

Radio-over-fibre technology for broadband wireless communication systems

Citation for published version (APA):

Ng'Oma, A. (2005). *Radio-over-fibre technology for broadband wireless communication systems*. [Phd Thesis 1 (Research TU/e / Graduation TU/e), Electrical Engineering]. Technische Universiteit Eindhoven. <https://doi.org/10.6100/IR592332>

DOI:

[10.6100/IR592332](https://doi.org/10.6100/IR592332)

Document status and date:

Published: 01/01/2005

Document Version:

Publisher's PDF, also known as Version of Record (includes final page, issue and volume numbers)

Please check the document version of this publication:

- A submitted manuscript is the version of the article upon submission and before peer-review. There can be important differences between the submitted version and the official published version of record. People interested in the research are advised to contact the author for the final version of the publication, or visit the DOI to the publisher's website.
- The final author version and the galley proof are versions of the publication after peer review.
- The final published version features the final layout of the paper including the volume, issue and page numbers.

[Link to publication](#)

General rights

Copyright and moral rights for the publications made accessible in the public portal are retained by the authors and/or other copyright owners and it is a condition of accessing publications that users recognise and abide by the legal requirements associated with these rights.

- Users may download and print one copy of any publication from the public portal for the purpose of private study or research.
- You may not further distribute the material or use it for any profit-making activity or commercial gain
- You may freely distribute the URL identifying the publication in the public portal.

If the publication is distributed under the terms of Article 25fa of the Dutch Copyright Act, indicated by the "Taverne" license above, please follow below link for the End User Agreement:

www.tue.nl/taverne

Take down policy

If you believe that this document breaches copyright please contact us at:

openaccess@tue.nl

providing details and we will investigate your claim.

Radio-over-Fibre Technology for Broadband Wireless Communication Systems

PROEFSCHRIFT

ter verkrijging van de graad van doctor aan de Technische
Universiteit Eindhoven, op gezag van de Rector Magnificus,
prof.dr.ir. C.J. van Duijn, voor een commissie aangewezen door
het College voor Promoties in het openbaar te verdedigen op
dinsdag 28 juni 2005 om 16.00 uur

door

Anthony Ng'oma

geboren te Kasama, Zambia

Dit proefschrift is goedgekeurd door de promotor:

prof.ir. A.M.J. Koonen

Copromotor:

prof.dr.ir. E.R. Fledderus

The work presented in this thesis was performed in the faculty of Electrical Engineering of the Eindhoven University of Technology, and was partly financially supported by the Dutch Ministry of Economic Affairs in the BTS project Broadband Radio@Hand within the BraBantBreedBand (B4) programme.

CIP-DATA LIBRARY TECHNISCHE UNIVERSITEIT EINDHOVEN

Ng'oma, Anthony

Radio-over-fibre technology for broadband wireless communication systems / by Anthony Ng'oma. – Eindhoven : Technische Universiteit Eindhoven, 2005.

Proefschrift. – ISBN 90-386-1723-2

NUR 959

Trefw.: optische telecommunicatie / microgolfttechniek / datatransmissie ; radiocommunicatie / breedbandcommunicatie / mobiele telecommunicatie.

Subject headings: optical fibre communication / millimetre wave generation / radio access networks / broadband networks / indoor radio.

Copyright © 2005 by Anthony Ng'oma

All rights reserved. No part of this publication may be reproduced, stored in a retrieval system, or transmitted in any form or by any means without prior written consent of the author.

Typeset using Microsoft Word 2003, printed in the Netherlands.

Summary

Wireless coverage of the end-user domain, be it outdoors or indoors (in-building), is poised to become an essential part of broadband communication networks. In order to offer integrated broadband services (combining voice, data, video, multimedia services, and new value added services), these systems will need to offer higher data transmission capacities well beyond the present-day standards of wireless systems. Wireless LAN (IEEE802.11a/b/g) offering up-to 54 Mbps and operating at 2.4 GHz and 5 GHz, and 3G mobile networks (IMT2000/UMTS) offering up-to 2 Mbps and operating around 2 GHz, are some of today's main wireless standards. IEEE802.16 or WiMAX is another recent standard aiming to bridge the last mile through mobile and fixed wireless access to the end user at frequencies between 2 – 66 GHz.

The need for increased capacity per unit area leads to higher operating frequencies (above 6 GHz) and smaller radio cells, especially in in-door applications where the high operating frequencies encounter tremendously high losses through the building walls. To reduce the system installation and maintenance costs of such systems, it is imperative to make the radio antenna units as simple as possible. This may be achieved by consolidating signal processing functions at a centralised headend, through radio-over-fibre technology.

The research in this thesis focussed on the feasibility of using both single-mode and multimode fibres to distribute high-frequency microwave signals to simplified remote radio antenna units. An alternative radio-over-fibre technique, termed Optical Frequency Multiplication (OFM) has been investigated. OFM entails the periodic filtering of a swept optical signal at the headend followed by photodetection at the radio access unit. A low sweep frequency (e.g. 3 GHz) is used. After photodetection at the remote radio access unit, high-frequency (>21 GHz) harmonic components of the sweep signal are generated. The desired microwave signal is selected by means of bandpass filtering, amplified, and radiated by the antenna. Modulated microwave carriers are generated by intensity modulating the frequency-swept optical signal.

Through modelling, simulations, and extensive experiments, the behaviour and performance of a radio-over-fibre downlink employing OFM was investigated. Simulation and comprehensive experimental results showed that OFM can be used to generate pure high-frequency microwave signals with very narrow linewidth and low SSB phase noise. This is because in the OFM process laser phase noise is inherently suppressed. The low-phase noise capability of OFM enables it to support the delivery

of carriers modulated not only by the simple ASK data format, but also by complex multilevel modulation formats such as BPSK, QPSK, and x-level QAM. Multicarrier signals such as Subcarrier Multiplexed signals, and OFDM signals used in wireless LANs are also supported. Low Error Vector Magnitudes (below 5%) were obtained for x-QAM modulation formats, including 64-QAM. BER measurements showed a modal dispersion penalty of about 1 dB for a 4.4 km MMF link under restricted launch condition.

It was established that OFM is chromatic dispersion tolerant and can support more than 10 times longer single-mode fibre transmission links (exceeding 50 km) than IM-DD systems, which suffer from the chromatic-dispersion-induced amplitude suppression. OFM also enables the delivery of microwave carriers exceeding the modal bandwidth of MMFs, by using the higher transmission passbands of the fibre response. Silica glass MMF links of more than 4 km are feasible. The maximum link length, which can be bridged with Polymer Optical Fibre (POF) is significantly shorter, owing to its higher attenuation values. Thus POF may be more attractive for in-building applications where link lengths of 500m are often sufficient.

Several different implementations of the Mach Zehnder Interferometer, and the Fabry Perot Interferometer filters were considered to determine their simplicity, performance, and applicability within the end-user environment. It was established that the wavelength of the optical FM source needs to be carefully aligned to the characteristics of the periodic optical filter. Therefore, it is preferred that both the source and the filter are co-located. This makes it easier to employ electronic tuning control of the filter (e.g. a fibre Fabry Perot Interferometer), so as to automatically track the alignment with the optical source, resulting in remarkable improvement of the OFM system stability.

The ability to achieve high frequency multiplication factors, good phase noise performance, the support for all modulation formats, and the ability to operate on both single-mode and MMFs, all make OFM ideal for use in high-frequency (>5 GHz) broadband wireless system applications.

Contents

Summary	iii
Contents	v
List of Acronyms	ix
1 Introduction	1
1.1 Wireless Communication Systems.....	1
1.2 Broadband Wireless Communication Systems	3
1.3 Challenges of Broadband Wireless Access Networks	4
1.4 Radio-over-Fibre Technology	6
1.4.1 What is RoF?	6
1.4.2 Benefits of RoF Technology	8
1.4.3 Limitations of RoF Technology	11
1.4.4 Applications of RoF Technology	11
1.5 Objectives and Outline of the Thesis	12
2 Techniques for Transporting RF Signals over Optical Fibre	15
2.1 Introduction	15
2.2 RF Signal Generation by Intensity Modulation and Direct Detection.....	16
2.2.1 Advantages of IM-DD	17
2.2.2 Disadvantages of IM-DD	17
2.3 RF Signal Generation by Remote Heterodyne Detection	18
2.3.1 The Principle of Optical Heterodyning	18
2.3.2 Optical FM-Filter System	20
2.3.3 Optical Frequency/Phase Locked-Loops (OFLL/OPLL)	22
2.3.4 Optical Injection Locking (OIL).....	24
2.3.5 Optical Injection Phase Locked Loop (OIPLL).....	26
2.3.6 Dual Mode Lasers	27
2.4 Techniques Based on Harmonics Generation	27
2.4.1 The FM – IM Conversion Technique	27

2.4.2	Modulation Sideband Techniques	29
2.4.3	Interferometer based Mixing	31
2.5	RoF Multiplexing Techniques	32
2.5.1	Sub-Carrier Multiplexing in RoF Systems	32
2.5.2	Wavelength Division Multiplexing in RoF Systems	33
2.6	Conclusions.....	34
3	Principle of Optical Frequency Multiplication	37
3.1	Introduction.....	37
3.2	Mach Zehnder Interferometer-based OFM System	39
3.2.1	Introduction.....	39
3.2.2	OFM Up-Conversion with the MZI.....	40
3.2.3	Impact of FM Index	41
3.2.4	Optimal Power Generation	43
3.2.5	Impact of Laser-Filter Misalignment.....	44
3.2.6	Intensity Modulation Depth	46
3.3	Fabry Perot Interferometer-based OFM System.....	49
3.3.1	Introduction.....	49
3.3.2	Up-conversion with FPI.....	52
3.3.3	Impact of FM Index on the FPI-based System	53
3.3.4	Impact of FPI's Finesse on the OFM System.....	56
3.3.5	Impact of Laser-Filter Misalignment in a FPI-based OFM system	58
3.4	Comparison of the MZI and FPI based OFM Systems.....	61
3.5	Impact of Laser Phase Noise on the OFM System	62
3.5.1	What is Laser Phase Noise?.....	62
3.5.2	Impact of Laser Phase Noise	63
3.6	Impact of Sweep Signal Phase Noise on the OFM System	64
3.6.1	What is Oscillator Phase Noise?.....	64
3.6.2	Impact of Sweep Signal Phase Noise	65
3.7	Conclusions.....	66
4	Impact of Fibre Dispersion on OFM.....	69
4.1	Introduction.....	69
4.2	Chromatic Dispersion	70
4.3	Impact of Chromatic Dispersion.....	70
4.4	Modal Dispersion.....	72
4.4.1	Modelling Modal dispersion.....	73
4.4.2	MMF Transfer Function	75
4.4.3	MMF Bandwidth.....	76
4.5	Impact of Modal Dispersion on OFM.....	77

4.6	Conclusions.....	80
5	Experimental Demonstration of an OFM-based RoF Downlink.....	81
5.1	Introduction.....	81
5.2	Optical FM Sources	82
5.3	FM Index Control.....	83
5.4	Microwave LO Generation with OFM.....	85
5.4.1	Experimental Set-up	85
5.4.2	Harmonic Component Selection.....	87
5.4.3	Impact of FM Index	88
5.5	Linewidth and Phase Noise of the OFM Generated Microwave LOs	89
5.5.1	Impact of Light Source Linewidth.....	89
5.5.2	Impact of Sweep Signal Phase Noise	90
5.6	Single Mode Fibre-based OFM Downlink.....	93
5.7	Multimode Fibre-based OFM Downlink	93
5.7.1	Single Mode Fibre Butt-Coupling	94
5.7.2	Coupling Through the Mode Scrambler	96
5.8	Polymer Fibre-based OFM Downlink.....	99
5.9	A Tunable Laser-based OFM System.....	101
5.10	Filter Implementations for the OFM System	103
5.10.1	Fibre based Fabry Perot Interferometer	104
5.10.2	Fibre Bragg Grating based Fabry Perot Interferometer	105
5.10.3	Wafer-based Fabry Perot Interferometer	106
5.10.4	Chip-Based MZI	108
5.11	Stability of OFM-Generated Carriers	108
5.11.1	MZI-Based OFM System.....	109
5.11.2	FPI-Based System.....	111
5.11.3	Stability of the Chip-based MZI	112
5.12	Transmission and Frequency Up-Conversion of Data Modulated Carriers	112
5.12.1	ASK Data Modulation	114
5.12.2	Complex Signal Modulation Formats.....	117
5.12.3	WLAN Signal Up-Conversion and Transmission	118
5.12.4	Bit Error Rate Measurements	122
5.13	Conclusions.....	123
6	Towards a Point-to-Multipoint RoF System Based on OFM.....	125
6.1	Introduction.....	37
6.2	Full-Duplex RoF System with OFM.....	126
6.3	Point-to-Multipoint OFM System.....	127

7	Conclusions and Recommendations	131
7.1	Conclusions.....	131
7.2	Recommendations.....	135
Appendix A:	Optical Frequency Multiplication based on MZI	137
References		139
List of Publications		149
Samenvatting		153
Acknowledgements		155
Curriculum Vitae		159

List of Acronyms

1G	First Generation
2G	Second Generation
3G	Third Generation
ASK	Amplitude Shift Keying
B4	BroadBand BraBant (research programme)
BBoF	Baseband-over-Fibre
BER	Bit-Error-Rate
BPSK	Binary Phase Shift Keying
BS	Base Station
CNR	Carrier-to-Noise Ratio
CW	Continuous Wave
DAS	Distributed Antenna System
dB	decibels
dBc	decibels relative to carrier
DFB	Distributed Feedback laser diode
dBm	decibels milliwatt
dBr	decibels relative
DR	Dynamic Range
DWDM	Dense Wavelength Division Multiplexing
EVM	Error Vector Magnitude
FBG	Fibre Bragg Grating
FFPI	Fibre-based Fabry Perot Interferometer
FFR	Far Field Radiation
FM	Frequency Modulation
FPI	Fabry Perot Interferometer
FSR	Free Spectral Range
FTTC	Fibre To The Curb
FTTH	Fibre To The Home
FWA	Fixed Wireless Access
FWHM	Full Width at Half Maximum
Gbps	Gigabit per second
GHz	GigaHertz
GIPOF	Graded Index Polymer Optical Fibre
GSCR	Grating assisted codirectional Coupler with rear Sampled grating Reflector
GSM	Global System for Mobile communications
IEEE	Institute of Electrical and Electronics Engineers

IF	Intermediate Frequency
IFoF	Intermediate Frequency-over-Fibre
IM	Intensity Modulation
IMD	Intensity Modulation Depth
IM-DD	Intensity Modulation with Direct Detection
IMT2000	International Mobile Telecommunications 2000
ISM	Industrial, Scientific, and Medical
LAN	Local Area Network
LMDS	Local Multipoint Distribution Systems
LO	Local Oscillator
Mbps	Megabit per second
MHz	Mega-Hertz
MMF	Multimode Fibre
MS	Mode Scrambler
MU	Mobile Unit
MZI	Mach-Zehnder Interferometer
MZM	Mach-Zehnder Modulator
NF	Noise Figure
O/E	Opto-Electrical
OFCG	Optical Frequency Comb Generator
OFDM	Orthogonal Frequency Division Multiplexing
OPLL	Optical Frequency-Locked Loop
OQPSK	Offset Quadrature Phase Shift Keying
OFM	Optical Frequency Multiplication
OIL	Optical Injection Locking
OPLL	Optical Phase Locked Loop
OTDM	Optical Time Division Multiplexing
PD	Photodetector
PLL	Phase Locked Loop
PM	Phase Modulation
POF	Polymer Optical Fibre
PZT	Piezo-electric Transducer
QAM	Quadrature Amplitude Modulation
QPSK	Quadrature Phase Shift Keying
rad	radians
RAP	Radio Access Point
RAU	Radio Access Unit / Remote Antenna Unit
RF	Radio Frequency
RFoF	Radio Frequency-over-Fibre
RHD	Remote Heterodyne Detection
RIN	Relative Intensity Noise
RoF	Radio-over-Fibre
SBS	Stimulated Brillouin Scattering
SCM	Sub-Carrier Multiplexing
SFDR	Spurious Free Dynamic Range
SMF	Single Mode Fibre
SSB	Single Side Band
UMTS	Universal Mobile Telecommunication System

VCSEL	Vertical Cavity Surface Emitting Laser diode
VPI	Virtual Photonics Inc. (simulation software manufacturer)
VSA	Vector Signal Analyser
VSG	Vector Signal Generator
WDM	Wavelength Division Multiplexing
WLAN	Wireless Local Area Network
WMAN	Wireless Metropolitan Area Network
WPAN	Wireless Personal Area Network
WTU	Wireless Terminal Unit

CHAPTER

1

Introduction

1.1 *Wireless Communication Systems*

Wireless communication has experienced tremendous growth in the last decade. In 1991 less than 1% of the world's population had access to a mobile phone. By the end of 2001, an estimated one in every six people had a mobile phone [1]. During the same period the number of countries worldwide having a mobile network increased from just three to over 90%. In fact the number of mobile subscribers overtook the number of fixed-line subscribers in 2002, as shown in Figure 1.1. It is predicted that this growth will continue to rise, and by 2010 there will be more than 1700 million mobile subscribers worldwide [2].

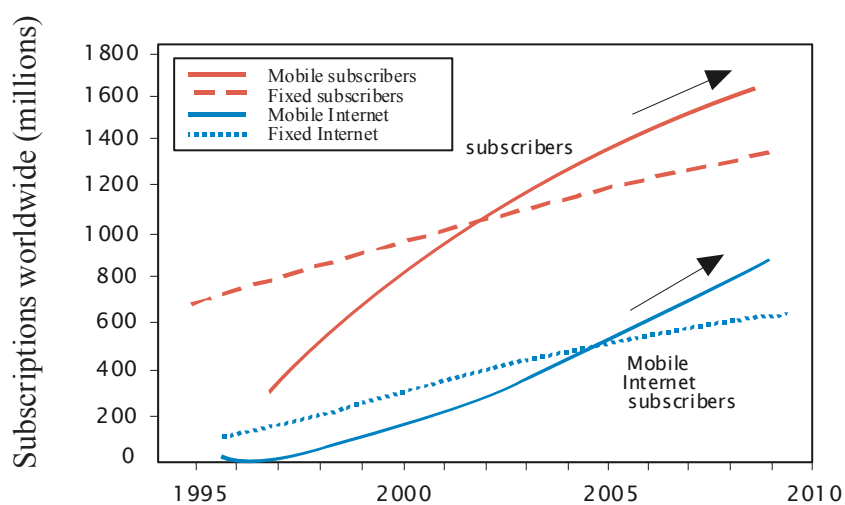



Figure 1.1: Global Growth of Mobile and Fixed Subscribers [2]

Apart from mobile telephone communications, Wireless Local Area Networks (WLANs), which came on the scene less than a decade ago (1997), have also experienced phenomenal growth. The rapid proliferation of WLAN hotspots in public places, such as airport terminals has been astounding. In fact WLANs have now made their way into homes, riding on the back of xDSL and cable access modems, which are now integrated with WLAN Radio Access Points (RAPs). As a result, the number of wireless Internet subscribers is expected to overtake the number of wired internet users quite soon, as shown in Figure 1.1. The growth of wireless data systems is also seen in the many new standards which have recently been developed or are currently under development (see Section 1.2).

The rapid growth of wireless communications is mainly attributed to their ease of installation in comparison to fixed networks [1]. However, technological advancement, and competition among mobile operators have also contributed to the growth. So far there have been three mobile telephone standards, launched in succession approximately every decade. The first-generation (1G) mobile systems were analogue, and were commissioned in the 1980s. In the 1990s, second-generation (2G) digital mobile systems such as the Global System for Mobile communications (GSM) came on the scene. The GSM standard has been extremely successful, providing not only national, but international coverage as well. Thus, GSM is currently the mainstream mobile communication system.

Table 1.1 Evolution of the WLAN Standards [3]



Year	WLAN Standard	Frequency	Modulation	Bit-Rate (Max)
1997	IEEE 802.11	2.4 GHz	Frequency Hopping and Direct Spread Spectrum	2 Mbps
1998	ETSI HomeRF	2.4 GHz	Wideband Frequency Hopping	1.6 Mbps
1999	IEEE 802.11b	2.4 GHz	Direct Sequence Spread Spectrum	11 Mbps
1999	IEEE 802.11a	5 GHz	OFDM	54 Mbps
2000	ETSI HiperLAN2	5 GHz	OFDM Connection-oriented	54 Mbps
2003	IEEE 802.11g	2.4 GHz	OFDM compatible with 802.11a	54 Mbps

Both 1G and 2G systems were designed primarily to provide voice applications, and to support circuit-switched services [4]. However, GSM does offer data communication services to users, although the data rates are limited to just a few tens of kbps. In contrast, WLANs originally designed to provide fixed data network extension, support Mbps data transmission rates. The WLAN standard – IEEE 802.11, also known as *Wi-Fi*, was first commissioned in 1997 and offered 2 Mbps. Since then, the standard has evolved several times responding to the sustained user demand for higher bit-rates as shown in Table 1.1. Currently, WLANs are capable of offering up-to 54 Mbps for the IEEE 802.11a/g, and HiperLAN2 standards operating

in the 2.4 GHz and 5 GHz license-free ISM bands. However, WLANs do not offer the kind of mobility, which mobile systems do.

1.2 Broadband Wireless Communication Systems

The explosive growth of the Internet, and the success of 2G systems together with WLANs have had a profound impact on our perception of communication. First of all, the vast majority of users now believe in the new notion of “always on” communication. We are now living in the era of *ubiquitous connectivity* or “communication anytime, anywhere, and with anything”. Secondly, the concept of broadband communication has caught on very well. As fibre penetrates closer to the end-user environment (Fibre To The Home/Curb/X, FTTH/C/X), wired transmission speeds will continue to rise. Transmission speeds such as 100 Mbps (Fast Ethernet) are now beginning to reach homes. The demand to have this broadband capacity also wirelessly has put pressure on wireless communication systems to increase both their transmission capacity, as well as their coverage.

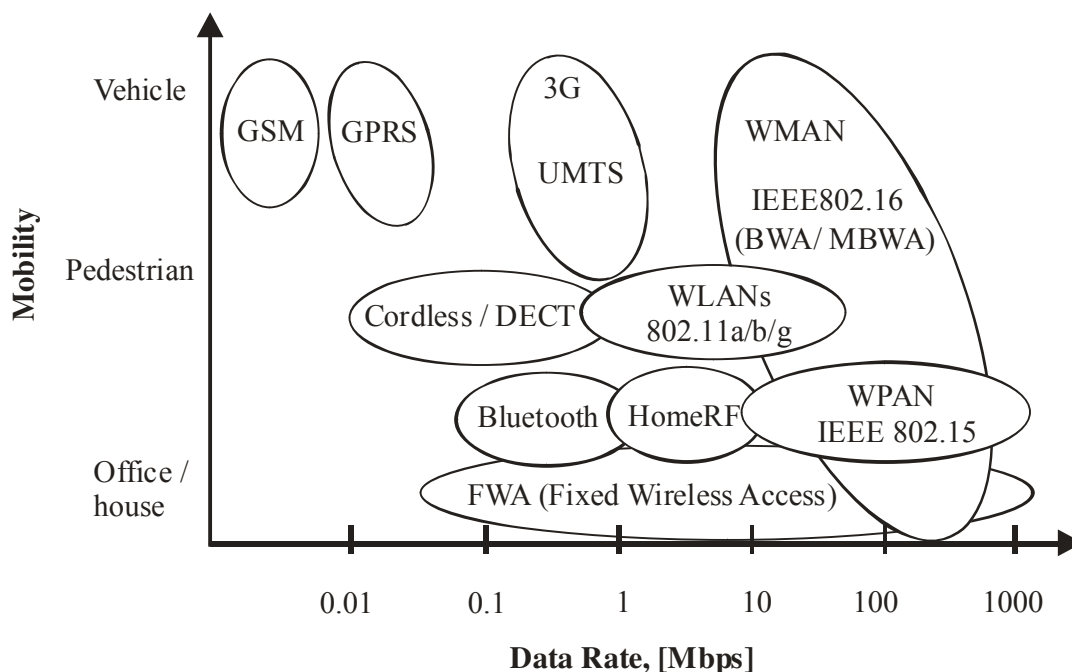


Figure 1.2: Overview of present and future wireless communication systems [2], [4], [5]

In general there is a trade off between coverage and capacity. Figure 1.2 shows the relationship between some of the various standards (present and future), in terms of mobility (coverage), and capacity. For instance, the cell size of Wireless Personal Area Networks (WPANs) is typically a few metres (picocell), while their transmission rates may reach several tens of Mbps. On the other hand 2G (e.g. GSM), and 3G (e.g. Universal Mobile Telecommunication System (UMTS) and the International Mobile Telecommunications (IMT2000)) systems have cells that extend several kilometres,

but have data rates limited to less than 2 Mbps. Therefore, as mobile communication systems seek to increase capacity, and wireless data systems seek to increase coverage, they will both move towards convergence. A case in point is the IEEE 802.16, otherwise known as WiMAX, which appears to lend weight to the notion of convergence, as shown in Figure 1.2. WiMAX seeks to provide high-bit rate mobile services using frequencies between 2 – 11 GHz. In addition, WiMAX also aims to provide Fixed Wireless Access (FWA) at bit-rates in the excess of 100 Mbps and at higher frequencies between 10 – 66 GHz [6].

1.3 Challenges of Broadband Wireless Access Networks

Figure 1.3 illustrates the configuration of narrowband wireless access systems (e.g. GSM) as we know them today. The central office handles call processing and switching, while the Base Stations (BS) act as the radio interfaces for the Mobile Units (MU) or Wireless Terminal Units (WTU). The BSs may be linked to the central office through either analogue microwave links or digital fibre optic links. Once the baseband signals are received at the BS, they are processed and modulated onto the appropriate carrier. The radius covered by the signal from the BS is the cell radius. All the MU/WTU within the cell, share the radio frequency spectrum. WLANs are configured in a similar fashion, with the radio interface called the Radio Access Point (RAP).

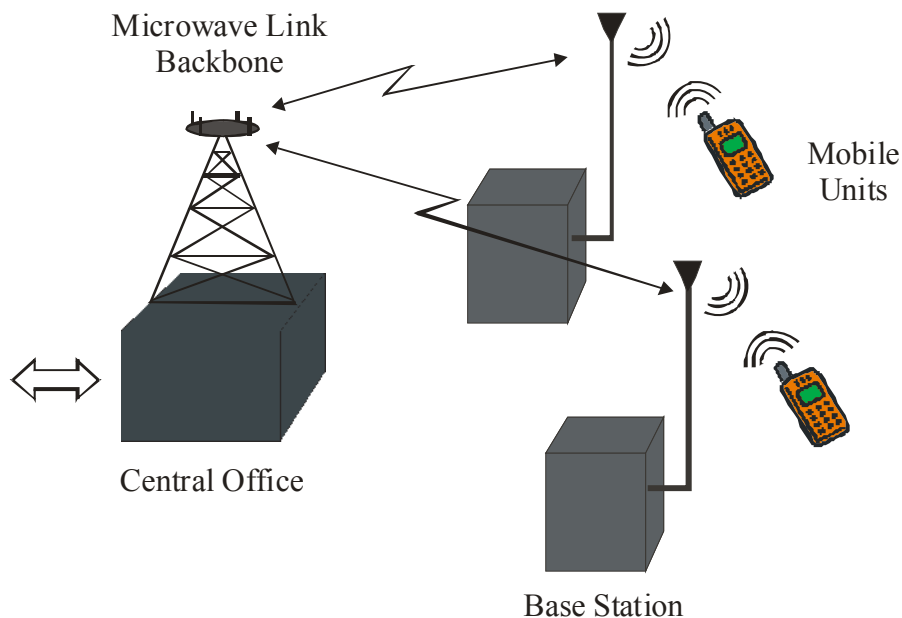


Figure 1.3: Schematic Showing the Components of a Narrowband Wireless Access Network

In general, low carrier frequencies offer low bandwidth. Therefore, part of the reason why narrowband wireless access systems (e.g. 2G) offer limited capacity is because they operate at low frequencies. For instance GSM operates at frequencies around

900 or 1800 MHz with 200 kHz allocated frequency spectrum. UMTS operates at frequencies around 2 GHz and has 4 MHz allocated bandwidth [7]. However, there is also stiff competition for frequency spectrum among the many wireless communication systems using carrier frequencies below 6 GHz. These include radio and TV broadcasts, and systems for (vital) communication services such as airports, police and fire, amateur radio users, wireless LANs, and many others. Low frequencies allow for low cost radio front-ends (in the BS and the MU/WTU). In addition, the efficiency of RF active devices (transistors) is higher at low frequencies, than at high frequencies. For instance, at millimetre wave frequencies the efficiency of active devices can be as low as 30 % [9]. Therefore, the low-power consumption advantage of systems operating at low frequencies is quite significant. Furthermore, low-frequency RF signals allow for larger cells, due to the longer reach of the radio waves. The larger cells enable high mobility, but lead to poor spectrum efficiency, since the spectrum is shared by all MUs/WTUs operating within the cell [7].

Therefore, one natural way to increase capacity of wireless communication systems is to deploy smaller cells (micro- and pico-cells). This is generally difficult to achieve at low-frequency microwave carriers, but by reducing the radiated power at the antenna, the cell size may be reduced somewhat. Pico-cells are also easier to form inside buildings, where the high losses induced by the building walls help to limit the cell size. In contrast, the high propagation losses, which radio waves experience at mm-wave frequencies, together with the line-of-site requirements, help to form small cells.


Another way to increase the capacity of wireless communication systems is to increase the carrier frequencies, to avoid the congested ISM band frequencies. Higher carrier frequencies offer greater modulation bandwidth, but may lead to increased costs of radio front-ends in the BSs and the MUs/WTUs.

Smaller cell sizes lead to improved spectral efficiency through increased frequency reuse. But, at the same time, smaller cell sizes mean that large numbers of BSs or RAPs are needed in order to achieve the wide coverage required of ubiquitous communication systems. Furthermore, extensive feeder networks are needed to service the large number of BSs/RAPs. Therefore, unless the cost of the BSs/RAPs, and the feeder network are significantly low, the system-wide installation and maintenance costs of such systems would be rendered prohibitively high. This is where Radio-over-Fibre (RoF) technology comes in. It achieves the simplification of the BSs/RAPs (referred to as Remote Antenna Units – RAUs) through consolidation of radio system functionalities at a centralised headend, which are then shared by multiple RAUs. In addition, a further reduction in system costs may be achieved if low-cost multimode fibres (see section 4.4) are used in the extensive feeder network [10].

Therefore, for broadband wireless communication systems to offer the needed high capacity, it appears inevitable to increase the carrier frequencies and to reduce cell sizes. This is evident from the new standards in the offing, which are aiming to use mm-waves. For example the recently formed IEEE 802.15 WPAN standard Task Group 3c is aiming to use the unlicensed mm-wave bands between 57 - 64 GHz for very-high-speed short-range communication offering up-to 2 Gbps [7]. The IEEE

802.16 (WiMAX) standard specifies frequencies between 10 – 66 GHz for the first/last mile Fixed Wireless Access (FWA). A summary of the operating frequencies for some of the current and future (broadband) wireless systems is given in Table 1.2.

Table 1.2 Frequencies for Broadband Wireless Communication Systems [2] - [5]



Frequency	Wireless System
2 GHz	UMTS / 3G Systems
2.4 GHz	IEEE 802.11 b/g WLAN
5 GHz	IEEE 802.11 a WLAN
2 – 11 GHz	IEEE 802.16 WiMAX
17/19	Indoor Wireless (Radio) LANs
28 GHz	Fixed wireless access – Local point to Multipoint (LMDS) /
38 GHz	Fixed wireless access, Picocellular
58 GHz	Indoor wireless LANs
57 – 64 GHz	IEEE 802.15 WPAN
10 – 66 GHz	IEEE 802.16 - WiMAX

1.4 Radio-over-Fibre Technology

1.4.1 What is RoF?

Radio-over-Fibre (RoF) technology entails the use of optical fibre links to distribute RF signals from a central location (headend) to Remote Antenna Units (RAUs). In narrowband communication systems and WLANs, RF signal processing functions such as frequency up-conversion, carrier modulation, and multiplexing, are performed at the BS or the RAP, and immediately fed into the antenna. RoF makes it possible to centralise the RF signal processing functions in one shared location (headend), and then to use optical fibre, which offers low signal loss (0.3 dB/km for 1550 nm, and 0.5 dB/km for 1310 nm wavelengths) to distribute the RF signals to the RAUs, as shown in Figure 1.4. By so doing, RAUs are simplified significantly, as they only need to perform optoelectronic conversion and amplification functions. The centralisation of RF signal processing functions enables equipment sharing, dynamic allocation of resources, and simplified system operation and maintenance. These benefits can translate into major system installation and operational savings [8], especially in wide-coverage broadband wireless communication systems, where a high density of BS/RAPs is necessary as discussed above.

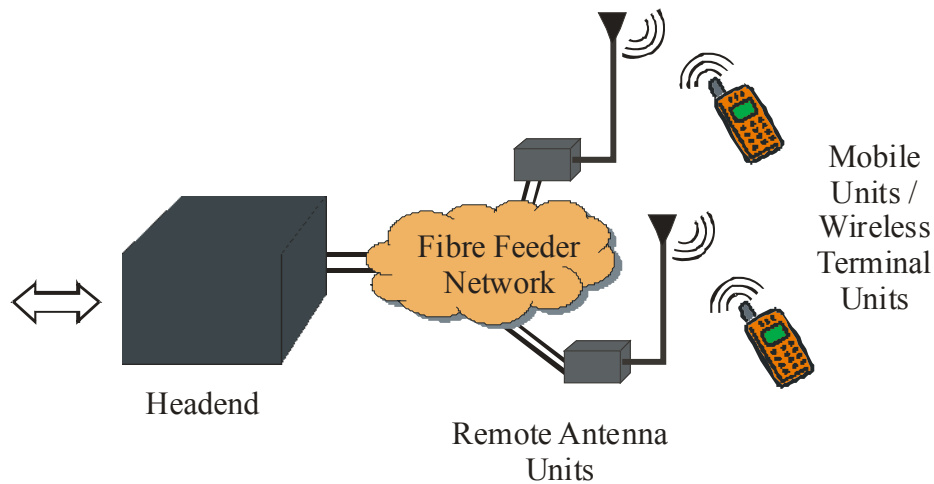


Figure 1.4: The Radio over Fibre System Concept

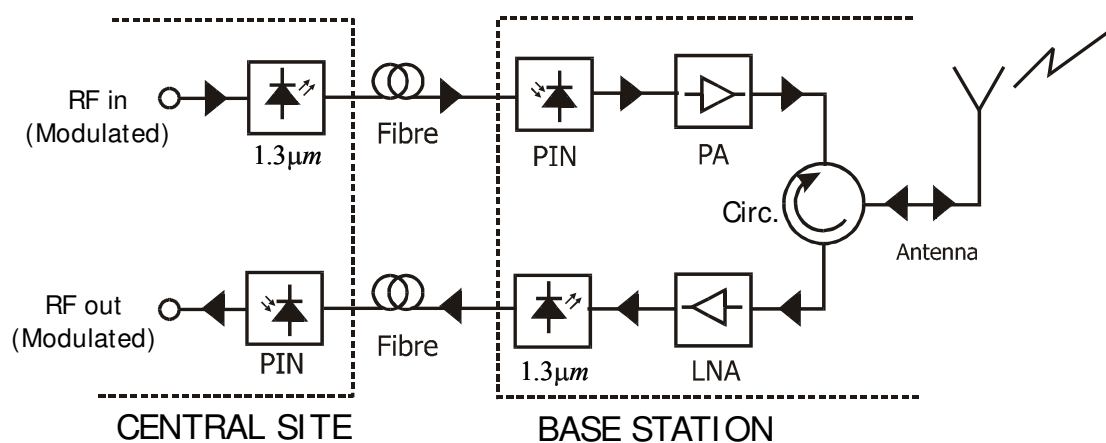


Figure 1.5: 900 MHz Fibre-Radio System

One of the pioneer RoF system implementations is depicted in Figure 1.5. Such a system may be used to distribute GSM signals, for example. The RF signal is used to directly modulate the laser diode in the central site (headend). The resulting intensity modulated optical signal is then transported over the length of the fibre to the BS (RAU). At the RAU, the transmitted RF signal is recovered by direct detection in the PIN photodetector. The signal is then amplified and radiated by the antenna. The up-link signal from the MU is transported from the RAU to the headend in the same way. This method of transporting RF signals over the fibre is called Intensity Modulation with Direct Detection (IM-DD), and is the simplest form of the RoF link.

While Figure 1.5 shows the transmission of the RF signal at its frequency, it is not always necessary to do that. For instance, a Local Oscillator (LO) signal, if available, may be used to down-convert the uplink carrier to an IF in the RAU. Doing so would allow for the use of low-frequency components for the up-link path in the RAU – leading to system cost savings. Instead of placing a separate LO in the RAU, it may be transported from the headend to the RAU by the RoF system. Once available at the RAU, the LO may then be used to achieve down-conversion of the uplink signals. This results in a much simpler RAU. In this configuration, the downlink becomes the crucial part of the RoF since it has to transport high-frequency signals. The transportation of high-frequency signals is more challenging because it requires high-frequency components, and large link bandwidth. This means that high-frequency signals are more susceptible to transmitter, receiver, and transmission link signal impairments.

Apart from IM-DD, other methods, which involve signal frequency up-conversion in addition to distribution are also used. These methods, which include Remote Heterodyning (RHD) and harmonic up-conversion are discussed in Chapter 2.

1.4.2 Benefits of RoF Technology

Some of the advantages and benefits of the RoF technology compared with electronic signal distribution are given below.

1.4.2.1 *Low Attenuation Loss*

Electrical distribution of high-frequency microwave signals either in free space or through transmission lines is problematic and costly. In free space, losses due to absorption and reflection increase with frequency [5]. In transmission lines, impedance rises with frequency as well, leading to very high losses [11]. Therefore, distributing high frequency radio signals electrically over long distances requires expensive regenerating equipment. As for mm-waves, their distribution via the use of transmission lines is not feasible even for short distances. The alternative solution to this problem is to distribute baseband signals or signals at low intermediate frequencies (IF) from the switching centre (headend) to the BS [1]. The baseband or IF signals are up-converted to the required microwave or mm-wave frequency at each base station, amplified and then radiated. This system configuration is the same as the one used in the distribution of narrowband mobile communication systems shown in Figure 1.3. Since, high performance LOs would be required for up-conversion at each base station, this arrangement leads to complex base stations with tight performance requirements. However, since optical fibre offers very low loss, RoF technology can be used to achieve both low-loss distribution of mm-waves, and simplification of RAUs at the same time.

Commercially available standard Single Mode Fibres (SMFs) made from glass (silica) have attenuation losses below 0.2 dB/km and 0.5 dB/km in the 1550 nm and the 1300 nm windows, respectively. Polymer Optical Fibres (POFs), a more recent kind of optical fibre exhibits higher attenuation ranging from 10 – 40 dB/km in the 500 - 1300 nm regions [12], [13]. These losses are much lower than those encountered in, say

coaxial cable, whose losses are higher by three orders of magnitude at higher frequencies. For instance, the attenuation of a ½ inch coaxial cable (RG-214) is >500 dB/km for frequencies above 5 GHz [14]. Therefore, by transmitting microwaves in the optical form, transmission distances are increased several folds and the required transmission powers reduced greatly.

1.4.2.2 *Large Bandwidth*

Optical fibres offer enormous bandwidth. There are three main transmission windows, which offer low attenuation, namely the 850 nm, 1310 nm, and 1550 nm wavelengths. For a single SMF optical fibre, the combined bandwidth of the three windows is in the excess of 50 THz [15]. However, today's state-of-the-art commercial systems utilize only a fraction of this capacity (1.6 THz). But developments to exploit more optical capacity per single fibre are still continuing. The main driving factors towards unlocking more and more bandwidth out of the optical fibre include the availability of low dispersion (or dispersion shifted) fibre, the Erbium Doped Fibre Amplifier (EDFA) for the 1550 nm window, and the use of advanced multiplex techniques namely Optical Time Division Multiplexing (OTDM) in combination with Dense Wavelength Division Multiplex (DWDM) techniques.

The enormous bandwidth offered by optical fibres has other benefits apart from the high capacity for transmitting microwave signals. The high optical bandwidth enables high speed signal processing that may be more difficult or impossible to do in electronic systems. In other words, some of the demanding microwave functions such as filtering, mixing, up- and down-conversion, can be implemented in the optical domain [16]. For instance, mm-wave filtering can be achieved by first converting the electrical signal to be filtered into an optical signal, then performing the filtering by using optical components such as the Mach Zehnder Interferometer (MZI) or Fibre Bragg Gratings (FBG), and then converting the filtered signal back into electrical form [17]. Furthermore, processing in the optical domain makes it possible to use cheaper low bandwidth optical components such as laser diodes and modulators, and still be able to handle high bandwidth signals [18].

The utilization of the enormous bandwidth offered by optical fibres is severely hampered by the limitation in bandwidth of electronic systems, which are the primary sources and receivers of transmission data. This problem is referred to as the “*electronic bottleneck*”. The solution around the electronic bottleneck lies in effective multiplexing. OTDM and DWDM techniques mentioned above are used in digital optical systems. In analogue optical systems including RoF technology, Sub-Carrier Multiplexing (SCM) is used to increase optical fibre bandwidth utilization. In SCM, several microwave subcarriers, which are modulated with digital or analogue data, are combined and used to modulate the optical signal, which is then carried on a single fibre [19], [20]. This makes RoF systems cost-effective.

1.4.2.3 *Immunity to Radio Frequency Interference*

Immunity to ElectroMagnetic Interference (EMI) is a very attractive property of optical fibre communications, especially for microwave transmission. This is so because signals are transmitted in the form of light through the fibre. Because of this

immunity, fibre cables are preferred even for short connections at mm-waves. Related to EMI immunity is the immunity to eavesdropping, which is an important characteristic of optical fibre communications, as it provides privacy and security.

1.4.2.4 Easy Installation and Maintenance

In RoF systems, complex and expensive equipment is kept at the headend, thereby making the RAUs simpler. For instance, most RoF techniques eliminate the need for a LO and related equipment at the RAU. In such cases a photodetector, an RF amplifier, and an antenna make up the RAU. Modulation and switching equipment is kept in the headend and is shared by several RAUs. This arrangement leads to smaller and lighter RAUs, effectively reducing system installation and maintenance costs. Easy installation and low maintenance costs of RAUs are very important requirements for mm-wave systems, because of the large numbers of the required RAUs. In applications where RAUs are not easily accessible, the reduction in maintenance requirements leads to major operational cost savings [8], [11]. Smaller RAUs also lead to reduced environmental impact.

1.4.2.5 Reduced Power Consumption

Reduced power consumption is a consequence of having simple RAUs with reduced equipment. Most of the complex equipment is kept at the centralised headend. In some applications, the RAUs are operated in passive mode. For instance, some 5 GHz Fibre-Radio systems employing pico-cells can have the RAUs operate in passive mode [21]. Reduced power consumption at the RAU is significant considering that RAUs are sometimes placed in remote locations not fed by the power grid.

1.4.2.6 Multi-Operator and Multi-Service Operation

RoF offers system operational flexibility. Depending on the microwave generation technique, the RoF distribution system can be made signal-format transparent. For instance the Intensity Modulation and Direct Detection (IM-DD) technique can be made to operate as a linear system and therefore as a transparent system. This can be achieved by using low dispersion fibre (SMF) in combination with pre-modulated RF subcarriers (SCM). In that case, the same RoF network can be used to distribute multi-operator and multi-service traffic, resulting in huge economic savings [8]. The principle of Optical Frequency Multiplication (OFM), which is the focus of this thesis can also be used to achieve multi-service operation in combination with either WDM or SCM, because it is tolerant to chromatic dispersion.

1.4.2.7 Dynamic Resource Allocation

Since the switching, modulation, and other RF functions are performed at a centralized headend, it is possible to allocate capacity dynamically. For instance in a RoF distribution system for GSM traffic, more capacity can be allocated to an area (e.g. shopping mall) during peak times and then re-allocated to other areas when off-peak (e.g. to populated residential areas in the evenings). This can be achieved by allocating optical wavelengths through Wavelength Division Multiplexing (WDM) as need arises [22]. Allocating capacity dynamically as need for it arises obviates the requirement for allocating permanent capacity, which would be a waste of resources

in cases where traffic loads vary frequently and by large margins [8]. Furthermore, having the centralised headend facilitates the consolidation of other signal processing functions such as mobility functions, and macro diversity transmission [22].

1.4.3 Limitations of RoF Technology

Since RoF involves analogue modulation, and detection of light, it is fundamentally an analogue transmission system. Therefore, signal impairments such as noise and distortion, which are important in analogue communication systems, are important in RoF systems as well. These impairments tend to limit the Noise Figure (NF) and Dynamic Range (DR) of the RoF links [23]. DR is a very important parameter for mobile (cellular) communication systems such as GSM because the power received at the BS from the MUs varies widely (e.g. 80 dB [8]). That is, the RF power received from a MU which is close to the BS can be much higher than the RF power received from a MU which is several kilometres away, but within the same cell.

The noise sources in analogue optical fibre links include the laser's Relative Intensity Noise (RIN), the laser's phase noise, the photodiode's shot noise, the amplifier's thermal noise, and the fibre's dispersion. In Single Mode Fibre (SMF) based RoF, systems, chromatic dispersion may limit the fibre link lengths and may also cause phase de-correlation leading to increased RF carrier phase noise [5]. In Multi-Mode Fibre based RoF systems, modal dispersion severely limits the available link bandwidth and distance. It must be stated that although the RoF transmission system itself is analogue, the radio system being distributed need not be analogue as well, but it may be digital (e.g. WLAN, UMTS), using comprehensive multi-level signal modulation formats such as xQAM, or Orthogonal Frequency Division Multiplexing (OFDM).

1.4.4 Applications of RoF Technology

RoF technology is generally unsuitable for system applications, where high Spurious Free Dynamic Range (SFDR = maximum output signal power for which the power of the third-order intermodulation product is equal to the noise floor) is required, because of the limited DR. This is especially true of wide coverage mobile systems such as GSM, where SFDR of > 70 dB (outdoor) are required. However, most indoor applications do not require high SFDR. For instance, the required (uplink) SFDR for GSM reduces from >70 dB to about 50 dB for indoor applications [23]. Therefore, RoF distribution systems can readily be used for in-building (indoor) distribution of wireless signals of both mobile and data communication (e.g. WLAN) systems. In this case the RoF system becomes a Distributed Antenna System (DAS). For high-frequency applications such as WPAN, the cell size will be small due to high losses through the walls, bringing the benefits of RoF discussed above. The in-building fibre infrastructure may then be used for both wired and wireless applications as shown in Figure 1.6. Using MMF or indeed POF instead of SMF fibres to feed the RAUs may further reduce system installation and maintenance costs, especially for in-door applications. In-building data communication LANs are often based on MMF.

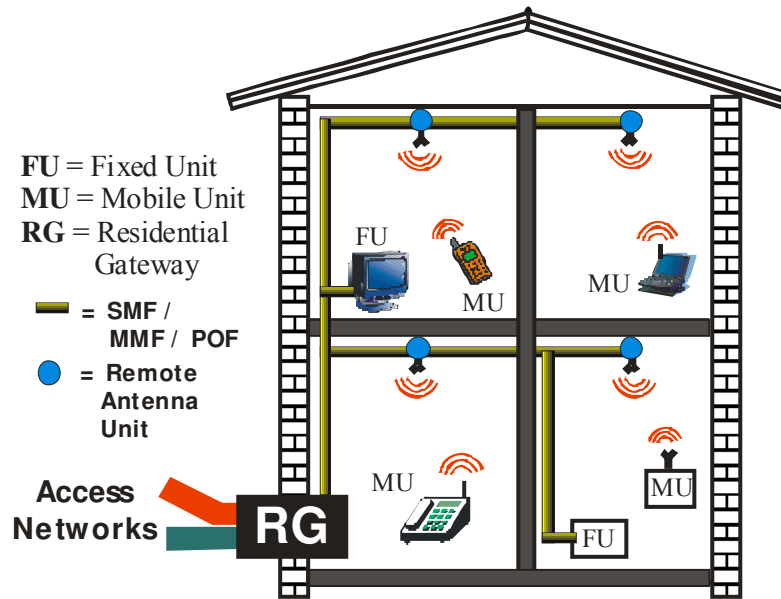


Figure 1.6: Using In-Building Fibre Infrastructure for Integrated Wired and Wireless System Applications

RoF systems are also attractive for other present and future applications where high SFDR is not required. For instance, UMTS MUs are required to control their transmitter power so that equal power levels are received at the BS. Thus, UMTS does not need the high SFDR required in GSM, so that RoF distribution systems may be used for both indoor and outdoor UMTS signal distribution [8]. Another application area is in Fixed Wireless Access (FWA) systems, such as WiMAX, where RoF technology may be used to optically transport signals over long distances bringing the significantly simplified RAUs closer to the end user, from where wireless links help to achieve broadband first/last mile access, in a cost effective way.

1.5 Objectives and Outline of the Thesis

It has been stated above that wireless communication systems require high-frequency carriers, and a high density of remote antenna units (RAUs) to achieve both high transmission capacity and wide signal coverage. In order to reduce system costs due to the large number of the required RAUs, the RAUs have to be significantly simplified. Furthermore, it has been stated that the new notion of *ubiquitous connectivity* has increased the importance of in-building coverage for all wireless communication systems. These requirements may be achieved by using RoF technology to centralise RF signal processing functions and using fibre optic links to distribute the RF signals to simplified RAUs. Therefore, in the RoF system, the transport of the LO or modulated microwave carrier over fibre links takes centre stage. Most RoF techniques utilise SMF to feed the RAUs, because the bandwidth of MMFs is severely limited by modal dispersion. However, most existing in-building fibre infrastructure for data communication is of a MMF nature. As a result many current RoF techniques may be used only for outdoor (SMF dominates) applications, but not indoor coverage (over MMFs).

This thesis proposes an alternative approach for delivering high-frequency signals to significantly simplified RoF RAUs. The method referred to as Optical Frequency Multiplication (OFM) involves interferometric filtering of a frequency-swept optical signal in order to generate high-frequency harmonic components of the sweep signal. Unlike some other techniques (see Chapter 2), OFM enables the use of only low-frequency electro-optical components at the headend. This helps to reduce the RoF system costs, while providing high-frequency operation at the RAU. OFM also allows for the use of both SMF and MMFs, as it does not rely on phase coherence as is the case in other techniques, such as heterodyne RoF techniques. A patent of the OFM technique has been filed [24].

Chapter 2 discusses some of the most widely used RoF techniques for distributing RF signals over fibre. The Chapter reviews the principle of operation for the various approaches, and considers their pros and cons. Chapter 3 describes the principle of operation of OFM and develops a theoretical model for the OFM system. The chapter also investigates the impact of device parameters, laser phase noise, and sweep signal phase noise on the behaviour and performance of the system. OFM systems based on both MZI and FPI filters are analysed.

In Chapter 4, the impact of both chromatic and modal dispersion on the performance of the OFM system is theoretically analysed. The practical realisation of a RoF downlink using OFM is presented in Chapter 5. The chapter reports on the extensive experiments conducted to validate the theoretical OFM model developed in Chapter 3, as well as the predicted impact of both chromatic and modal dispersion on the OFM system. Three types of fibres are used in the experiments – namely SMF, silica MMF, and Graded Index Polymer Optical Fibre (GIPOF). Various filter implementations of the MZI and the FPI types are explored. In addition, factors influencing the stability of the RF carriers generated by OFM are identified, and their mitigation investigated. The delivery of microwave LOs is demonstrated, and the phase noise performance of the OFM system verified. OFM is also used to deliver carriers modulated with both simple ASK and complex multi-level modulation formats. Both EVM and BER measurements of the received data were performed, in order to assess the feasibility of OFM to support high-capacity wireless communication systems.

Chapter 6 discusses the use of the OFM generated LOs for the system up-link, and highlights some of the important issues regarding point-to-multi-point system realisation. The thesis ends with Chapter 7, where conclusions are drawn, and recommendations made, about the performance of OFM and its suitability as a RoF method for realising ubiquitous broadband connectivity.

CHAPTER

2

Techniques for Transporting RF Signals over Optical Fibre

2.1 Introduction

There are several optical techniques for generating and transporting microwave signals over fibre. By considering the frequency of the RF signal fed into the RoF link at the headend in comparison with the signal generated at the RAU the RoF techniques may be classified into three categories – namely RF-over-fibre (RFoF), IF-over-Fibre (IFoF), or baseband-over-Fibre (BBoF) [5]. RFoF involves the transmission of the actual RF signal over the fibre. However, in IFoF and BBoF the desired microwave signal is generated at the RAU through up-conversion with a LO, which is either provided separately at the RAU, or is transported remotely to the RAU. Therefore, depending on the transmission method used, the RAU may be more complex or simpler.

Schemes requiring a separate LO at the RAU (i.e. either BBoF or IFoF) may render the RAU more costly, especially in mm-wave applications [5]. However, such systems exhibit improved receiver sensitivity. A comparison of the receiver sensitivities of three different RoF data transmission techniques – namely BBoF, IFoF, and RFoF is reported in [5]. Using an IF signal frequency of 2 GHz, and a LO signal frequency at 27 GHz, the three schemes were used to generate a 29 GHz RF signal modulated with 155 Mbps downstream data. It was found that the BBoF scheme exhibited better sensitivity than the IFoF scheme by 4 dB. On the other hand, the IFoF scheme had 2 dB better sensitivity than the RFoF scheme.

The transport of wireless signals as RFoF has the advantage that simpler RAUs may be used, since no frequency up-conversion is required. But this comes at a cost in

terms of the requirement for high-frequency equipment at the headend. The RFoF system is also susceptible to the effects of fibre dispersion on the RF power and phase noise [5]. BBoF and IFoF schemes may overcome such effects, but this may occur at the cost of increased RAU complexity, unless the upstream LO is delivered remotely.

RoF techniques may also be classified in terms of the underlying modulation/detection principles employed. In that case, the techniques may be grouped into three categories, namely Intensity Modulation – Direct Detection (IM-DD), Remote Heterodyne Detection (RHD) [25], and harmonic up-conversion techniques. RFoF systems fall under the IM-DD category. IFoF and BBoF systems, which involve the use of a LO at the RAU may also employ IM-DD to transmit the baseband data or IF to the RAU. However, in most cases, IFoF and BBoF schemes rely on RHD for RF signal generation.

This chapter presents the principles behind the various RF signal transport methods and discusses their pros and cons. Where necessary, some examples of RoF systems are given to emphasise some aspects of the techniques involved.

2.2 RF Signal Generation by Intensity Modulation and Direct Detection

The simplest method for optically distributing RF signals is simply to directly modulate the intensity of the light source with the RF signal itself and then to use direct detection at the photodetector to recover the RF signal. This method falls under the IM-DD, as well as the RFoF categories. There are two ways of modulating the light source. One way is to let the RF signal directly modulate the laser diode's current. The second option is to operate the laser in continuous wave (CW) mode and then use an external modulator such as the Mach-Zehnder Modulator (MZM), to modulate the intensity of the light. The two options are shown in Figure 2.1. In both cases, the modulating signal is the actual RF signal to be distributed. The RF signal must be appropriately pre-modulated with data prior to transmission. Thus RFoF requires costly high-frequency electro-optic equipment at the headend.

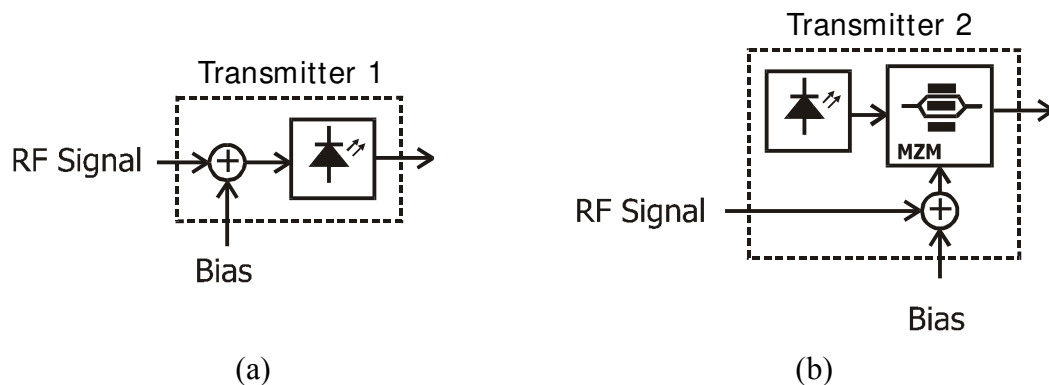


Figure 2.1: Generating RF Signals by Direct Intensity Modulation (a) of the Laser, (b) Using an External Modulator

After transmission through the fibre and direct detection on a photodiode, the photocurrent is a replica of the modulating RF signal applied either directly to the laser or to the external modulator at the headend. The photocurrent undergoes trans-impedance amplification to yield a voltage that is in turn used to excite the antenna. If the RF signal used to modulate the transmitter is itself modulated with data, then the detected RF signal at the receiver will be carrying the same data. The modulation format of the data is preserved.

Most RoF systems, including IM-DD RoF systems, use SMFs for distribution. However, the use of the IM-DD RoF technique to transport RF signals over multimode fibre, by utilising the higher order transmission passbands, has also been demonstrated for WLAN signals below 6 GHz [19], [20], [26].

2.2.1 Advantages of IM-DD

The advantage of this method is that it is simple. Secondly, if low dispersion fibre is used together with a (linearised) external modulator, the system becomes linear. Consequently, the optical link acts only as an amplifier or attenuator and is therefore transparent to the modulation format of the RF signal [25]. That is to say that both Amplitude Modulation (AM) and multi-level modulation formats such as xQAM may be transported. Such a system needs little or no upgrade whenever changes in the modulation format of the RF signal occur. Sub-Carrier Multiplexing (SCM) can also be used in such systems. Furthermore, unlike direct laser bias modulation, external modulators such as the Mach Zehnder Modulator (MZM) can be modulated with mm-wave signals approaching 100 GHz, though this comes at a huge cost regarding power efficiency [9], [11], and linearization requirements.

2.2.2 Disadvantages of IM-DD

One draw back of the RFoF or IM-DD technique is that it is difficult to use for high-frequency mm-wave applications. This is so because to generate higher frequency signals such as mm-waves, the modulating signal must also be at the same high frequency. For direct laser modulation, this is not possible due to limited bandwidth, and laser non-linearity, which lead to inter-modulation product terms that cause distortions. On the other hand, external modulators such as the MZM can support high frequency RF signals. However, they require high drive voltages, which in turn leads to very costly drive amplifiers [9], [11].

A further disadvantage of RFoF is that it is susceptible to chromatic dispersion, which induces frequency- or length-dependent amplitude suppression of the RF power, if Double Side Band modulation of the optical signal is used [5], [27] (see section 4.3). The amplitude suppression effect may be modelled by the modulation transfer of the externally-modulated IM-DD system, which is given in equation (2.1) [27]:

$$\frac{i_{\text{RF}}}{I_0} = -\sqrt{2}m \cdot \cos \omega_m \tau \cdot \cos \left(\frac{\beta_2 L_f \omega_m^2}{2} - \frac{\pi}{4} \right) \quad (2.1)$$

Where ω_m is the modulation frequency, β_2 is the second derivative of the propagation constant β (i.e. $\beta_2 = d^2\beta/d\omega^2$), L_f is the fibre length, and $\tau = t - (z/v_g)$ with v_g being the group velocity. From this equation, the fibre span of a 60 GHz IM-DD system operating at 1550 nm may be limited to just 1.5 km, when the first null occurs. The amplitude suppression effects may be overcome by using dispersion tolerant techniques such as Optical Single Side Band modulation [5], [27], which eliminates the transmission of a second sideband. This may be achieved by either filtering one of the sidebands off [28], [29] or by using dual drive intensity modulators [5]. All of this makes the OSSB IM-DD RoF system more complex.

2.3 RF Signal Generation by Remote Heterodyne Detection

2.3.1 The Principle of Optical Heterodyning

Most RoF techniques rely on the principle of coherent mixing in the photodiode to generate the RF signal. These techniques are generally referred to as Remote Heterodyne Detection (RHD) techniques (see Figure 2.2 and Figure 2.5). While performing O/E conversion, the photodiode also acts as a mixer thereby making it a key component in RHD-based RoF systems.

The principle of coherent mixing may be illustrated as follows [11]. Two optical fields of angular frequencies, ω_1 and ω_2 can be represented as:

$$E_1 = E_{01} \cos(\omega_1 t) \quad (2.2)$$

$$E_2 = E_{02} \cos(\omega_2 t) \quad (2.3)$$

If both fields impinge on a PIN photodetector, the resulting photocurrent on the surface will be proportional to the square of the sum of the optical fields. That is, the normalised photocurrent i_{PD} , will be:

$$i_{\text{PD}} = (E_1 + E_2)^2 \quad (2.4)$$

$$i_{\text{PD}} = E_{01}E_{02} \cos[(\omega_1 - \omega_2)t] + E_{01}E_{02} \cos[(\omega_1 + \omega_2)t] + \text{other terms} \quad (2.5)$$

The term of interest is $E_{01}E_{02} \cos[(\omega_1 - \omega_2)t]$, which shows that by controlling the difference in frequency between the two optical fields, radio signals of any frequency can be generated. The only upper limit to the signal frequencies that can be generated by this method is the bandwidth limitation of the photodiode itself [11]. If we

consider optical power signals instead of optical fields, then the generated photocurrent is given by equation (2.6):

$$i_{\text{PD}}(t) = 2R\sqrt{p_1(t)p_2(t)} \cdot \cos[\{\omega_1(t) - \omega_2(t)\}t + \phi_1(t) - \phi_2(t)] + \text{other terms} \quad (2.6)$$

where R is the responsivity of the photodetector, t is the time, $p_1(t)$ and $p_2(t)$ are the two instantaneous optical power signals with instantaneous frequencies, $\omega_1(t)$ and $\omega_2(t)$, respectively. The instantaneous phases of the signals are given by $\phi_1(t)$ and $\phi_2(t)$ respectively.

Equation (2.6) shows that the stability of the instantaneous frequency of the RHD-generated signal depends on the instantaneous frequency difference between the two optical carriers being mixed. Therefore, in RHD, it is necessary to control the instantaneous frequency difference accurately in order to keep the frequency of the generated signal stable. In other words, absolute shifts in emission frequencies are not important, but the offset between them only. Normally, only one of the two optical carriers is modulated with data. Equation (2.6) shows that the phase noise of the generated signal is influenced by the optical linewidth of the two optical carriers (= the sum of the linewidths of the optical carriers).

Given that the laser emission frequency is highly sensitive to temperature variations, phase noise and other effects, techniques to maintain the required frequency offset and phase noise performance have to be used. There are several methods for controlling the frequency offset between the two lasers. These include:

- Optical Frequency-Locked Loop (OFLL)
- Optical Phase-Locked Loop (OPLL)
- Optical Injection Locking (OIL) and
- Optical Injection Phase-Locked Loop (OIPLL)

These techniques are discussed in the sections that follow.

There are several ways of generating the two optical carriers for coherent heterodyning. One approach is to use an optical phase modulator to generate several optical side bands, and then selecting the required components. Another approach is to use two separate laser sources. The two laser diodes are made to emit light at frequencies (wavelengths) separated by the required microwave frequency. The techniques mentioned above are then used to keep the offset frequency between the two optical carriers stable and phase correlated.

2.3.1.1 *Advantages of Optical Heterodyning*

Using optical heterodyning, very high frequencies can be generated, limited only by the photodetector bandwidth. Furthermore, heterodyning yields high-detected power (higher link gain) and higher carrier-to-noise ration (CNR). This is so because the

optical powers of the two optical fields both contribute to the power of the generated microwave signal.

Remote heterodyning has an inherent advantage concerning chromatic dispersion. If only one of the two optical carriers is modulated with data, system sensitivity to chromatic dispersion can be reduced greatly. This is not possible in direct intensity modulation based methods, where the two optical sidebands end up both being modulated with data. Reducing chromatic dispersion effects is very important in phase noise sensitive modulation formats such as xQAM, where dispersion causes a power penalty [30].

Another important attribute of RHD is that it permits low-frequency data modulation at the headend since high-frequency electro-optical components are not required. Therefore, in contrast to IMDD, the RHD modulator at the headend may be driven either with baseband data or by a low-frequency RF signal. Low-frequency modulators generally have low half-wave voltages, V_{π} and therefore require lower drive levels. Consequently, low-frequency modulators are easier to linearise. Furthermore, linear drive amplifiers are more readily available and less costly for baseband or low-frequency modulation applications. At the RAU, the need for mm-wave frequency filters is eliminated when baseband data is used.

A further advantage of optical heterodyning is that it is capable of producing signals with 100% intensity modulation depth [31]. Other benefits of RHD include photonic signal processing and radio system function capabilities such as phase control, filtering, and frequency conversion [25].

2.3.1.2 *Disadvantages of Optical Heterodyning*

The major drawback of RHD is the strong influence of laser phase noise and optical frequency variations on the purity and stability of the generated RF carriers. Since semiconductor lasers have large spectral widths, extra measures to reduce the linewidth of the generated RF signals, have to be taken. These measures often lead to more complex systems. Techniques used to reduce phase noise sensitivity include Optical Phase Locked Loops (OPLL) and Optical Injection Locking (OIL), which are discussed in Sections 2.3.3, and 2.3.4.

2.3.2 **Optical FM-Filter System**

The Optical FM-Filter technique is a single-laser technique that involves modulating the optical frequency by applying an electrical signal to one of the laser's terminals. This generates a series of optical spectral lines (sidebands) all spaced by the drive frequency as shown in Figure 2.2. Two sidebands, separated by the required mm-wave are then selected. The selected sidebands subsequently impinge on the surface of the photodiode and mix coherently to generate the desired RF signal as explained earlier.

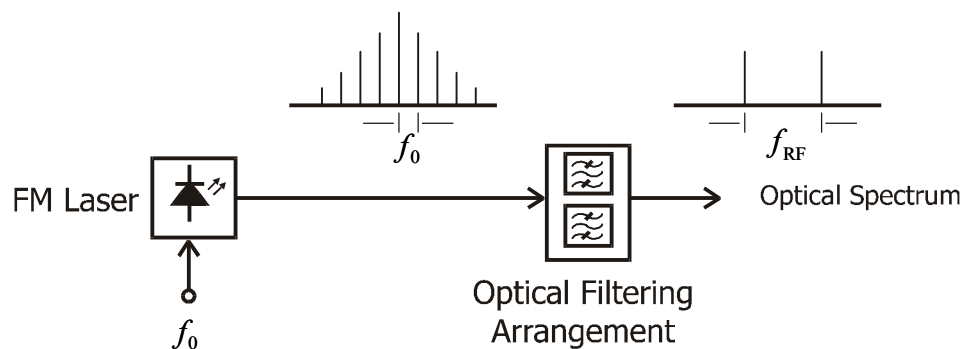


Figure 2.2: Principle of Optical Coherent Mixing based on the FM Laser

Two commonly used methods for selecting the required sidebands are:

- Optical filtering – also referred to as spectrum slicing, and
- Injection-locked lasers

Using an optical filter, the required sidebands are selected while the rest are rejected. This approach was used to remotely deliver mm-wave signals at 54 GHz, 90 GHz and 126 GHz to a RAU fed by a 9 km SMF link [32]. An optical phase modulator was driven by an IF signal at either 13.5 GHz or 22.5 GHz, to generate a series of sidebands, as shown in Figure 2.3. A tuneable Fibre Fabry Perot Interferometer (FFPI) was used to select two sidebands separated by the desired mm-wave frequency. The FFPI had a Free Spectral Range (FSR) of 17.963 GHz, and a Finesse of 100 (see Section 3.3.1). The filtered optical signal was transmitted over the length of the fibre link, amplified, and detected with a waveguide based photomixer. The power of the detected mm-wave signal at 90 GHz was -8 dBm. The measured phase noise of the 90 GHz signal at 100 kHz offset was -95 dBc/Hz, which was 13 dB higher than that of the 22.5 GHz reference signal. Two problems with this scheme were highlighted – namely polarisation sensitivity attributed to the photomixer, and the severely limited tuning range, which was just 360 MHz (6 dB) [32].

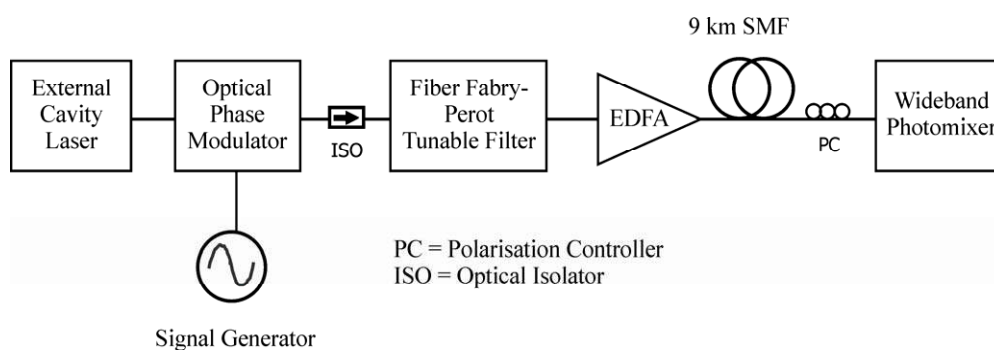


Figure 2.3: Remote Heterodyning by Using a Filter to Select the Mixing Sidebands [32]

The second approach of using injection-locked lasers to selecting the required sidebands to heterodyne is discussed in Section 2.3.4.

2.3.2.1 *Advantages of the FM-Filter Method*

Since the mixing sidebands are generated by the same laser source, they are well correlated. Therefore the FM-Filter technique, is capable of generating high-frequency mm-wave signals with very narrow linewidth. For instance, a linewidth of just 10 Hz at 35 GHz has been reported [11].

2.3.2.2 *Disadvantages of the FM-Filter Method*

The major disadvantage lies in the fact that the sideband selection system must accurately track any shifts in the position of the sidebands. In addition to this, very selective (high-Q) optical filtering is required. These issues tend to increase the complexity of the RoF system. Furthermore, the tunability of the system is very limited (e.g. 360 MHz only at 90 GHz [32]).

2.3.3 **Optical Frequency/Phase Locked-Loops (OFLL/OPLL)**

The basic configuration of OFLL and OPLL techniques is shown in Figure 2.4. It consists of a free running master laser, a PIN photodiode, a microwave amplifier, a frequency or phase detector, a loop filter, a slave laser and a microwave reference oscillator. The combined outputs of the master and slave lasers are split into two parts. Part of the optical signal is used in the OPLL/OFLL at the headend while the other part is transmitted to the RAU. The optical signal at the headend is heterodyned on a photodiode to generate a microwave signal. The generated microwave signal is compared to the reference signal. A phase error signal in the case of OPLL (and a frequency error signal in the case of the OFLL) is fed back to the slave laser. In this way, the slave laser is forced to track the master laser at a frequency offset corresponding to the frequency of the microwave reference oscillator.

As the names suggests, OFLL strives to maintain the required mean frequency offset. It does not suppress small-scale frequency variations caused by phase noise. On the other hand, OPLL is able to track small scale phase perturbations as well. A packaged OPLL system based on semiconductor lasers capable of producing microwave signals up to 14 GHz is reported in [33].

2.3.3.1 *Advantages of OFLL/OPLL*

Because OPLL techniques track small phase variations they are capable of producing high quality RF signals with narrow linewidth. OPLLs also have good temperature tracking capabilities. In addition, OPLLs exhibit a wide locking range. On the other hand, OFLL techniques have the advantage that they can be realised with standard and fairly inexpensive DFB lasers [11].

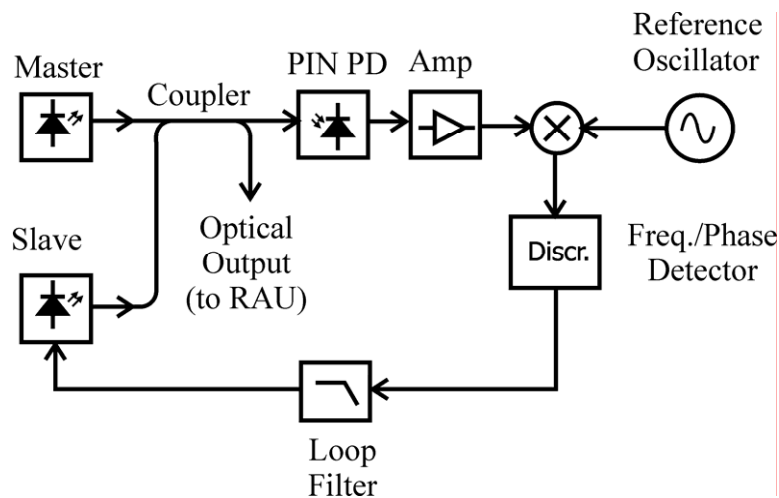


Figure 2.4: Principle of Optical Frequency-/Phase-Locked Loop

2.3.3.2 Disadvantages of OFLL/OPLL

The main disadvantage of OFLL techniques is that they generate microwave signals with broad linewidths. The linewidth of the signal generated by the OFLL system is roughly the sum of the linewidths of the lasers. This is a consequence of the fact that OFLLs maintain only the mean frequency offset. In addition to this, the instantaneous frequency of the generated microwave signal is equal to the instantaneous frequency difference between the two beating optical fields. Therefore, in order to produce narrow linewidth microwave signals using OFLL, lasers with narrow linewidths are necessary. However reducing the source linewidth reduces the maximum power that can be transmitted in the fibre without experiencing severe attenuation due to Stimulated Brillouin Scattering (SBS) [11]. Therefore, there is a practical limit to how narrow the laser linewidth is allowed to be.

The major drawback of OPLLs is that they require far more complex laser structures such as 3-contact DFBS. This requirement is a direct consequence of the fact that to track the frequency perturbations of the master laser, the tuning rate of the slave laser must be sufficiently high. This also implies that sufficient feedback bandwidth must be available. The required feedback bandwidth is determined by the summed laser linewidth, the requirements for loop stability, and phase noise requirements placed on the optical microwave signal by the system in which the OPLL is to be applied. A wide feedback bandwidth is necessary if semiconductor lasers are used, because they have a large amount of phase noise. In order to achieve the wide feedback bandwidth, the loop-propagation delay must be small. In addition to this, the response bandwidths of the microwave components, together with the slave laser FM response, must be wide and uniform in both magnitude and phase [33]. These requirements are not easy to fulfil. They make the design and construction of OPLL components challenging.

2.3.4 Optical Injection Locking (OIL)

Optical Injection Locking (OIL) is a technique that involves modulating the master laser with a low-frequency signal, f_{REF} , which is a sub-harmonic of the cavity round trip time of the slave laser. The spectrum of the master laser therefore comprises several sidebands separated by the sub-harmonic frequency, f_{REF} . The modulating signal of the master is the reference signal.

Part of the output of the master laser is fed into the slave laser. Since f_{REF} is a sub-harmonic of the slave laser's resonant frequency, there will be an n^{th} sideband of the modulated master laser's output that will coincide with the slave laser's frequency as shown in Figure 2.5. This will cause the slave laser to lock onto the master's sideband frequency and resonate there. The offset of the slave laser's emission frequency from the master laser's will therefore vary with both the master central frequency and the reference signal, f_{REF} . If f_{REF} is kept constant, the slave laser's emission frequency will be able to track variations in the master laser's emission frequency, keeping the frequency of the emitted mm-wave signal constant. Using this technique, the generation of a 35 GHz mm-wave signal with a detuning frequency range larger than 300MHz has been demonstrated [34]. In [35], OIL was used to generate a 38 GHz signal, using DSB SC modulation. However, the locking range was only 14 MHz. A RoF system based on the OIL technique and used to generate a 63 GHz mm-wave signal carrying 155 Mbps data is reported in [36].

Another way to generate the sidebands is to use an amplified fibre loop Optical Frequency Comb Generator (OFCG) as shown in Figure 2.6 [37]. The OFCG generates a wide comb of optical frequencies. Two sidebands with the desired frequency difference are selected and subsequently heterodyned to generate the desired microwave signal. The filtering is achieved by using two slave lasers mode-locked on two different frequencies separated by the required microwave. This technique is therefore a combination of OFCG and OIL techniques. With the OFCG system, mm-waves at extremely high frequencies may be generated. For example the technique was used to generate precise signals of high spectral purity from 10 to 110 GHz [37]. A high speed Uni-Travelling-Carrier Photodiode (UTC-PD) was used in the experiments.

2.3.4.1 Advantages of OIL

One advantage of using OIL is that cheaper broad-linewidth lasers can still be used to generate stable narrow electrical linewidth signals. Secondly, OIL exhibits good phase noise suppression because the mixing sidebands are phase correlated. Thirdly, because the slave laser locks on to a sub-harmonic of its resonance frequency, low-frequency reference signals are used. These are simpler and easier to achieve. Fourthly, the mode-locked OFCG technique provides rapid frequency hopping (<1 ns) and an ultra-wide frequency tuning range. These features are very important in DWDM systems [38].

2.3.4.2 Disadvantages of OIL

The major disadvantage of OIL is that it has a small frequency detuning range. Optimum phase noise suppression occurs only at one point of slave laser detuning relative to the free-running frequency [33].

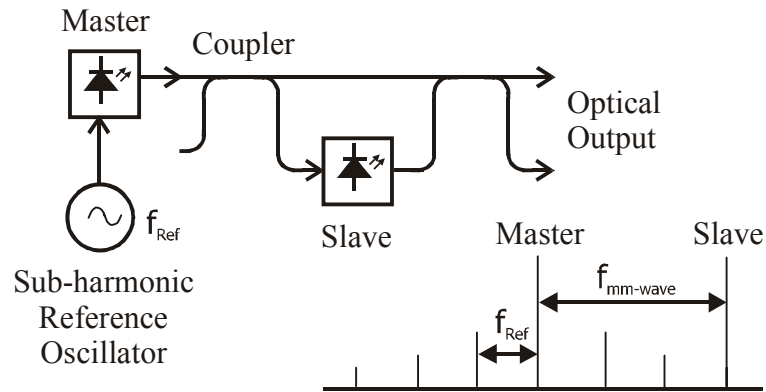


Figure 2.5: Principle of Optical Injection Locking

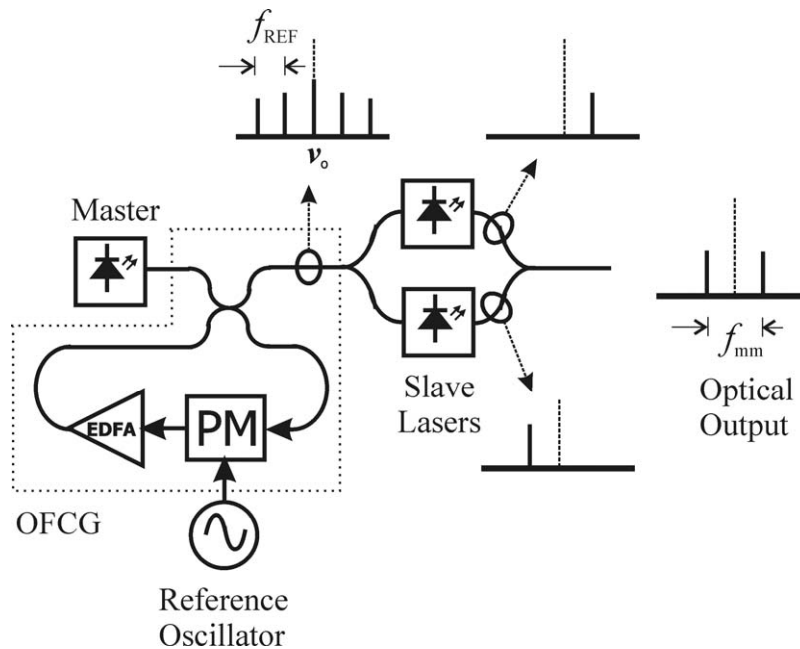


Figure 2.6: Optical Frequency Comb Generator for Carrier Generation through Heterodyning

2.3.5 Optical Injection Phase Locked Loop (OIPLL)

The Optical Injection Phase Locked Loop (OIPLL) technique, illustrated in Figure 2.7, combines both OPLL and OIL principles. The objective is to combine the benefits of both techniques and to complement their weaknesses. In the OIPLL system, the master laser is modulated at a sub-harmonic frequency of the desired mm-wave just like in OIL. A small part of the master's output is then injected into the slave laser through the optical circulator. The slave laser is then tuned to lock to the n^{th} harmonic sideband of the injected master laser's light. The outputs of both the master and the slave lasers are combined and sent to the output. Just as it is in OIL the required mm-wave frequency is the offset between the two optical frequencies. A small part of the combined optical signals is sent to the OPLL. At the photodetector heterodyning takes place. The generated microwave signal at the photodetector is amplified and then compared with the reference signal. This comparison takes place in a balanced mixer, which is sub-harmonically pumped. The output is then passed through the loop filter. The filtered signal is converted to a current signal and then added to the injection current of the slave laser. In this way, two-phase control mechanisms - OIL and OPLL are combined.

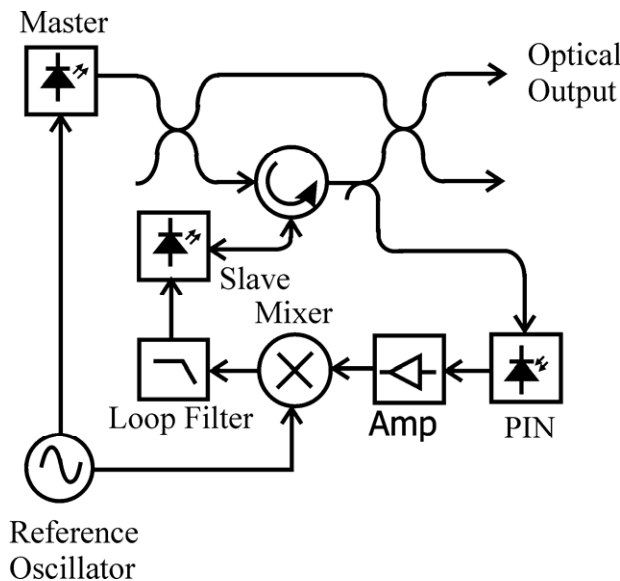


Figure 2.7: The Principle of the Optical Injection Phase Locked Loop (OIPLL)

This technique has been used to generate 36 GHz mm-waves of very narrow linewidth of a few kHz only [39]. OIPLL has been shown to have the ability to increase the locking range of an OIL system from 2 GHz to 30 GHz when OPLL is activated [39]. A Radio-over-Fibre system employing the OIPLL technique to generate a 36 GHz microwave signal modulated with 140 Mbps is reported in [40].

2.3.5.1 Advantages of OIPLL

OIPLL benefits from the low phase noise exhibited by OIL while having an extended locking range provided by the OPLL part of the system. In addition, the short loop

propagation delay required in OPLL becomes less important. Furthermore, OIPLL does not require narrow linewidth lasers but performs well with ordinary broad linewidth lasers, which are cheaper.

2.3.5.2 *Disadvantages of OIPLL*

The disadvantage of OIPLL lies in the complexity of the system itself, being a hybrid of two complex techniques.

2.3.6 **Dual Mode Lasers**

As stated earlier the major drawback of optical heterodyning-based techniques is the sensitivity to phase noise of the two heterodyning signals, and the dependence of the RF beat signal on the polarisation state difference of the two heterodyning carriers. Several techniques used to improve beat signal phase noise have been described above. A different approach to reducing beat signal phase noise is to ensure that the heterodyning optical modes are correlated. When this happens, the beat noise cancels out. Correlation of optical modes can be achieved by having both optical modes in the same cavity. One way to do so is to remove the phase shift in the DFB laser so that no oscillation occurs at the Bragg frequency. This results in a device called the Dual Mode Laser (DML) because it emits two modes - one on either side of the Bragg frequency. The required mode separation is obtained by tuning the grating strength coefficient [31].

A dual mode laser designed to test the viability of this technique showed that direct electrical injection at a sub-harmonic of the beat frequency was still needed in order to generate a pure mm-wave [31]. In the reported experiment, a 57 GHz mm-wave was generated using a 6.3 GHz (9th sub-harmonic) injected reference signal.

The main advantage of the DML approach is that it does not require complex feedback circuitry as does the different optical injection locking methods discussed above. However, the method has limitations regarding tunability, because of its narrow locking range [41].

2.4 ***Techniques Based on Harmonics Generation***

2.4.1 **The FM – IM Conversion Technique**

The FM - IM conversion technique is an interesting method that thrives on the otherwise undesired fibre chromatic dispersion, to work. The conversion from an FM modulated signal to an Intensity Modulated one is performed by the fibre's chromatic dispersion itself. A laser is optically FM modulated by applying a drive signal to one of its terminals. This produces an optical spectrum that consists of spectral lines spaced by the drive frequency. The FM optical signal then propagates over dispersive fibre. Due to chromatic dispersion effects, the relative phasing of the optical sidebands is altered leading to intensity fluctuations of light at harmonics of the drive

frequency. This technique of generating microwaves has been analysed theoretically and demonstrated experimentally in [31] and [42]. For the case of an FM modulated optical signal and standard SMF with chromatic dispersion, the instantaneous optical intensity received after propagating through the fibre is given by [31]:

$$i(t) = I_0 + \sum_{p=1}^{\infty} 2|I_p| \cos(p\omega t + \zeta_p) \quad (2.7)$$

where I_p is the p th harmonic component of intensity variation given by equation (2.7), and I_0 the dc photocurrent. The parameter ω is the modulating angular frequency, and ζ_p is the phase of the p^{th} harmonic. The harmonic intensity, I_p is given by

$$I_p = J_p(2\beta \sin(p\phi)) \quad (2.8)$$

where $J_p(x)$ is the Bessel function of the first kind, β is the FM modulation index (or phase modulation index) and ϕ is an angle characterizing the fibre dispersion given by

$$\phi = -\frac{\omega^2}{4\pi} \frac{D\lambda^2}{c} z \quad (2.9)$$

where λ is the free space wavelength of the laser, c is the speed of light, z is the fibre length, and D is the fibre group dispersion parameter.

If the modulation depth M_p of the p^{th} harmonic is defined as the ratio of the amplitude of the alternating photocurrent at the p^{th} harmonic to the dc photocurrent, then M_p will be given by

$$M_p = |2J_p(2\beta \sin(p\phi))| \quad (2.10)$$

In demonstration experiments, the FM-IM technique was used to generate mm-waves up to 60 GHz (15th harmonic of 4 GHz drive signal). In theory, the maximum achievable modulation depth is 60% for the 10th harmonic. However, only 13% modulation depth was achieved in practice. This was attributed to inherent intensity modulation present in the laser output (i.e. optical signal was not pure FM) [42].

2.4.1.1 Advantages of the FM-IM Method

FM – IM conversion technique can be used to generate mm-waves at very high frequencies efficiently. It is a simple technique to implement, which exploits the undesirable fibre chromatic dispersion to operate.

2.4.1.2 Disadvantages of the FM-IM Method

The obvious drawback of this technique is that the modulation depth varies with the fibre length. However, it can be argued that varying the FM index can compensate for the effect of length dependency of the modulation depth. Unfortunately, lasers with good broadband FM response are not readily available. The FM laser must be capable of wide optical frequency deviation at microwave rates. In general the peak-to-peak frequency deviation must at least be equal to the millimetre-wave frequency desired [31]. To solve the problem of intensity modulation inherent in the directly modulated FM laser, an external phase modulator in combination with a CW laser could be used. Using this approach, theoretical modulation depths are realizable in practice.

2.4.2 Modulation Sideband Techniques

There are two modulation side band techniques dubbed $2f$ and $4f$ methods. Unlike the FM-IM technique, these techniques generate high order harmonics without the necessity for dispersive fibre, by relying on the non-linear transfer characteristic of the Mach Zehnder amplitude modulator (MZM). The output of the MZM in terms of the E-field can be described by [11]:

$$E_{\text{out}}(t) = E_{\text{in}}(t) \cos\left(\frac{\pi}{2} \frac{V_{\text{mod}}(t)}{V_{\pi}}\right) \quad (2.11)$$

where $E_{\text{in}}(t)$ is the optical field applied to the input of the modulator, $V_{\text{mod}}(t)$ is the modulating voltage applied to the modulator, and V_{π} is the modulating voltage required to totally suppress the output. If the modulating voltage $V_{\text{mod}}(t)$ is sinusoidal, it can be shown that the output field may be written in the form [11]:

$$\begin{aligned} E_{\text{out}}(t) = & \frac{1}{2} J_0\left(\alpha \frac{\pi}{2}\right) \cos\left(\frac{\pi}{2}(1+\varepsilon)\right) \cos(\Omega t) \\ & - \frac{1}{2} J_1\left(\alpha \frac{\pi}{2}\right) \sin\left(\frac{\pi}{2}(1+\varepsilon)\right) \cos(\Omega t \pm \omega t) \\ & + \frac{1}{2} J_2\left(\alpha \frac{\pi}{2}\right) \cos\left(\frac{\pi}{2}(1+\varepsilon)\right) \cos(\Omega t \pm 2\omega t) \\ & - \frac{1}{2} J_3\left(\alpha \frac{\pi}{2}\right) \sin\left(\frac{\pi}{2}(1+\varepsilon)\right) \cos(\Omega t \pm 3\omega t) \\ & + \dots \end{aligned} \quad (2.12)$$

where J_i is the i^{th} Bessel function of the first kind, ε is the normalised bias, and α is the drive level. Equation (2.12) shows that by adjusting the bias to appropriate levels $\varepsilon=0$, or $\varepsilon=1$, the 2nd or 4th order harmonics of the drive signal may be generated.

2.4.2.1 *The 2f Method*

When the MZM is biased so that $\varepsilon = 0$ (at V_π), the optical carrier is suppressed together with the even modulation sidebands at $\Omega \pm 2\omega$, $\Omega \pm 4\omega$, etc. What remain are two strong components separated by 2ω and centred on Ω as illustrated in Figure 2.8, plus higher order odd terms. The higher order terms have lower amplitudes and can be reduced to 15dB below the two major components by careful control of the bias point [43]. The modulated optical signal is transported across the fibre length to the RAU. When the two strong components separated by 2ω impinge on the photodiode, they are heterodyned to generate a microwave signal with angular frequency equal to 2ω . In other words, the drive frequency is doubled, or $f_{\text{mm}} = 2f_{\text{mod}}$. The doubling in frequency is what leads to the name *2f method*. Adding data modulation to the generated mm-waves is achieved by filtering one of the optical sideband components and then modulating it with the data before combining and transmitting both sidebands, as shown in Figure 2.8.

A bi-directional system realised by using the *2f* method is reported in [44]. The technique was used to transport the mm-wave LO (at $\frac{1}{2}$ the LO frequency equal to 17.42 GHz) over 20 km SMF to a RAU, together with baseband data at 622 Mbps. The remotely generated 34.8 GHz LO was then extracted electrically by filtering, and part of it used to up-convert the baseband data to the mm-wave. The other part of the LO was used to down-convert the uplink signal from the MU, from 37.5 GHz to an IF at 2.7 GHz. The 2.7 GHz IF was used to modulate an LED and transported back to the headend, using WDM multiplexing.

2.4.2.2 *4f Method*

The *4f* method is the same as the *2f* method discussed above, except that in this case $\varepsilon = 1$ is used. The spectrum then comprises the optical carrier at the centre with sidebands at 2ω on either side. By carefully choosing the drive voltage α such that $J_0(\alpha\pi/2) = 0$, the central component at Ω can also be suppressed. The resulting optical spectrum now consists of two main components separated by four times the drive frequency of the modulator. Heterodyning at the photodiode produces a signal at frequency, $f_{\text{mm}} = 4f_{\text{mod}}$ – hence the term *4f method*.

2.4.2.3 *Advantages of the 2f and 4f methods*

Both the *2f* and *4f* methods rely on optical heterodyning. Therefore, they are capable of generating high-frequency mm-waves. Since the same laser generates both optical fields, the phase noise is highly correlated resulting in very narrow linewidth mm-waves. In fact, the performance of these methods in terms of phase noise is comparable to the OPLL system. The modulation depths achievable with these techniques in practice are larger than in FM-IM techniques. For instance the maximum modulation depth for the 3rd harmonic is about 0.7. A comparison between the theoretical and the practically achievable modulation depths is reported in [31].

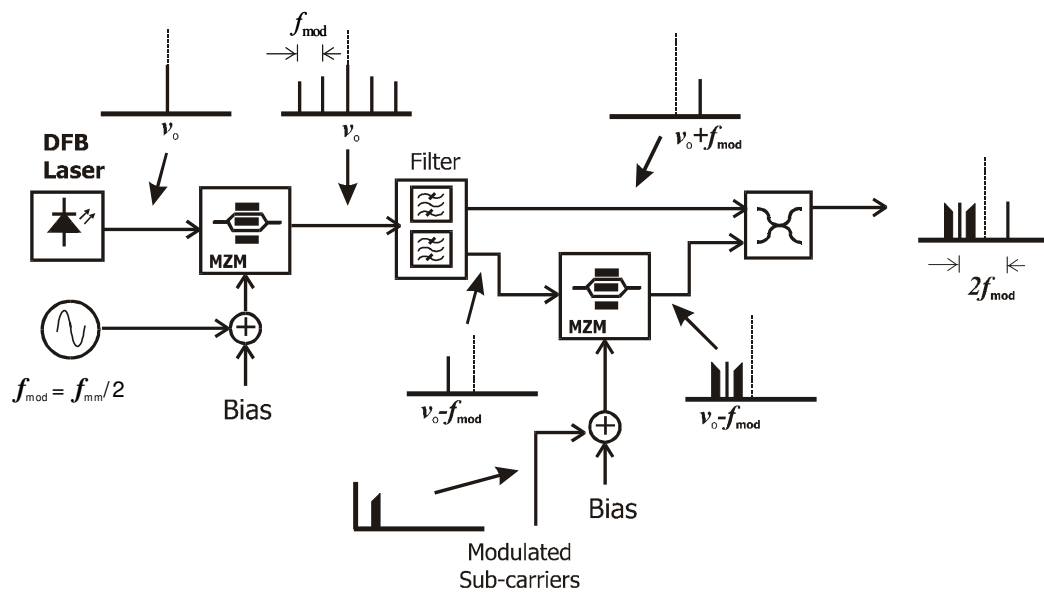


Figure 2.8: The $2f$ Technique for Generating Millimetre-Waves

2.4.2.4 Disadvantage of the $2f$ and $4f$ methods

The main disadvantage of these techniques is the need for filtering one of the sidebands for data modulation. Temperature control is very important in order to keep the filter aligned with the optical side band to be filtered.

2.4.3 Interferometer based Mixing

Another harmonic up-conversion method that uses an interferometer to achieve mixing is illustrated in Figure 2.9 [17], [18], [45]. In this method a LO signal and an RF signal are used to modulate a laser diode, and then mixed in a MZI/photodiode configuration. The FSR of the MZI is chosen so as to maximise the mixing product. The challenge in this approach regards the fact that both the laser wavelength and filter response must be stabilised against environmental disturbances. In addition, the system performance is very sensitive to polarisation perturbations.

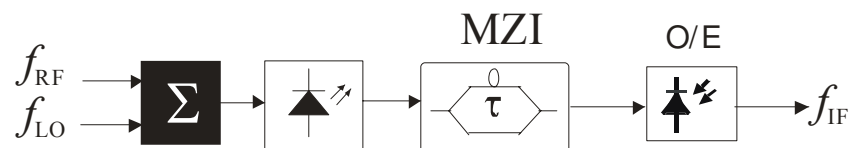


Figure 2.9: Frequency Conversion Through Mixing by a Mach Zehnder Interferometer [18]

2.5 RoF Multiplexing Techniques

2.5.1 Sub-Carrier Multiplexing in RoF Systems

Subcarrier Multiplexing (SCM) is a maturing, simple, and cost effective approach for exploiting optical fibre bandwidth in analogue optical communication systems in general and in RoF systems in particular. In SCM, the RF signal (the subcarrier) is used to modulate an optical carrier at the transmitter's side. This results in an optical spectrum consisting of the original optical carrier f_0 , plus two side-tones located at $f_0 \pm f_{SC}$, where f_{SC} is the subcarrier frequency. If the subcarrier itself is modulated with data (analogue or digital), then sidebands centred on $f_0 \pm f_{SC}$ are produced as illustrated in Figure 2.10.

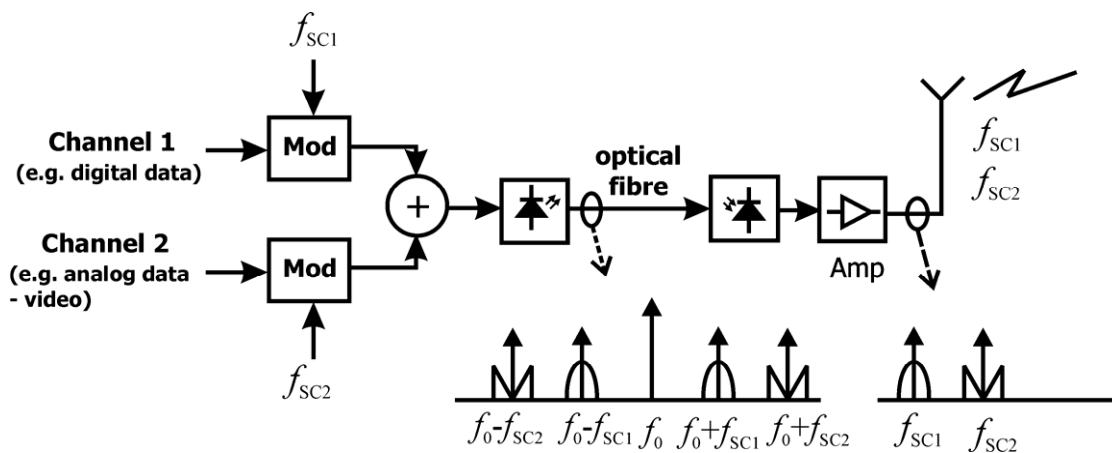


Figure 2.10: Sub-Carrier Multiplexing of Mixed Digital and Analogue Signals

To multiplex multiple channels on to one optical carrier, multiple sub-carriers are first combined and then used to modulate the optical carrier as shown in Figure 2.10. At the receiver's side the sub-carriers are recovered through direct detection and then radiated. Different modulation schemes may be used on separate sub-carriers. One sub-carrier may carry digital data, while another may be modulated with an analogue signal such as video or telephone traffic. In this way, SCM supports the multiplexing of various kinds of mixed mode broadband data. Modulation of the optical carrier may be achieved by either directly modulating the laser, or by using external modulators such as the MZM.

SCM may be used in both IM-DD and RHD RoF techniques. SCM in combination with IM-DD has been used in RoF systems fed by multimode fibre. However, these systems have been used mainly for transmitting WLAN signals at frequencies below 6 GHz [19], [20].

A practical application of SCM in a 60 GHz RHD-based RoF communication system is reported in [46]. Two sub-carriers were used to multiplex two data streams. Since the set-up was based on OIL, each of the sub-carriers (1.27 GHz and 1.79 GHz) was first OQPSK (Offset Quadrature Phase Shift Keying) modulated with 155 Mbps data and then used to modulate one of the two slave lasers. The two resulting phase modulated optical carriers were transmitted through the fibre together with a third reference optical carrier. After heterodyning at the photodiode, the two sub-carriers were up-converted to 62.07 GHz and 62.21 GHz respectively, and radiated. BER measurements on the data recovered at the RAU confirmed the performance of the SCM based RoF system. Another SCM-RoF system employing a combined modulator/detector at the RAU is reported in [47].

2.5.1.1 Advantages of Sub-Carrier Multiplexing

One of the main advantages of SCM is that it supports mixed mode data traffic. Each subcarrier may transport a signal having an independent modulation format. Therefore, it can be used for a wide range of applications such as CATV, wireless LANs and mm-wave applications to name but a few. This is a consequence of the fact that the modulation technique used and data carried on each subcarrier are independent of the subcarriers used. Furthermore, because the subcarriers are at low frequencies, components required for SCM-based systems are readily available. Modulators, mixers and amplifiers employed in cable (or community) TV (CATV) and other satellite systems can still be used in SCM systems leading to low system costs.

2.5.1.2 Disadvantages of Sub-Carrier Multiplexing

The disadvantage of SCM is that being an analogue communication technique, it is more sensitive to noise effects and distortions due to non-linearities. This places stringent linearity requirements on the performance of components especially for applications such video, where a Carrier-to-Noise-Ratio (CNR) > 55 dB may be required. The light source's Relative Intensity Noise (RIN) is the major source of noise and should be kept as low as possible [8], [23].

2.5.2 Wavelength Division Multiplexing in RoF Systems

The use of Wavelength Division Multiplexing (WDM) for the distribution of RoF signals has gained importance recently. WDM enables the efficient exploitation of the fibre network's bandwidth. However, the transmission of RFoF signals is seen as inefficient in terms of spectrum utilisation, since the modulation bandwidth is always a small fraction of the carrier signal frequency. Therefore, methods to improve the spectrum efficiency have been proposed [5]. RoF on WDM systems have been reported. Carriers modulated with mm-waves are dropped from and added to a fibre ring using Optical Add-Drop Multiplexers (OADM). The OADM are placed at base stations and tuned to select the desired optical carriers to drop [47], [48], [49], [50], [114].

2.6 Conclusions

The state-of-the art techniques for distributing RF signals over fibre optic links have been reviewed. The different RoF techniques for transporting RF signals over optical fibres may be classified in terms of the frequency at which the signals are transported or the underlying optical modulation/detection principles involved. In terms of frequency, RoF techniques may be classified as RF-over-fibre, IF-over fibre, or baseband-over-fibre. In terms of modulation/detection, they may be classified as Intensity Modulation – with Direct Detection (IM-DD), Remote Heterodyne Detection (RHD), or harmonic up-conversion. Therefore a RoF technique may belong to one or more categories, or may combine the different aspects of several techniques.

The simplest method for transmitting RF signals over fibre is the RF over Fibre method using IM-DD, because no frequency up/down-conversion at the RAU is required. This leads to simple RAUs. However, high-frequency RoF system applications require complex high-frequency electro-optical interface equipment at the headend, which leads to increased system costs, or poor performance. In addition, RFoF is susceptible to chromatic dispersion-induced carrier suppression when simple DSB modulation is used.

Many RoF techniques rely on the principle of Remote Heterodyne Detection (RHD), where two optical carriers are coherently mixed in the photodiode. Several methods may be used to generate the optical carriers, including, optical FM/PM, sideband generation with the Mach Zehnder intensity Modulator, and dual mode lasers. With RHD, RF signals at very high frequencies (limited only by photodetector bandwidth) may be generated. However, the requirement for additional beat frequency stabilisation and phase noise suppression schemes in RHD-based RoF systems, renders them rather complex. These schemes include optical phase/frequency locked loops, and optical injection locking, or a combination of both.

Presently, RoF technology is applied mainly in SMF-based systems. For MMF-RoF systems, only the IM-DD approach for WLAN applications has been reported. The reported signals transmitted over such links are generally below 6 GHz. Therefore, considering the increasing importance of in-building coverage for wireless systems, the need for high-frequency signal distribution over multimode fibre, which constitutes the main in-building fibre infrastructure becomes equally important.

The following chapter presents an alternative approach for the generation and transportation of high-frequency RF signals – Optical Frequency Multiplication (OFM). OFM is capable of generating very pure RF signals without the use of complex optical injection locking mechanisms for phase noise suppression as is the case in RHD. Furthermore, OFM offers very wide tunability as it does not employ closed loop feedback schemes such as PLL. Unlike RFoF, OFM is inherently chromatic dispersion tolerant. Therefore, OFM can be used in SMF-based RoF systems with very long link lengths. In addition, OFM can operate in MMF links as well. In addition, OFM requires only low-frequency electro-optical interface

equipment at the headend, while offering mm-wave signal distribution to the RAUs. This helps to reduce the overall system costs of the OFM-based RoF system.

CHAPTER

3

Principle of Optical Frequency Multiplication

3.1 Introduction

This chapter describes, and analyses the principle of Optical Frequency Multiplication (OFM) for up-converting frequencies of RF signals. A theoretical model of an OFM system, without any fibre link is developed. Using the OFM model and software simulations, the behaviour of the OFM system is analysed. Factors influencing the performance of the OFM system are identified. The performance of the OFM system when implemented with two kinds of interferometers - the Mach-Zehnder Interferometer (MZI) and the Fabry-Perot Interferometer (FPI), is analysed. The impact of laser phase noise and sweep signal phase noise on the OFM-generated carriers is also considered.

OFM is a method by which a low-frequency RF signal is up-converted to a much higher microwave frequency through optical signal processing. This is achieved by periodic filtering and photo-detection of an optical signal whose wavelength is continuously swept by the low-frequency RF signal, f_{sw} , as shown in Figure 3.1. The desired microwave signal is selected by the bandpass filter [10], [24], [116]. The OFM system is split into two main parts, namely the headend and the Radio Access Unit (RAU) as shown in Figure 3.1. The RAU may be remoted from the headend by an optical fibre link. In that case, the radio access unit is also referred to as a Remote Antenna Unit (also RAU).

Periodic filtering is achieved by using an interferometer whose response is characterized by multi-passband transmission characteristics. The Mach-Zehnder Interferometer (MZI), and Fabry Perot Interferometer (FPI) are some of the common filters that may be used. A wavelength-swept optical signal may be achieved by

driving a tunable laser with the sweep signal [10] (see also Section 5.9) or by using the combination of a CW laser diode followed by an Optical Phase Modulator [51].

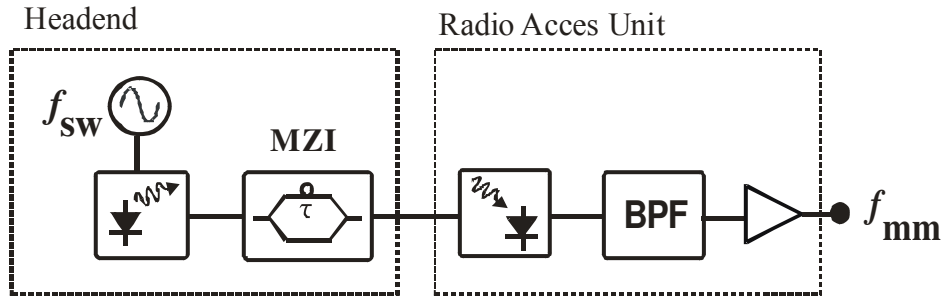


Figure 3.1: Principle of Optical Frequency Multiplication

Tuning of the laser diode wavelength may be achieved through temperature tuning, the use of a movable external cavity diffraction grating, or by changing the carrier density (and so the resonant conditions) inside an active region of the laser diode. Tuning speeds of temperature-tuned lasers, and external cavity tunable lasers are limited to a few milliseconds. Three section lasers such as the Distributed Bragg Reflector (DBR) tunable lasers have faster tuning speeds, but they are still limited to just several tens of nanoseconds [15]. This means that in general the tunable laser option is only available for limited sweeping rates of a few hundred MHz at best. For faster tuning speeds of laser wavelength, the use of commercially-available phase modulators is a more practical option.

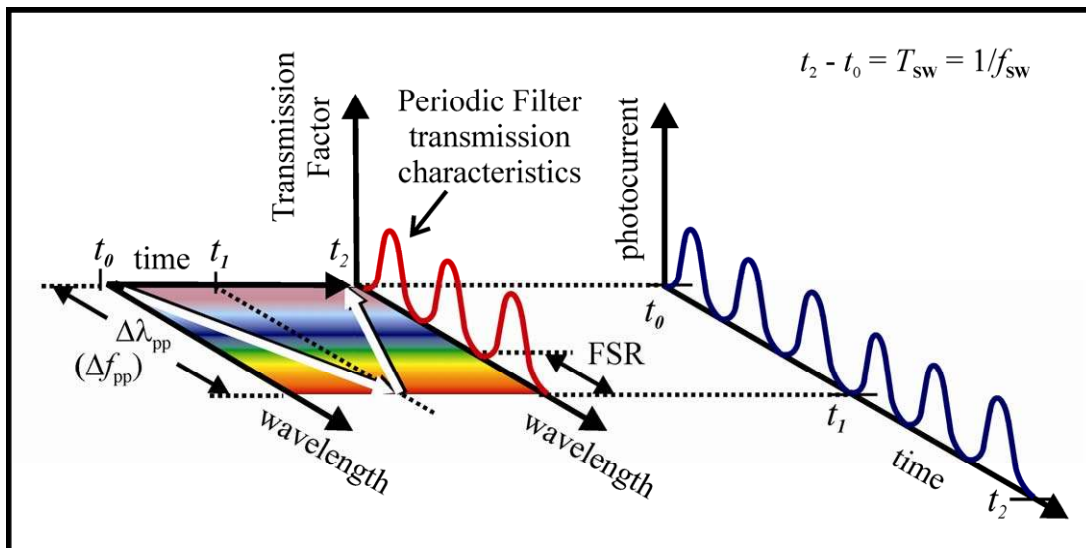


Figure 3.2: Illustration of the method of Optical Frequency Multiplication

Figure 3.2 illustrates what happens when a wavelength-swept optical signal passes through an interferometer, followed by detection by a photo-receiver. For simplicity's sake, a linear wavelength sweep is used here. Beginning at time t_0 , the wavelength is

swept to produce the peak-to-peak optical frequency deviation of $\Delta\lambda_{pp}$ in nanometres (equivalent to Δf_{pp} , in Hz) at t_1 . The wavelength returns to its initial value at t_2 , completing one cycle. The period of this cycle is determined by the low-frequency sweep signal, f_{sw} and equals $T_{sw} = 1/f_{sw} = t_2 - t_0$.

If Δf_{pp} is chosen such that it is N multiple times the Free Spectral Range (FSR) of the periodic filter, then $2 \cdot N$ transmission peaks of the filter are traversed during a single wavelength swing cycle resulting in the production of $2 \cdot N$ intensity bursts of photocurrent at the output of the photodiode as shown in Figure 3.2. Therefore, the generated electrical signal exhibits a smaller period of $T_{mm} = T_{sw}/2N$. This implies an increased signal frequency of $f_{mm} = 2N \cdot f_{sw}$, signifying a base frequency up-conversion factor of $2N$, where $N = \Delta f_{pp}/\text{FSR}$ [51], [52].

3.2 Mach Zehnder Interferometer-based OFM System

3.2.1 Introduction

An ideal Mach Zehnder Interferometer (MZI) consists of two 3 dB couplers forming two branches as shown in Figure 3.3. One of the branches is made longer than the other in order to obtain a differential path delay equal to τ . It can be shown that the impulse response of the MZI, h_{MZI} is given by equation (3.1), which shows that the MZI is of the Finite Impulse Response (FIR) type.

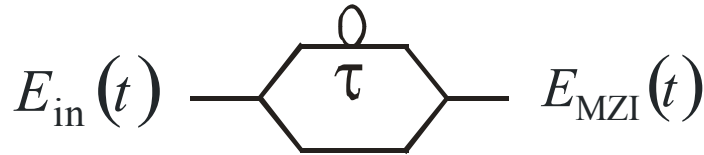


Figure 3.3: Modelling a MZI-based Optical Frequency Multiplication System

$$h_{MZI} = \frac{1}{2}[\delta(t) + \delta(t - \tau)] \quad (3.1)$$

The power transfer function, $|H_{MZI}(f)|^2$ of the MZI is given by equation (3.2) [53].

$$|H_{MZI}(f)|^2 = \cos^2\left(\frac{\pi f}{\text{FSR}}\right) \quad (3.2)$$

where FSR is the period of the frequency response called the Free Spectral Range. Equation (3.2) may be of the sine type if the coupler output on the same side as the input port is used as the filter's output port. The FSR is related to the differential path delay, τ by equation (3.3):

$$\text{FSR} = \frac{1}{\tau} = \frac{c}{n\Delta L} \quad (3.3)$$

where c is the speed of light in a vacuum, n is the refractive index of fibre, and ΔL is the path length difference between the two branches. Therefore, to obtain a FSR of 10 GHz, the path length difference should be 2 cm, assuming the refractive index of the fibre is 1.5. This corresponds to a path length difference delay of $\tau = 100$ ps.

A plot of the power transfer function of the MZI is given in Figure 3.4. The difference between the passband's peak and the valley is the contrast ratio of the filter. In the ideal case the MZI has an infinite contrast ratio, because maximum interference between the two optical beams is assumed. But, in reality the contrast ratio of the MZI is limited, since the level of interference is hampered by the lack of absolute polarisation matching between the two beams.

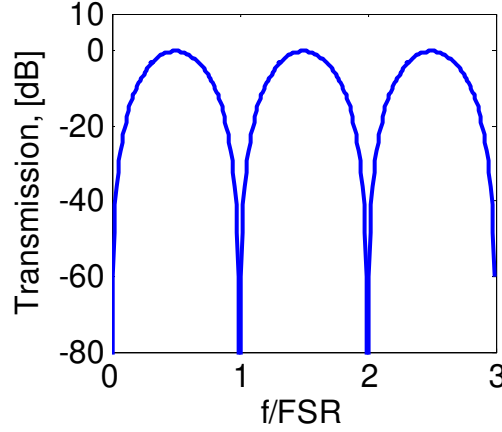


Figure 3.4: Frequency Response of a MZI Filter

3.2.2 OFM Up-Conversion with the MZI

If a Mach Zehnder Interferometer (MZI) is used as the periodic filter in the OFM system, then the detected optical signal may be modelled by considering the input and output fields applied to the MZI as shown in Figure 3.3.

The variable, τ refers to the differential delay time between the two MZI branches. Assuming a sinusoidal sweep frequency, f_{sw} , and a peak optical frequency deviation of Δf_{pk} from the CW optical frequency f_0 , the swept input field $E_{in}(t)$ is given by equation (3.4). In this case, β is the frequency modulation index defined by ratio of the peak optical frequency deviation to the sweep frequency. The electric field at the output of the MZI is obtained by the convolution of the input field with the impulse response of the MZI, $h_{MZI}(t)$. The detected intensity $I_{PD}(t)$, is then given by equation (3.5) [see Appendix A]

$$E_{\text{in}}(t) = E_0 e^{j[\omega_0 t + \beta \sin(\omega_{\text{sw}} t)]} \quad (3.4)$$

$$I_{\text{PD}}(t) = \frac{1}{2} |E_0|^2 \cdot \left\{ \begin{array}{l} 1 + \cos(\omega_0 \tau) \cdot \left\{ J_0(z) + 2 \sum_{k=1}^{\infty} (-1)^k J_{2k}(z) \cdot \cos \left[2k \cdot \left(\omega_{\text{sw}} t - \frac{\omega_{\text{sw}} \tau}{2} \right) \right] \right\} \\ + 2 \sin(\omega_0 \tau) \cdot \sum_{k=1}^{\infty} (-1)^k J_{2k-1}(z) \cdot \cos \left[(2k-1) \cdot \left(\omega_{\text{sw}} t - \frac{\omega_{\text{sw}} \tau}{2} \right) \right] \end{array} \right\} \quad (3.5)$$

where $z = 2\beta \cdot \sin\left(\frac{\omega_{\text{sw}} \tau}{2}\right)$, $\tau = \frac{1}{\text{FSR}}$ is the path length delay, FSR is the filter's Free

Spectral Range, and $J_{2k}(\cdot)$ is the Bessel function of the first kind and of the order $2k$. Equation (3.5) assumes that there is complete coherence between the electric field in both arms of the MZI of the laser. If that is not the case, then the detected intensity is scaled by a corresponding factor less than 1.

It is observed from equation (3.5) that apart from a DC component, even $\{2k \cdot \omega_{\text{sw}}\}$ and odd $\{(2k-1) \cdot \omega_{\text{sw}}\}$ higher order harmonics of the sweep signal are generated. The relative amplitudes of the even and odd harmonic components are given by equations (3.6) and (3.7) respectively.

$$X = |E_0|^2 \cdot \cos(\omega_0 \tau) \cdot J_{2k} \left(2\beta \sin \left(\frac{\omega_{\text{sw}} \tau}{2} \right) \right) \quad (3.6)$$

$$Y = |E_0|^2 \cdot \sin(\omega_0 \tau) \cdot J_{2k-1} \left(2\beta \sin \left(\frac{\omega_{\text{sw}} \tau}{2} \right) \right) \quad (3.7)$$

Equations (3.6) and (3.7) show that the FM index, β , the MZI's path-length delay, τ , and the alignment of the optical wavelength and the MZI ($\cos \omega_0 \tau$, and $\sin \omega_0 \tau$), are all important variables in the OFM system based on the MZI. The effects of these parameters are discussed below.

3.2.3 Impact of FM Index

Equations (3.6), and (3.7) show that the amplitudes of the generated harmonic components are affected by the FM index, β . Figure 3.5 shows what happens when the FM index is varied from 0 to 6 for an OFM system having a MZI with the FSR = 10 GHz and with the sweep frequency, $f_{\text{sw}} = 3$ GHz. The figure shows that each harmonic component has specific values of β , which yield peak power. Furthermore, these values of β are greater for higher order harmonic components. For instance in order to generate the 6th harmonic component (18 GHz in this case), with maximum

power, an FM index β equal to 4.7 would be required, while peak power for the 2nd harmonic requires just $\beta = 2$ [50], [54].

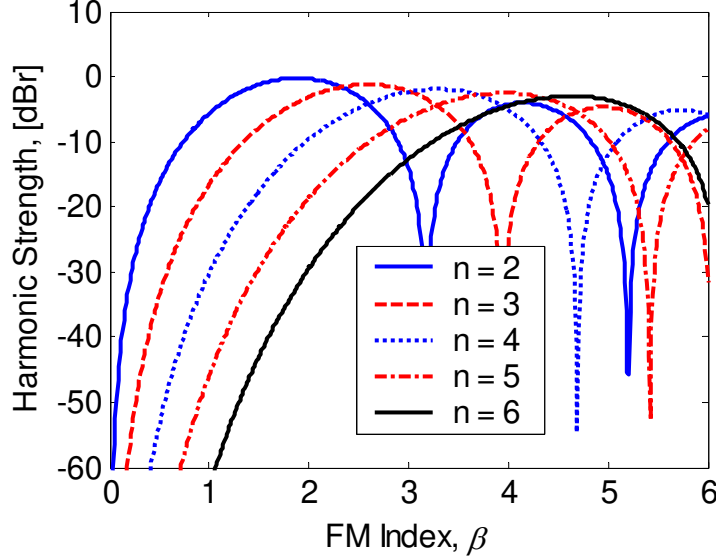


Figure 3.5: Effect of the FM Index, β on the intensity of the generated harmonics in a MZI-based Optical Frequency Multiplication system

A greater FM index implies a larger peak optical frequency deviation. Therefore, it follows that in general, the optical spectral efficiency of the OFM system drops with increased frequency up-conversion factors. However, by careful selection of the MZI's FSR, the required frequency up-conversion factor may be obtained with a minimal peak optical frequency deviation and thus better spectral efficiency. The criterion for having the optimal or lowest FM index, β_{opt} is given by equation (3.8).

$$\left(\frac{\omega_{sw}\tau}{2}\right) = (2n+1) \cdot \frac{\pi}{2}; \quad \text{for integer } n \geq 0 \quad (3.8)$$

$$\Rightarrow \text{FSR} = \frac{2}{2n+1} \cdot f_{sw}; \quad \text{for integer } n \geq 0$$

For instance, in the example given above the effective peak frequency deviation can be reduced from 14.1 GHz to 11.4 GHz by using a MZI with a FSR equal to 6 GHz. The optimal FM index is then $\beta_{\text{opt}} = 3.8$. The occupied optical bandwidth estimated by using Carson's rule [55] is then reduced from 34 GHz to 29 GHz. This represents a 16% reduction in the occupied optical bandwidth.

Furthermore, given that the generated harmonic power does not vary rapidly around the optimal FM index, β_{opt} , a small power performance may be traded off for better optical spectral efficiency. For example a 6 dB RF power trade-off allows a further reduction of the FM index to just 3. In that case, the peak frequency deviation is just

9 GHz, and the occupied bandwidth is equal to 24 GHz according to Carson's rule, representing a total bandwidth saving of nearly 30%. Because the filter's FSR is not easily tunable, the latter may be a more practical solution to increasing the system spectral efficiency in applications where spectral efficiency is important, such as in WDM systems. However, in systems employing Fabry-Perot Interferometer (FPI) filters, the FSR can be tuned quite easily, which makes the choice of the required FM index much more flexible (see Section 3.3).

3.2.4 Optimal Power Generation

In order to obtain the maximum harmonic power for a particular CW laser wavelength and MZI's FSR, it is necessary to maximize the value of the Bessel functions in equations (3.6) and (3.7). This will occur when

$$z = 2\beta \sin\left(\frac{\omega_{\text{sw}}\tau}{2}\right) = J'_{n,1} \quad (3.9)$$

where $J'_{n,1}$ is the first zero of the derivative of the n th Bessel function. In this case $n = 2k$, and $n = (2k - 1)$ for the even and odd harmonics respectively. The values of $J'_{n,1}$ and the corresponding FM Index, β for the first 8 harmonics are given in Table 3.1. The values computed for the optimum FM Index, β_{opt} given in Table 3.1 were verified by independent system simulations in VPI simulation package (see Section 3.3.1).

Table 3.1 Computation of the Necessary Condition for Maximum Harmonic Power

n	First Zero (z_0) of $J'_{n,1}(z)^*$	$J_n(z_0)^*$	β_{opt}
0	0.0	1	0.62
1	1.90	0.58	1.17
2	3.11	0.49	1.92
3	4.26	0.43	2.63
4	5.38	0.40	3.32
5	6.48	0.37	4.00
6	7.56	0.35	4.67
7	8.64	0.34	5.34
8	9.71	0.32	6.00

$$* z = 2\beta \sin\left(\frac{\omega_{\text{sw}}\tau}{2}\right)$$

Thus to obtain the maximum RF power of the n th harmonic at the output of the photodetector it is necessary to adjust the FM index β for the particular sweep

frequency f_{sw} and MZI's FSR. This value of β_{opt} can be reduced by careful selection of the sweep frequency and the MZI's FSR as discussed in section 3.2.3. This will occur when the condition given in equation (3.10) is satisfied.

$$f_{sw} = (2n + 1) \cdot \frac{FSR}{2}; \text{ for integer } n \geq 0 \quad (3.10)$$

3.2.5 Impact of Laser-Filter Misalignment

Equations (3.6) and (3.7) indicate that the strengths of the harmonic components are strongly dependent on the relationship between the CW (peak) laser wavelength and the MZI's path-length delay, τ (i.e. the MZI's FSR). The necessary condition for maximising the even harmonics is

$$f_{0, \text{even}} = m \cdot \frac{FSR}{2}; \text{ for integer } m \geq 1 \quad (3.11)$$

where f_0 is the CW laser optical frequency. For the odd harmonics, the necessary condition is

$$f_{0, \text{odd}} = (2m + 1) \cdot \frac{FSR}{4}; \text{ for integer } m \geq 0 \quad (3.12)$$

By maximising even harmonics, odd harmonics are themselves minimised and vice-versa. Thus, by carefully tuning the CW laser wavelength it is possible to completely eliminate one set of harmonics, while enhancing the strength of the other harmonics. In other words, when condition (3.11) is satisfied, only even harmonics will be generated while condition (3.12) results in the generation of odd harmonics only.

Equations (3.6) and (3.7) indicate a serious practical implication in the operation of the MZI-based OFM system. That is, fluctuations in the CW laser's (peak) wavelength will result in the alteration of the strength of the generated harmonics. A distinction is made between two kinds of wavelength variations, namely short-term, and long-term variations [15]. Short term-variations are caused by temperature and other environmental (ambient) conditions. Long-term variations are those wavelength variations, which are associated with the aging of the laser. Figure 3.6 shows what happens when the laser wavelength varies by about 7 GHz (about 0.04 nm). This value is a typical wavelength drift that a DFB laser would experience when the laser current is increased by about 15mA while operating above the threshold current, at constant temperature. Harmonic power variation between the minimum and the maximum is observed. Laser current fluctuations are easily prevented by laser current control circuitry. But, the laser's wavelength remains quite sensitivity to temperature fluctuations even under temperature control circuitry [56]. Therefore, to stabilise the laser wavelength, special control schemes such as the one employing fibre gratings may be required [56]. Alternatively, laser wavelength perturbations may be compensated for by employing feedback control of the filter. This technique was

successfully used in an experiment to eliminate laser wavelength induced intensity fluctuations (see Section 5.11.2).

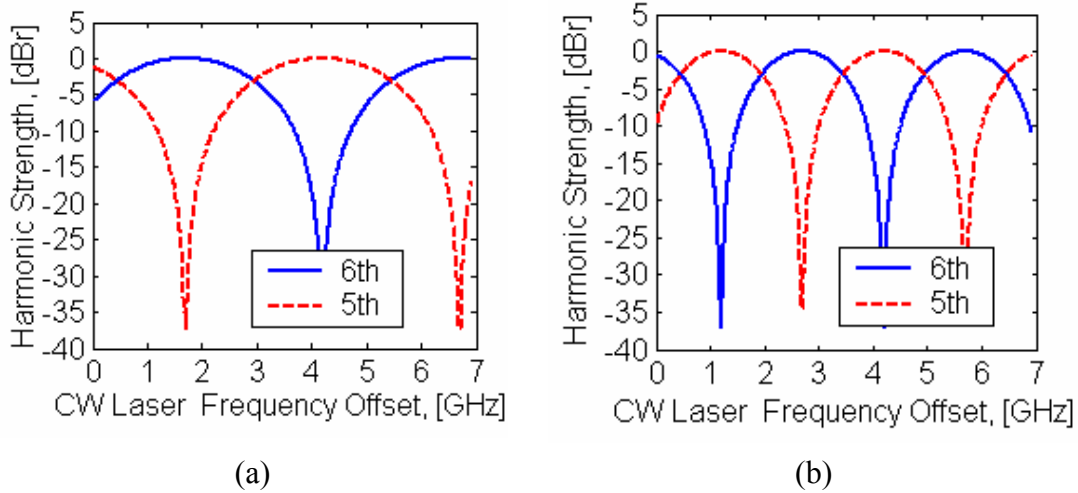


Figure 3.6: Effect of peak laser wavelength drift on the strength of the generated microwave frequency harmonics for FSR = (a) 10 GHz, and (b) 6 GHz

In the first case (Figure 3.6a), the MZI's FSR is 10 GHz, while in the second case (Figure 3.6b) the MZI's FSR is 6 GHz. In both cases the FM index is 3.8, which is the optimum FM index for the system with 6 GHz FSR. The sweep frequency is 3 GHz in both cases.

It is observed that laser peak wavelength drift can have a major impact on the strength of the generated harmonic components. As the peak wavelength drifts downwards (or upwards), the strength of the harmonic components vary between the maximum and the minimum. At the peak of the even harmonics, the odd harmonics are eliminated and vice-versa.

Figure 3.6 also shows that the system's sensitivity to laser wavelength fluctuations depends on the "biasing" of the MZI, which is the position of the laser wavelength with respect to the MZI's passbands. Clearly, the best operating point is at the peak of either the even or the odd harmonic components, which provides the largest tolerance in the laser wavelength drift.

It is also observed from Figure 3.6 that the system tolerance to peak wavelength drift depends on the FSR of the MZI used. In the case of the 10 GHz MZI's FSR, a maximum -3dB wavelength drift tolerance of 2.5 GHz is obtained. This tolerance drops by 1 GHz to 1.5 GHz when the FSR is reduced to 6 GHz, which is the optimum value for obtaining best spectral efficiency (see section 3.2.3 above). In both cases the maximum wavelength drift tolerance is 25 % of the MZI's FSR. It is apparent from the forgoing that there is a trade-off between spectral efficiency and wavelength drift tolerance in the choice of the MZI's FSR. The larger the FSR is, the lower the OFM system sensitivity to the laser wavelength drift is, and the lower the spectral efficiency.

Even though the above discussion focuses on the fluctuations in the peak wavelength of the laser, the same effects would occur if the FSR of the MZI fluctuated instead. This would happen if the short or long paths of the MZI experienced independent length variations due to (localised) environmental temperature changes or other effects. Such effects are generally slowly varying in nature and may be compensated for by the use of a PZT in a feedback loop in the case of fibre-based MZIs [57], and temperature control in the case of chip based MZIs [45]. In the case of the OFM system, we may therefore speak about the requirement of the relative stability between the peak wavelength of the laser and the FSR of the MZI filter. To ease system operation, it is therefore preferred to put the periodic filter at the headend, close to the laser, in order to facilitate stabilisation of the laser CW frequency with respect to the MZI. Such a stabilisation scheme would be more complicated if the MZI were placed at the radio access unit.

3.2.6 Intensity Modulation Depth

The Intensity Modulation Depth (IMD), M_k , of the k th harmonic component is a measure of the efficiency of the frequency up-conversion process. It is defined as the ratio of the amplitude of the alternating photocurrent at the k th harmonic to the dc photocurrent [31].

For the MZI-based OFM system, the IMD is given by equations (3.13), and (3.14) for the even and odd harmonics respectively.

$$M_{2k} = 2 \cdot \frac{\left| \cos(\omega_0 \tau) \cdot J_{2k} \left\{ 2\beta \cdot \sin\left(\frac{\omega_{sw} \tau}{2}\right) \right\} \right|}{\left| 1 + \cos(\omega_0 \tau) \cdot J_0 \left\{ 2\beta \cdot \sin\left(\frac{\omega_{sw} \tau}{2}\right) \right\} \right|} \quad (3.13)$$

$$M_{2k-1} = 2 \cdot \frac{\left| \sin(\omega_0 \tau) \cdot J_{2k-1} \left\{ 2\beta \cdot \sin\left(\frac{\omega_{sw} \tau}{2}\right) \right\} \right|}{\left| 1 + \cos(\omega_0 \tau) \cdot J_0 \left\{ 2\beta \cdot \sin\left(\frac{\omega_{sw} \tau}{2}\right) \right\} \right|} \quad (3.14)$$

It is clear from equations (3.13), and (3.14) that the IMD is determined by the FM index, the MZI's path-length delay, τ , and the laser wavelength alignment, just like the harmonic intensity given in equations (3.6) and (3.7). This dependence is shown in Figure 3.7, where the IMD of the first six harmonic components is plotted against the FM index and Figure 3.8, where the effect of laser wavelength drift is plotted against the IMD. As expected, the IMD oscillates up and down with increasing FM Index.

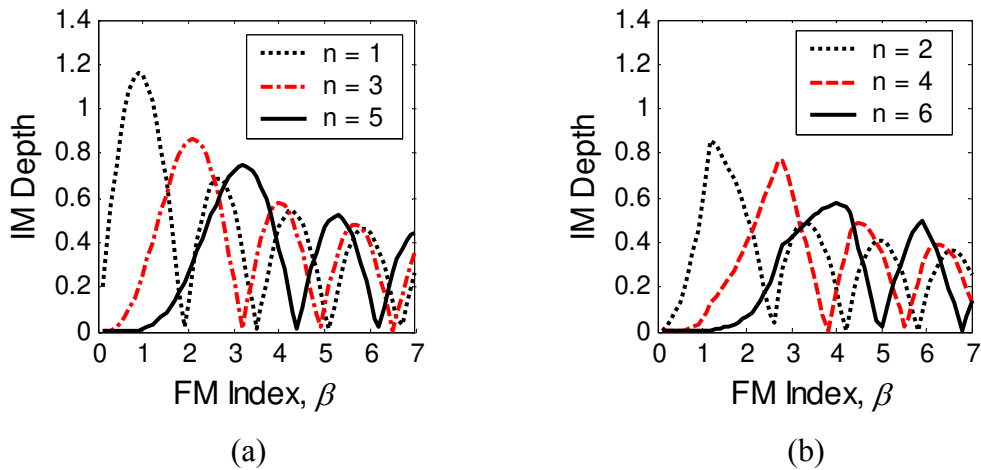


Figure 3.7: Effect of the FM modulation index on the maximum Intensity Modulation Depth of the OFM-generated microwave frequency harmonics for the case when laser wavelength is aligned for maximum (a) odd harmonics, and (b) even harmonics

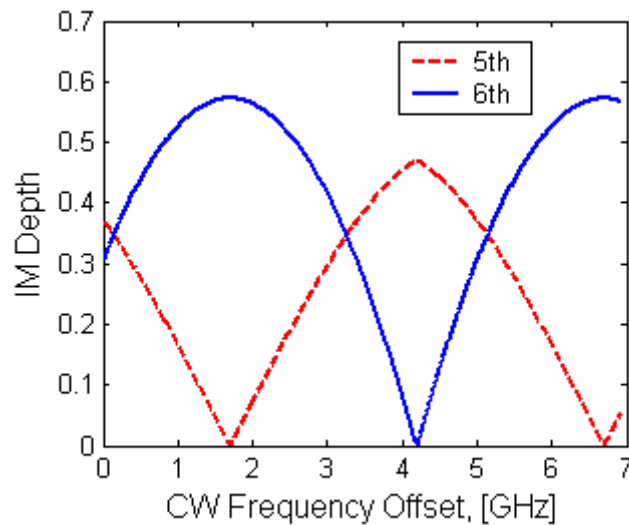


Figure 3.8: Effect of peak laser wavelength drift on the Intensity Modulation Depth of the OFM-generated microwave frequency harmonics (FM index = 4.8; FSR = 10 GHz)

To achieve the maximum IMD, it is necessary to align the laser wavelength to obtain unity for the cosine ($\cos\omega_0\tau$) or the sine ($\sin\omega_0\tau$) components. As mentioned earlier maximisation of even harmonics results in the elimination of odd harmonics and vice versa. Thus, assuming that the laser wavelength is chosen to maximise even or odd harmonics, the corresponding IMD depths are then given by equations (3.15), and (3.16), respectively. The expression for the IMD of the odd harmonics of the OFM system then resembles that of the FM-IM system, which relies on dispersive fibre to convert an optical FM signal to an intensity modulated signal, [31].

$$M_{2k} = 2 \cdot \frac{\left| J_{2k} \left\{ 2\beta \cdot \sin \left(\frac{\omega_{sw} \tau}{2} \right) \right\} \right|}{\left| 1 + J_0 \left\{ 2\beta \cdot \sin \left(\frac{\omega_{sw} \tau}{2} \right) \right\} \right|} \quad (3.15)$$

$$M_{2k-1} = 2 \cdot \left| J_{2k-1} \left\{ 2\beta \cdot \sin \left(\frac{\omega_{sw} \tau}{2} \right) \right\} \right| \quad (3.16)$$

It follows from equation (3.16) that in the case of the odd harmonics, the greatest IMD possible for the $(2k-1)^{\text{th}}$ harmonic component is equal to twice the maximum value (the first maxima) of the $(2k-1)^{\text{th}}$ Bessel function. If the sweep frequency and the MZI's FSR are chosen such that the FM index, β is minimised (i.e. according to equation (3.10)), then the maximum IMD will occur when

$$2\beta = J'_{2k-1, 1} \quad (3.17)$$

where $J'_{2k-1, 1}$ is the first zero of the derivative of the $(2k-1)^{\text{th}}$ Bessel function. The maximum values of the IMD for the first 6 harmonic components are given in **Table 3.2**. The maximum IMD of the 6th harmonic component is 0.58 obtained at the FM Index of about 4.0.

The impact of laser wavelength drift on the IMD shown in Figure 3.8 is similar to its impact on the harmonic intensity discussed in Section 3.2.5. It shows once again the importance of the relative stability between the laser wavelength and the MZI's FSR (or long arm's delay).

Table 3.2 Maximum Intensity Modulation Depth of the MZI-based OFM System

n	Maximum IMD, M_n	FM Index, β
1	1.16	0.9
2	0.86	1.2
3	0.87	2.1
4	0.77	2.7
5	0.75	3.2
6	0.58	4.0

3.3 Fabry Perot Interferometer-based OFM System

As stated earlier, OFM involves the periodic filtering of a wavelength swept optical signal, prior to photodetection. Section 3.2 discusses the OFM system based on a MZI filter. This section focuses on the OFM system using a Fabry Perot Interferometer (FPI) as the periodic filter.

3.3.1 Introduction

A Fabry Perot Interferometer (FPI) is an optical filter having an Infinite Impulse Response (IIR). It is generally realised by using two parallel reflecting mirrors to form an optical cavity [58] as shown in Figure 3.9.

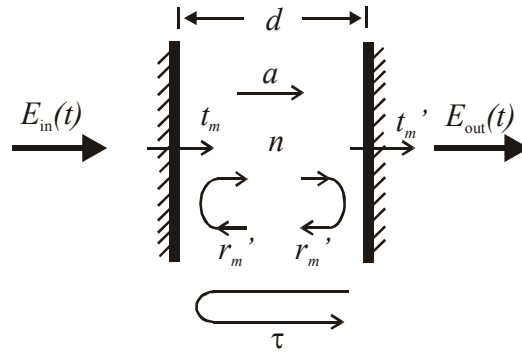


Figure 3.9: Schematic of an ideal single cavity Fabry Perot Interferometer

The electric field $E_{in}(t)$, of a light beam entering the optical cavity experiences a transmission loss, t_m through the first mirror. The amplitude of the beam is then attenuated by a factor a as it propagates through the cavity medium towards the second mirror. The refractive index of the cavity medium is n . At the second mirror, part of the beam is reflected by factor r'_m and the rest is transmitted with an amplitude attenuation, t'_m . Because of multiple reflections within the optical cavity, the optical beam exiting the second mirror is a summation of several components of the original optical beam (delayed by integer multiples of the cavity roundtrip delay, τ) that entered the cavity through the first mirror. As a result, only an input with wavelength λ satisfying the resonance relation $d = k\lambda/2$ where k is a positive integer, experiences maximum transmission through the FPI. All other wavelengths interfere destructively with each other resulting in varying degrees of their extinction.

From the foregoing, the electric field of the optical beam leaving the optical cavity through the second mirror may be represented by

$$E_{out}(t) = t_m t'_m a \cdot E_{in}(t) + t_m t'_m a^3 (r'_m)^2 \cdot E_{in}(t - \tau) + t_m t'_m a^5 (r'_m)^4 \cdot E_{in}(t - 2\tau) + \dots \quad (3.18)$$

which reduces to

$$E_{\text{out}}(t) = E_{\text{in}}(t) * t_m t'_m \cdot \sum_{k=0}^{\infty} a^{2k+1} \cdot [(r'_m)^2]^k \cdot \delta(t - k\tau) \quad (3.19)$$

Thus, the impulse response of the FPI is

$$h_{\text{FPI}}(t) = T \cdot \sum_{k=0}^{\infty} a^{2k+1} \cdot R^k \cdot \delta(t - k\tau) \quad (3.20)$$

where $T = t_m t'_m$ is the power transmissivity, and $R = (r'_m)^2$ the power reflectivity of the mirrors. The cavity round trip is given by

$$\tau = \frac{2dn}{c} = \frac{1}{\text{FSR}} \quad (3.21)$$

where FSR is the period of the FPI frequency response called the Free Spectral Range. Given the impulse response in equation (3.20), the field transfer function $H_{\text{FPI}}(f)$ may be obtained, leading to the intensity transfer function $|H_{\text{FPI}}(f)|^2$ given by [53], [59]:

$$|H_{\text{FPI}}(f)|^2 = \frac{T_0}{1 + \left[\frac{2}{\pi} F_R \cdot \sin\left(\frac{\pi f}{\text{FSR}}\right) \right]^2} \quad (3.22)$$

where T_0 is the maximum transmission factor given by

$$T_0 = \frac{A \cdot (1 - R)^2}{(1 - A \cdot R)^2} \quad (3.23)$$

and F_R is the reflectivity finesse given by

$$F_R = \pi \frac{\sqrt{A \cdot R}}{1 - A \cdot R} \quad (3.24)$$

The factor A is the attenuation factor of the light intensity. It is related to a , the attenuation of the electric field by $A = |a|^2$. Equation (3.22) is commonly referred to as the *Airy function*.

Finesse is a common figure of merit of the FPI. It is related to the contrast ratio of the filter. According to equation (3.24), Finesse is a function of both the plate reflectivity and the loss of the medium between the plates. Figure 3.10 shows the intensity frequency responses of a FPI for 3 different values of plate Reflectivity, namely $R =$

0.1, 0.6, and 0.9, assuming a lossless medium between the plates (i.e. $A = 1$). These reflectivity values correspond to reflectivity finesse of $F_R = 1.1$, 6.0, and 29.8.

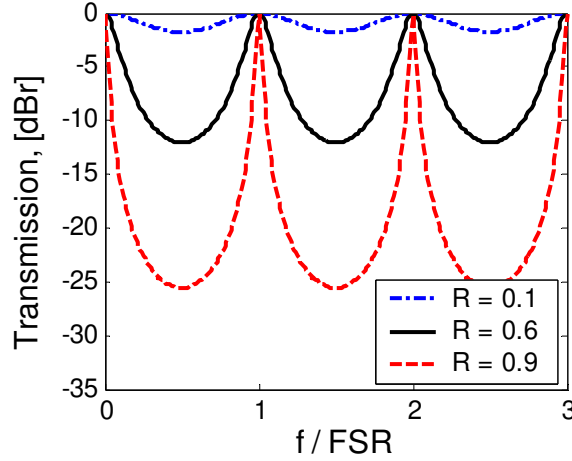


Figure 3.10: Effect of plate Reflectivity on the frequency response (intensity) of Fabry-Perot Interferometer plotted against optical frequency normalised to the FSR

In most filtering applications an important figure of merit is the contrast ratio, or contrast factor, which is the ratio between the maximum and the minimum transmission of the filter. The contrast ratio is important because it determines the cross-talk attenuation of the filter [53], [59]. For the FPI, the contrast ratio, C is therefore given by

$$C = \left[\frac{(1 + A \cdot R)}{(1 - A \cdot R)} \right]^2 \quad (3.25)$$

In Figure 3.10, the contrast ratio is the difference between the maximum transmission peak and the minimum valley. Thus a contrast ratio of 25.6 dB corresponds to the plate reflectivity of $R = 0.9$. The contrast ratio will affect the modulation depth in the OFM system [51].

The -3dB bandwidth, or Full Width at Half Maximum (FWHM) bandwidth of the FPI's passband is given by

$$BW_{3dB} = \frac{FSR}{F} \quad (3.26)$$

where F is the effective finesse of the FPI.

From the foregoing, it is clear that the plate reflectivity is the most important parameter of the FPI since it determines the filter's finesse, contrast ratio, and bandwidth. However, this is only true for the case when the optical beam is fully collimated and perpendicular to the first reflective plate, which is also assumed to be

perfectly flat. In practical applications, this is hardly the case. Thus, the effective finesse of the FPI depends also on the flatness of the plates. The resulting finesse is referred to as the instrument finesse, F_I given by [59], [60]:

$$\frac{1}{F_I^2} = \frac{1}{F_R^2} + \frac{1}{F_F^2} \quad (3.27)$$

where F_F is the flatness finesse given by

$$F_F = \frac{M}{2} \quad (3.28)$$

where M is the fractional wavelength deviation from true flatness or parallelism across the mirror aperture. Mirror flatness is commonly specified as λ/M at a standard wavelength of 546 nanometres.

In spectroscopy and related applications, the pinhole finesse, F_P which determines the degree of collimation of the light passing through the FPI, must also be included. The total instrument finesse then becomes

$$\frac{1}{F_I^2} = \frac{1}{F_R^2} + \frac{1}{F_F^2} + \frac{1}{F_P^2} \quad (3.29)$$

where F_P is the associated pinhole finesse given by

$$F_P = \frac{4\lambda f^2}{D^2 d} \quad (3.30)$$

where D is the pinhole diameter and f is the focal length of the lens between the FPI and the pinhole.

Wavelength tuning of the FPI may be achieved by adjusting the reflective plate spacing or by rotating the interferometer with respect to the input beam, [59], [61]. Furthermore, in applications where sharper filter responses are required, the simple single cavity plane filter discussed above may be cascaded in series, or used in multi-pass configurations [53], [59]. In addition FPI's with spherical reflective plates or mirrors rather than flat plate surfaces may be used [58]. Furthermore, (and more recently), FPI have also been made from Fibre Brag Gratings (FBG). However, these devices tend to be more complex and operate only for a limited range of wavelengths (see Section 5.10.2).

3.3.2 Up-conversion with FPI

The Fabry-Perot Interferometer (FPI) discussed in Section 3.3.1 is normally used as a general purpose filter in Wavelength Division Multiplexing (WDM) systems, and

Spectrometry. This section describes the use of the FPI as a periodic filter in the OFM system.

Since the equations describing the OFM process in a FPI-based system are in a form that is difficult to analyse numerically, the *VPI Transmission Maker (Ver 6.0)*, an optical simulation platform from *VPIsystems Inc.* was used to simulate and analyse the FPI-based system and to compare it with the MZI-based system. In order to have reliable simulation results, the simulation system was validated by first simulating the MZI-based OFM system and then comparing the simulation results with the analytical results. As Figure 3.11 shows, there was complete agreement of results, in this case regarding the effect of the FM index on the intensity of the generated harmonic components. Several other simulations were carried out and comparisons made, but Figure 3.11 is only given as a representative summary of the results obtained.

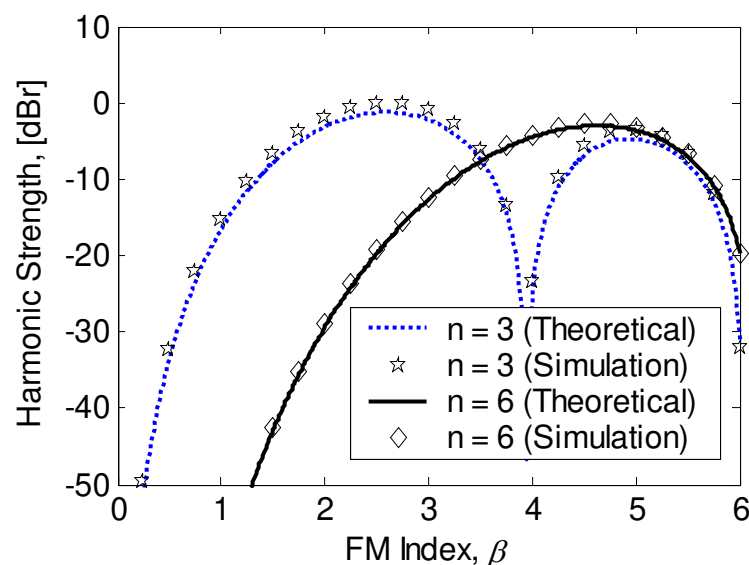


Figure 3.11: Comparison of theoretical and simulation models of the MZI-based OFM system with $\text{FSR} = 10 \text{ GHz}$, and $f_{\text{sw}} = 3 \text{ GHz}$

3.3.3 Impact of FM Index on the FPI-based System

The impact of the FM Index, β on the FPI-based OFM system was investigated by varying the FM Index between 0 and 12 in the VPI simulation. The results of the simulation are shown in Figure 3.12. In this simulation, the laser wavelength was set for either maximum even harmonics or maximum odd harmonics (see Section 3.3.5). The FPI's FSR was 10 GHz and the Reflectivity, R , was equal to 0.6.

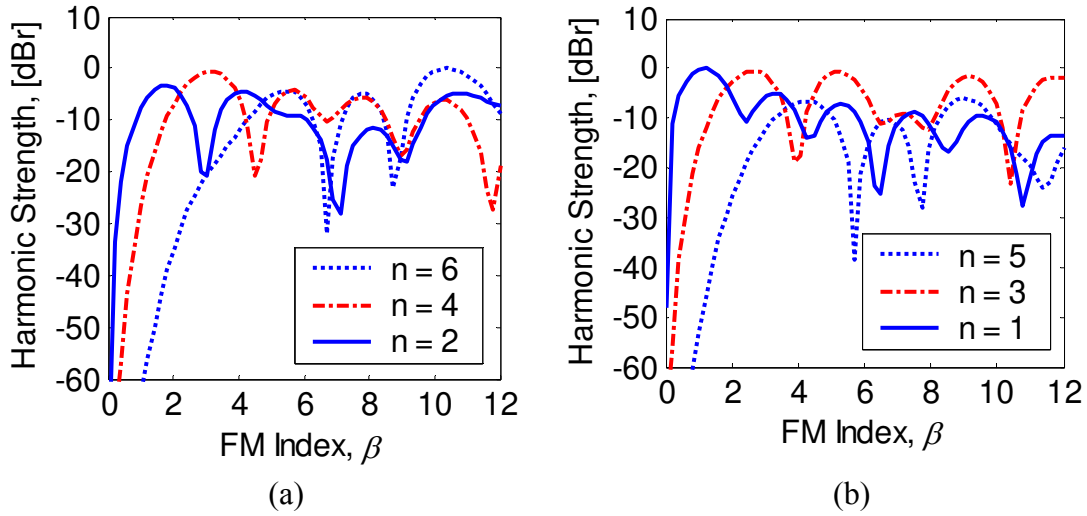


Figure 3.12: Effect of the FM Index on the intensity of the generated harmonics in a FPI-based OFM system with $R = 0.6$; (a) Even harmonics; (b) Odd harmonics

It was observed that the intensity of the harmonics generated by a FPI-based OFM system is affected by the FM index, just as is the case in the MZI-based system. However, the system behaviour is not as smooth and regular as it is in the MZI-based system (see Figure 3.5). In the case of the MZI-based system the peaks of the harmonic strengths decrease monotonically. This is not the case in the FPI-based system, where the peaks of harmonics first decrease and then increase again for higher FM Indices. For instance the first peak of the 6th harmonic component occurs around $\beta = 5$ and is about -5 dB_r strong. The next peak occurs around $\beta = 8$ and is slightly lower in amplitude. However, at $\beta = 10$, another peak, which is much stronger (0 dB_r) than even the first peak is observed.

The FPI-based system also exhibits valleys of minimum (or zero) harmonic strength for certain values of β as shown in Figure 3.12. That means that for certain values of β , the strength of the particular harmonic is severely reduced. For the 6th harmonic, these values are $\beta = 6.7, 8.7$, etc. Therefore these values of the FM Index would have to be avoided in a practical FPI-based system with FSR = 10 GHz, if the 6th harmonic component is the desired microwave frequency to be generated.

The effect of the Reflectivity, R on the sensitivity of the system to the FM Index was also investigated. The results are summarised in Figure 3.13, where 3 curves showing the impact of the FM Index for $R = 0.4$, $R = 0.6$, and $R = 0.9$ (corresponding to finesse values, $F_R = 3.3, 6.1$, and 29.8 respectively) for the 6th and 5th harmonic components are plotted against the FM index, β . For comparison's reasons, the curves of the MZI-based system are also shown in Figure 3.13 for the corresponding harmonic components. In order to make a fair comparison, the MZI-based system was completely identical to the FPI-based system except of course for the use of the MZI filter in place of the FPI filter. The laser wavelength alignment (i.e. FSR/2 for the even harmonics and FSR/4 for the odd harmonics) and the filter's FSRs (10 GHz) were also identical. Therefore, Figure 3.13 also gives a fair indication of the relative conversion efficiency of the two systems.

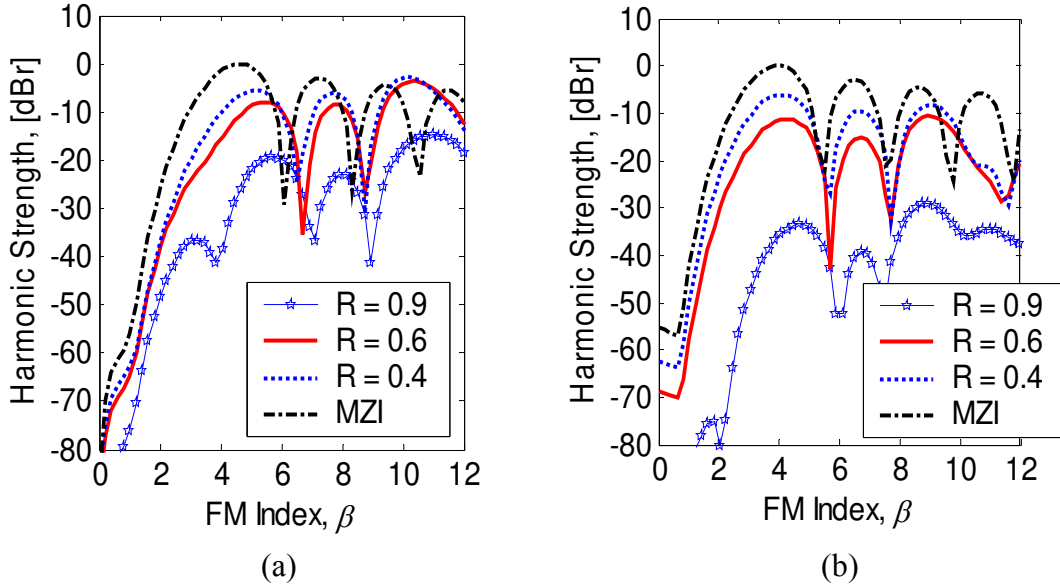


Figure 3.13: Impact of Reflectivity, R , on the effect of the FM Index on the intensity of the generated harmonics in a FPI-based OFM system; (a) $n = 6$ (b) $n = 5$.

We can make the following conclusions about the FPI-based system:

- (i) The Reflectivity, R does affect the peak intensity of the harmonics. This is obvious from the fact that filter finesse or, equivalently, the contrast ratio affects harmonic strength (see Section 3.3.4).
- (ii) The FM index required to obtain peak harmonic strength increases slightly with increasing R . For instance in the case of the 6th harmonic component, $\beta = 5.1$ is needed to obtain peak power for $R = 0.4$ (the first peak). This value of the FM index, β increases to 5.7 when $R = 0.9$ is used. Looking at Figure 3.13, it is as though higher values of Reflectivity push the Harmonic Strength-FM Index curves towards higher β values. In other words, it can be said that in general the conversion efficiency and spectral efficiency of the FPI-based system depreciate with increasing plate Reflectivity, R .
- (iii) Given that the MZI-based system needed $\beta = 4.7$ to obtain the first peak (see Section 3.2.3), while the FPI-based system required $\beta = 5.1$ or more to obtain the first peak, coupled with the fact that the peak of the MZI-based system is more than 5 dB higher than the highest peak of the three FPI-based peaks, it looks as though the MZI-based system is more efficient than the FPI-based system, at least in theory. However, it must be stated that the MZI used in the simulations is assumed to be ideal, with a large contrast ratio of more than 30 dB. Such a large contrast ratio for a MZI is not easy to obtain in practice, because it is not possible to achieve perfect polarisation and phase alignment of the interfering optical beams in practice [57]. This means that the conversion efficiencies of the MZI-based system obtained in practice will be lower than the theoretical ones. On the other hand, the Reflectivity of FPIs can be controlled quite accurately,

making it possible to reproduce the theoretical performance indicated in Figure 3.13. Therefore, the apparent conversion efficiency advantage of the MZI-based system is not expected to exist in practice. That is to say that in practice the power performances of the FPI- and the MZI-based systems should be comparable.

3.3.4 Impact of FPI's Finesse on the OFM System

Finesse, F_R is a common figure of merit of Fabry Perot Interferometers (FPIs). It is determined by the Reflectivity, R of the plates defining the optical cavity of the filter, and the loss of the cavity medium (see Section 3.3.1). The relationship between finesse and R is given by equation (3.24).

To investigate the impact of plate Reflectivity, R , and Finesse F_R , on the harmonics generated by the OFM system, all system parameters were fixed and the Reflectivity, R of the FPI varied between 0 and 9. The laser wavelength was aligned at FSR/8 so as to obtain both even and odd harmonics with comparative strength (see Section 3.2.5). The filter's FSR was 10 GHz, the sweep frequency, f_{sw} was 3 GHz, and the FM index was set to $\beta=5$.

The results of the simulation are summarised in Figure 3.14. As expected, various values of R produce varying strengths of harmonics. In general Reflectivity values of around $R = 0.3$ to 0.7 are desirable to produce strong harmonic components. These values of R correspond to Finesse values of 2.5 to 9, respectively. Figure 3.14 (b) shows the relationship between the strength of the harmonic components and the Reflectivity Finesse. The figure shows that in general, a high finesse is not required for maximum harmonic power generation. That is to say that OFM does not require costly high Q filters. This is an important advantage, which translates into major system cost benefits [51], [62].

In the case of a linearly (e.g. triangularly) swept OFM system, the detected photocurrent is given by equation (3.31) [10], [51], [52], [63].

$$i(t) = i_0 \cdot \frac{1-R}{1+R} \cdot \left\{ 1 + 2 \sum_{n=1}^{\infty} R^n \cos(4\pi n N f_{sw} \cdot t) \right\} \quad (3.31)$$

where N represents the number of peaks traversed by the peak frequency deviation, Δf_{pk} . In such a system, the relationship between harmonic strength and Finesse is given in Figure 3.15. As can be seen moderately higher finesse values may be necessary for high harmonic order operation.

In the case of the triangularly swept system, the maximum power of the n^{th} harmonic component occurs for a specific value of the Reflectivity, R_n given by equation (3.32).

$$R_n = \frac{(\sqrt{1+n^2})-1}{n} \quad (3.32)$$

And the Intensity Modulation Depth, M_n for the n^{th} harmonic component increases with increasing Reflectivity, R as described by equation (3.33) [51]. The behaviour of the linearly swept system is analysed in more detail in [10], [51].

$$M_n = 2R^n \quad (3.33)$$

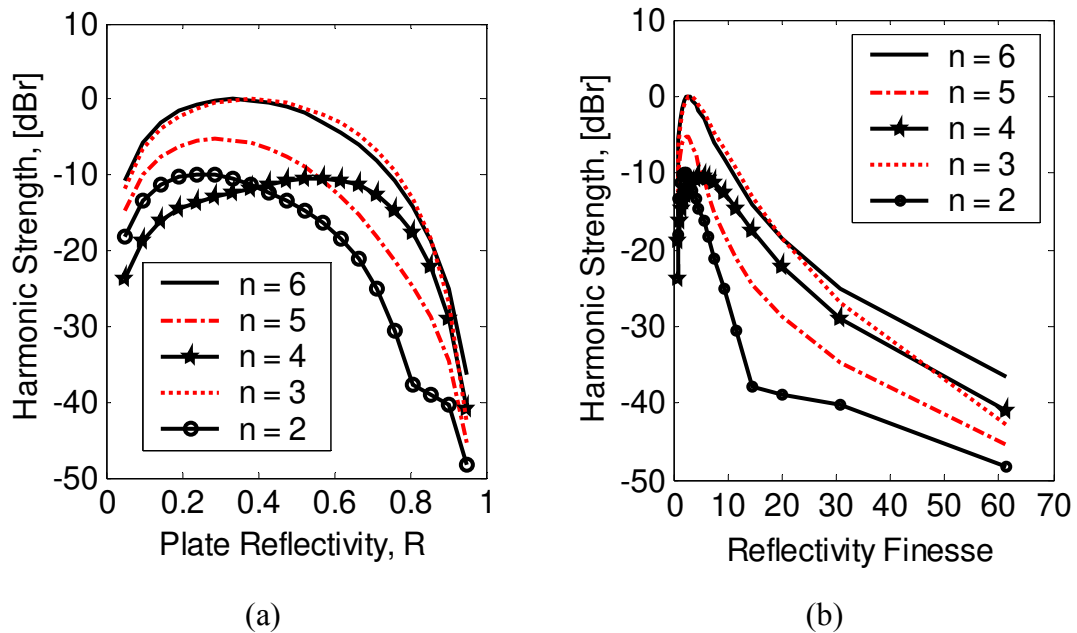


Figure 3.14: Effect of plate Reflectivity, R (a), and Finesse, F_R (b), on the strength of the generated harmonic components in a FPI-based OFM system with FM Index = 5 and laser wavelength FPI biasing = FSR/8.

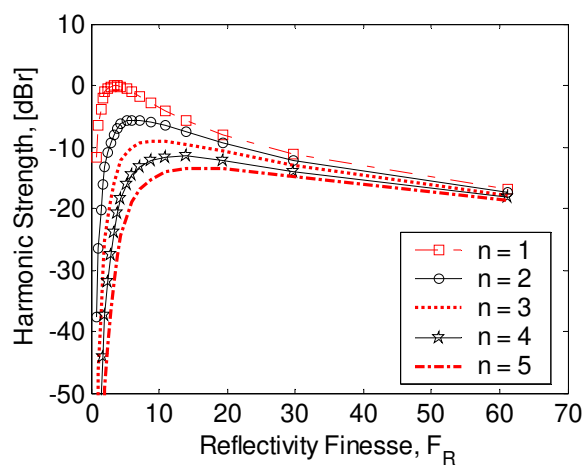


Figure 3.15: Effect of Reflectivity Finesse, F_R , on the strength of the generated harmonic components in a linearly swept FPI-based OFM system.

A combination of the impacts of laser wavelength-filter alignment and Reflectivity, R , is shown in Figure 3.16. Here we see that by enhancing even harmonics, we suppress odd harmonic components and vice-versa. For instance, by “biasing” the FPI at $FSR/2$, odd harmonic components are suppressed by 40 dB. The impact of laser wavelength-filter alignment is discussed in more details in Section 3.3.5.

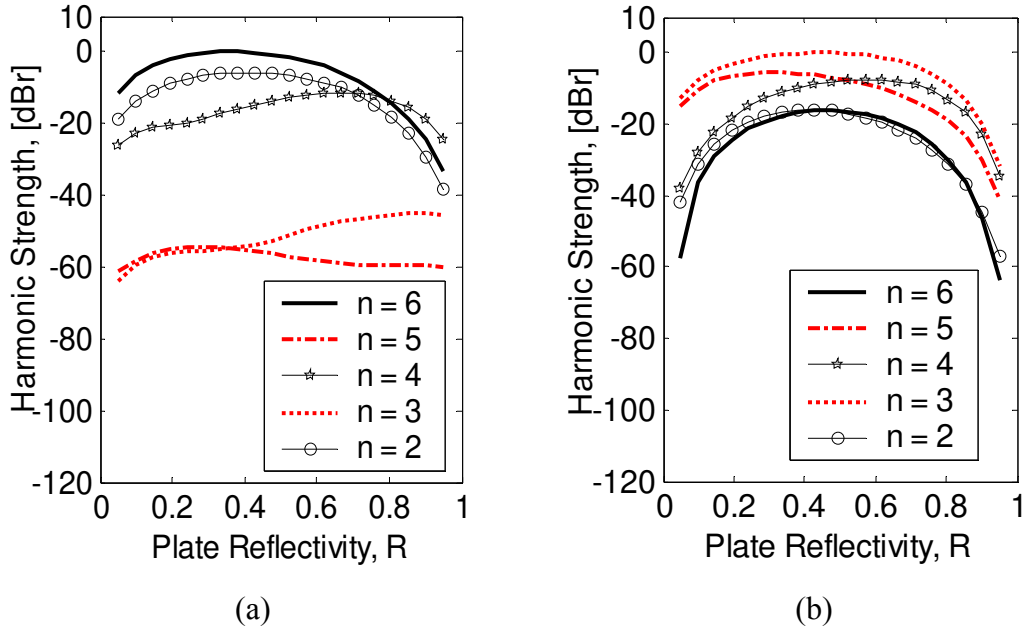


Figure 3.16: Effect of plate Reflectivity, R , on the strength of the generated harmonic components in a FPI-based OFM system with FM Index = 5 and laser wavelength-FPI biasing = (a) $FSR/2$; (b) $FSR/4$.

3.3.5 Impact of Laser-Filter Misalignment in a FPI-based OFM system

Figure 3.17 shows what happens when the laser wavelength fluctuates in a FPI-based system. In the simulation, the laser wavelength was varied by a total of 20 GHz peak-to-peak; i.e. by 10 GHz to either side of the CW wavelength. The FSR of the FPI was 10 GHz. The FPI was biased on the dark spot (FPI valley) as shown in Figure 3.17. From the figure, it is quite clear that the effect of laser wavelength drift on the 5th and 6th harmonic components is not as smooth and regular as that of the MZI-based system discussed in Section 3.2.5. Furthermore, among the two graphs, the 5th harmonic looks more regular.

The 6th harmonic component shows several minima, which belong to four sets of levels. The deepest set, hereafter referred to as the *absolute minima* occurs at values of the wavelength offset of ± 3.4 GHz and ± 6.6 GHz. In terms of percentage, these values represent wavelength offsets of about 34% and 66% of the FSR. The second level of minima occurs at wavelength offsets equal to 0 and equal to the FSR. The

third level occurs around 18% and 82% of the FSR. The final and highest set of minima occurs at wavelength offsets equal to half the FSR. This behaviour is periodic and repeats for wavelength drifts of between the FSR and twice the FSR (20 GHz in this case), and so on and so forth. The absolute minima of the 5th harmonic component are more regular and occur at wavelength drifts of 0%, 50%, and 100% of the FSR. This is similar to the behaviour of the MZI-based OFM system. The second set of minima occurs at wavelength drifts of 25%, and 75% of the FSR.

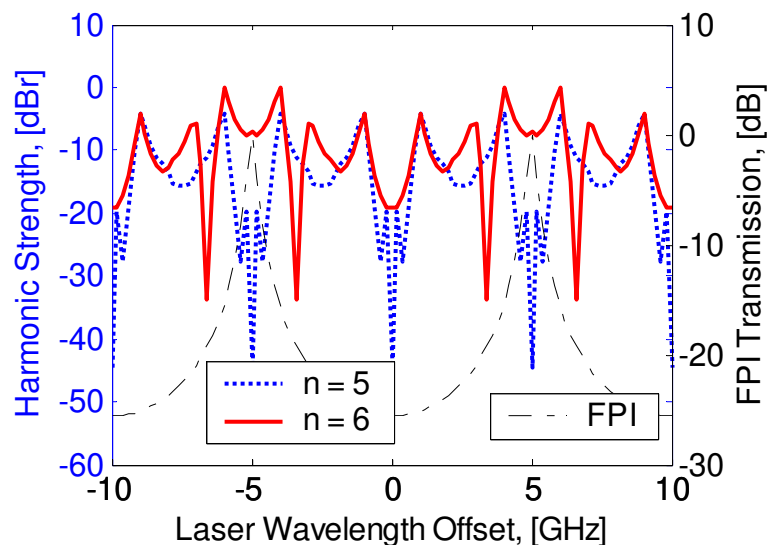


Figure 3.17: Impact of Laser wavelength drift on harmonic components generated by a FPI-based OFM system, with $R = 0.9$.

The maxima of both the 5th and 6th harmonic components all have very sharp peaks. These peaks would not be desirable operating points in a practical system because that would render the system susceptible to acute sensitivity to laser wavelength drifts. The higher minima would be more stable operating points, albeit with slightly lower power performance.

Unlike in the case of the MZI-based OFM system, where the sensitivity (and tolerance) to laser wavelength drift are independent of the order of the harmonic component, the behaviour of the FPI-based system is different. Figure 3.18 shows the comparison of the FPI-based system sensitivity to wavelength drift for both the low and high order even and odd harmonic components. It is clear that system sensitivities are unique for each harmonic component. In the case of the even harmonics, the absolute minima occur at different wavelength offsets – an intriguing observation. But, the maxima tend to occur at the same wavelength offsets, namely at offsets equal to $FSR/2$. This behaviour is similar to the MZI-based system, where the necessary condition for maximizing even harmonic components is given by Equation (3.11).

As for the odd harmonic components, the absolute minima occur at the same wavelength offsets, namely when the offset is $FSR/2$, including the zero offset. As mentioned above, this condition results in maximum even harmonics. The maxima of odd harmonics are more difficult to predict, just like the minima of the even harmonics.

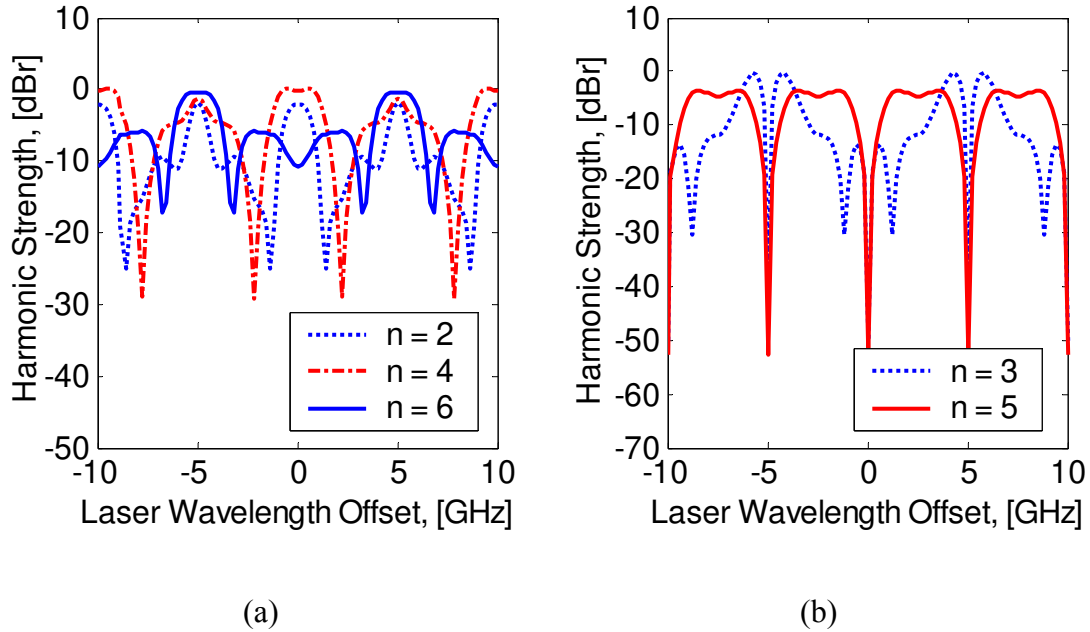


Figure 3.18: Comparison of the impact of laser wavelength drift on the strength of the generated low and high order microwave frequency harmonic components in a FPI-based OFM system; (a) even harmonics, (b) odd harmonics

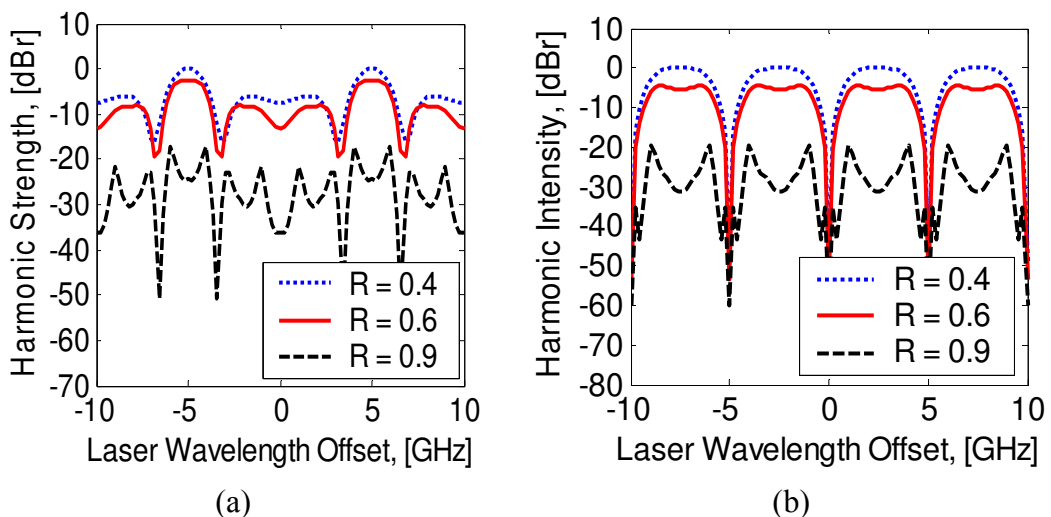


Figure 3.19: Effect of Reflectivity, R on laser wavelength drift sensitivity in a FPI-based OFM system; (a) $n = 6$, (b) $n = 5$

In the case of the MZI-based system, both the minima and maxima of the wavelength drift sensitivity for the even and odd harmonic components are easy to find (see

Section 3.2.5). Apart from the fact that they occur at the same offsets for each set of harmonics (even & odd), they also occur alternately. That is each maximum for the even harmonics coincides with an absolute minimum for the odd harmonics and vice versa. Therefore, a minimum for one set of harmonics (e.g. odd) can be used to identify the maximum for the other set (i.e. even), and vice versa. Thus, a convenient strategy in the stabilisation control circuit might involve the minimisation of an odd harmonic in order to maximise an even component. However in the case of the FPI-based system, only the minima of the odd harmonics may be used to locate the maxima of the even components, according to Figure 3.17. The reverse is not possible. Understanding of this behaviour may require an analytical model of the system.

The impact of the FPI's plate Reflectivity, R on the system sensitivity to laser wavelength drift was investigated. It was observed that better and smoother sensitivity is obtained with lower values of R . This behaviour is shown in Figure 3.19. Two interesting observations are made. Firstly, the presence and position of the absolute minima remain unchanged for both the 5th and the 6th harmonic components. Secondly, the non-absolute minima appear only for high values of R , and they appear in the places where the maxima existed. It can be said that the non-absolute minima go deeper with increasing Reflectivity, R (or finesse), and they are responsible for the deteriorating wavelength drift sensitivity.

3.4 Comparison of the MZI and FPI based OFM Systems

From the discussions above, it is clear that the OFM systems based on either the MZI or the FPI filters behave similar in most respects. However, some differences do exist. In this section, some of the theoretical similarities and significant differences are highlighted.

3.4.1.1 Similarities

- Both systems generate odd and even harmonic components.
- In both systems, the FM index, β , determines the relative strengths of the harmonic components. Higher frequency multiplication factors require increased FM Indices.
- Both systems require similar laser-filter alignment conditions (also called filter biasing) for enhancing the even harmonics and suppressing the odd harmonic components. In general, this occurs when the filter is biased at FSR/2 as given by equation (3.11). Under this condition all odd harmonic components are suppressed or eliminated altogether in both systems (see Figure 3.6, Figure 3.17, Figure 3.18, and Figure 3.19). However, the conditions necessary for suppressing even harmonics in the FPI systems are not the same as those for the MZI-based system.

3.4.1.2 Differences

- The finesse, and thus the contrast ratio of the FPI-based system is easily controlled by varying plate reflectivity, R or plate flatness, as well as beam collimation as given by equation (3.29). Therefore, plate

reflectivity, R , offers an extra system optimisation parameter for the FPI-based system.

- The two systems have different system sensitivities to laser wavelength-filter misalignment. The behaviour of the MZI-based system is more regular and smoother than that of the FPI-based system, which is very irregular for high values of finesse.
- The condition necessary for minimizing even harmonics (and so maximising odd harmonics) is not the same for the two systems. The MZI-based system requires a filter biasing of $FSR/4$ given by equation (3.12), which is not valid in the case of the FPI-based system. In fact, the minima of the different even harmonic components occur at different values of filter biasing. In other words, while locating a harmonic minimum automatically locates a harmonic maximum in the case of the MZI-based system, the same is not true in the case of the FPI-based system. In particular, the occurrence of an even harmonic minimum does not necessarily point to the occurrence of an odd harmonic maximum (see Figure 3.17).
- The FPI has an advantage that it can easily be tuned, a feature which is useful in the implementation of feedback stabilisation schemes (see 5.11.2).
- Regarding co-integration with a laser, the MZI filter is easier to integrate. The FPI requires an optical isolator to prevent back reflected light from interfering with the laser.
- The MZI-based system is easier to model mathematically because of the Finite Impulse Response (FIR) of the filter.

3.5 Impact of Laser Phase Noise on the OFM System

3.5.1 What is Laser Phase Noise?

The primary cause of random laser phase noise is spontaneous emission originating in the active laser cavity. The emissions change the phase of the free-running laser frequency. The process is magnified by physical effects within the laser cavity, leading to a broader spectral linewidth. The radiated spectrum of single-mode lasers such as the Distributed Feedback (DFB) and VCSELs is of the Lorentzian shape [15], [64] with the Full Width at Half Maximum (FWHM) linewidth defined by equation (3.34) [64]:

$$\delta\nu = \frac{1}{4\pi P} n_{sp} (1 + \alpha_e^2) h\nu \frac{\log(1/R)}{\tau_p \tau_{rt}} \quad (3.34)$$

where P is the optical power, n_{sp} is the spontaneous emission factor, α_e is the linewidth enhancement factor, which is the effective amplitude-phase coupling coefficient, h is Planck's constant, ν is the optical frequency, R is the laser facet

reflectivity, τ_p is the cold cavity photon lifetime, and τ_{rt} is the laser cavity round trip delay.

Therefore, laser linewidth is inversely proportional to optical power, P , and is proportional to the rate of spontaneous emission n_{sp} , and the square of the linewidth enhancement factor, α_e . DFB lasers emitting up-to 30mW of optical power exhibit linewidths of 1 MHz or less [15].

The power spectrum of the Lorentzian linewidth shape is given by equation (3.35) [65]:

$$\tilde{S}_E(f) \approx \frac{1}{1 + \left(\frac{f}{\delta\nu/2}\right)^2} \quad (3.35)$$

where $\delta\nu$ is the FWHM linewidth.

3.5.2 Impact of Laser Phase Noise

The detected intensity comprising the odd and even harmonics components described in equation (3.5), assumes an ideal laser emitting just a single spectral line with no phase noise. In order to determine what effect laser linewidth has on the generated harmonics, equation (3.4) is modified to include a laser phase noise term producing a laser linewidth of $\delta\omega$ ($= 2\pi \cdot \delta\nu$). The detected intensity is then described by [50], [66].

$$I_{PD}(t) = I_0 \cdot \left\{ \begin{array}{l} 1 + \cos(\omega_0\tau + \delta\omega \cdot \tau) \left\{ J_0(z) + 2 \sum_{k=1}^{\infty} (-1)^k J_{2k}(z) \cdot \cos \left[2k \cdot \left(\omega_{sw}t - \frac{\omega_{sw}\tau}{2} \right) \right] \right\} \\ + 2 \sin(\omega_0\tau + \delta\omega \cdot \tau) \sum_{k=1}^{\infty} (-1)^k J_{2k-1}(z) \cdot \cos \left[(2k-1) \cdot \left(\omega_{sw}t - \frac{\omega_{sw}\tau}{2} \right) \right] \end{array} \right\} \quad (3.36)$$

where $I_0 = |E_0|^2/2$.

Equation (3.36) shows that laser phase noise is converted into intensity noise of the generated harmonics. However, since in the OFM system the laser linewidth (few MHz) is much smaller than the FSR (few GHz) of the interferometer (i.e. $\delta\omega \ll 2\pi/\tau$), equation (3.36) shows that laser phase noise has in fact virtually no impact on the OFM system. This conclusion is in line with analyses of similar systems reported in [67], [68]. A more rigorous general analysis of the impact of phase noise in both coherent and incoherent interferometric systems using the statistical approach is reported in [69]. The analysis also arrives at the same conclusion. It should be noted

that the condition $\delta\omega \ll 2\pi/\tau$ implies that in fact the OFM system operates in the coherent regime [69].

Elimination of laser phase noise in the OFM system is a major operation and performance advantage. In many heterodyne detection-based RoF systems, the phase noise of the generated microwave signal is often broader than those of the laser sources, which are in MHz (see Section 2.3). Thus in order to generate low-phase noise microwave signals (to eliminate laser phase noise), additional functionality (such as Phase Locked Loops (PLL), and Optical Injection Locking, OIL) is often required around the basic system [39], [40], [70]. This leads to more complex and costly systems. However, in the case of OFM, this is not necessary, making it simpler.

3.6 Impact of Sweep Signal Phase Noise on the OFM System

The OFM system depicted in Figure 3.1 needs two sources – one optical and the other electrical. The electrical source is a low frequency LO, f_{sw} used to sweep the optical frequency. In section 3.5 the impact of laser phase noise on OFM has been analysed, and found to be insignificant. This section explores the impact of sweep signal phase noise on the OFM system.

3.6.1 What is Oscillator Phase Noise?

Phase noise refers to the short-term random fluctuation in the frequency or phase of an oscillator signal. It is defined as the ratio of power in one phase modulation sideband per Hertz (Hz) to the total signal power at a given offset frequency f_m , from the signal frequency. Phase noise is denoted by $L_\phi(f_m)$, and is usually expressed in decibels relative to the carrier power per Hz of bandwidth, i.e. dBc/Hz.

Sources of phase noise in oscillators include thermal noise (kTB), which sets the noise floor, and flicker noise, $1/f$, which is attributed to random fluctuations of the carrier density in the active devices used (transistors) [9]. Other noise sources come from the VCO, and include reference signal leakage in the PLL, harmonics of the VCO, and spurious frequencies generated by the phase detector. All the noise within the passbands of the oscillator feedback loop is amplified, thereby increasing its effective contribution to the total oscillator phase noise. To reduce phase noise, a VCO usually has to deploy a high-Q cavity filter for frequency selectivity. This commonly implies that the VCO is more difficult to sweep.

Oscillator phase noise is important in wireless systems because it reduces receiver performance by increasing the BER (or Error Vector Magnitude, EVM) by causing decision errors in digitally modulated signals (e.g. xQAM), and by degrading the selectivity of the receiver through reciprocal mixing [9].

A common way of representing a sinusoidal signal, $y(t)$ with small ($\beta \ll 1$) phase perturbations, $\theta(t)$ is equation (3.37).

$$y(t) = V_{\text{pk}} \cos(\omega_0 t + \theta_p \sin \omega_m t) \quad (3.37)$$

where $\theta(t) = \theta_p \sin \omega_m t$, and θ_p is the peak phase deviation defined in (3.38), (which is equal to the FM index, β in the corresponding FM modulation) and, f_m is the modulating signal frequency.

$$\theta_p = \frac{\Delta f}{f_m} \quad (3.38)$$

If phase variations are small, then it can be shown that small phase or frequency deviations in the signal, $y(t)$ result in modulation side bands at $\omega_0 \pm \omega_m$ on either side of the carrier signal, and that the amplitude of the side bands is $0.5\theta_p$. This means that Single Side Band (SSB) phase noise, $L_\phi(f_m)$, which is the ratio of noise power in a single sideband to the carrier power will be given by equation (3.39)

$$L_\phi(f_m) = \frac{\theta_p^2}{4} = \frac{\theta_{\text{rms}}^2}{2} \quad (3.39)$$

where θ_p , and θ_{rms} are the peak and *rms* phase deviations respectively. The two sided power spectral density associated with phase noise is then a combination of power in the two sidebands [9]:

$$S_\theta(f_m) = 2 \cdot L_\phi(f_m) = \frac{\theta_p^2}{2} = \theta_{\text{rms}}^2 \quad (3.40)$$

3.6.2 Impact of Sweep Signal Phase Noise

In RoF systems where a reference LO, an IF, or the actual microwave signal have to be transported over the fibre, the noise added by the optical system determines the quality of the delivered LO or microwave signal [71]. It has been demonstrated above that laser phase noise does not impact the OFM process. In order to determine the relationship between the phase noise of the sweep signal, f_{sw} and the phase noise of the OFM-generated microwave harmonics, f_{mm} , lets consider an instantaneous frequency drift $\pm\delta\omega$ in the sweep signal, $\omega_{\text{sw}} = 2\pi f_{\text{sw}}$, so that the new instantaneous frequency becomes $\omega_{\text{sw}} \pm \delta\omega$. From equation (3.5), the generated harmonic components will be:

$$i_N(t) = I_0 \cdot \sum_{N=1}^{\infty} (-1)^N \cdot A \cdot \cos \left[N \cdot \left((\omega_{\text{sw}} \pm \delta\omega) \cdot t - \frac{\omega_{\text{sw}} \tau}{2} \right) \right] \quad (3.41)$$

where N = the order of the harmonic, and $A = X$ or Y given in equations (3.6), and (3.7) for even and odd harmonic components, respectively. Since the FM index, β is the same as before, equation (3.41) shows that the change in the peak frequency deviation as a result of the change in the instantaneous frequency is proportional to the order of the harmonic component. That is, the new peak frequency deviation becomes $N \cdot \Delta f$, and the new peak phase deviation $N \cdot \theta_p$. Therefore the new SSB phase noise $L_N(f_m)$, at the same frequency offset, f_m is related to the phase noise of the sweep signal, f_{sw} by:

$$L_N(f_m) = N^2 \cdot L_\phi(f_m) \quad (3.42)$$

That is to say the phase noise of the generated frequency components of order N , is higher than that of the sweep signal by the multiplication factor, N . In other words the increase in the phase noise is :

$$\Delta L_{N,\text{dB}}(f_m) = 20 \cdot \log[N] \quad (3.43)$$

From equation (3.43), the SSB phase noise of the second harmonic component increases by 6 dB, that of the third harmonic component by 9.5 dB, and so on and so forth.

3.7 Conclusions

The Optical Frequency Multiplication (OFM) system has been modelled and its principle of operation analysed theoretically. The following are some of the key conclusions that are drawn from the analysis in this Chapter.

Firstly, OFM generates several frequency components, which are harmonics of the sweep signal, f_{sw} . Therefore, the choice of the sweep signal depends on the desired microwave carrier frequency, which should be a multiple of the sweep signal. Frequency multiplication factors of more than 6, for the generation of microwave carriers with reasonable intensity and intensity modulation depth (IMD) are feasible.

The intensity of the generated harmonics depends on three factors, namely the quality of the filter, the biasing of the filter, and the value of the FM Index, β used. By appropriate biasing of the filter, one set of harmonics (even or odd) is either enhanced or suppressed (eliminated). However, it is also possible to bias the filter in such a way as to generate both even and odd harmonic components. By appropriate tuning of the FM index, the desired harmonic(s) may be further enhanced, or suppressed.

In general, the generation of high order harmonic components requires a greater FM index. Thus, for very high multiplication factors, the OFM system might be less efficient spectrally, when compared to some other optical methods for transporting

high frequency signals. However, by careful selection of the filter's FSR, the FM index, β_{opt} required for optimum power performance may be reduced, resulting in some significant optical bandwidth saving.

The intensity of the OFM generated harmonics is susceptible to intensity fluctuations induced by wavelength-filter variations. The FSR of the filter places a limit on the required laser source-filter stability. The relative stability may also be achieved through optical feedback. If the filter is kept in a central location, the stabilisation scheme, which could be a combined laser-filter stabilisation scheme, may be shared by many antenna sites thereby reducing the extra system cost.

The MZI-based, and FPI-based OFM systems have many similarities. However, they also have some differences. The contrast ratio of the FPI-based system may be more accurately controlled by adjusting the reflectivity, R . No such parameter exists for the MZI-based system. In both systems, even harmonics are enhanced over odd harmonics by biasing the filter at FSR/2. The odd harmonics are enhanced, and the even harmonics suppressed when the biasing is FSR/4, for the MZI-based system. However, this is not the case for the FPI-based system. In fact, in terms of the sensitivity to laser wavelength fluctuations, the MZI-based system behaves in a more regular manner than the FPI-based system. In the MZI-based system, a minimum of one harmonic may be used to identify a maximum of another harmonic. But, in the case of the FPI-based system, this is not so, because the maximums of even harmonics do not always coincide with the minimums of the odd harmonics.

The analysis of the OFM process shows that it suppresses laser phase noise completely. Therefore, an OFM-based system does not require extra circuitry such as Phase Locked Loops (PLLs) and Optical Injection Locking (OIL, which increase system complexity) to suppress laser phase noise, as is the case in most Remote Heterodyne Detection (RHD) techniques. This is a major advantage of the OFM method over methods such as RHD, and injection locking schemes.

The phase noise of the generated frequency components is related to that of the sweep signal f_{sw} . For the up-converted harmonics the SSB phase noise increases by a factor that is proportional to the square of the multiplication factor. However, this is not peculiar to OFM.

Impact of Fibre Dispersion on OFM

4.1 Introduction

The principle of Optical Frequency Multiplication (OFM) for generating high frequency microwave signals is discussed in Chapter 3. The modelling in Chapter 3 does not include a fibre link between the headend and the antenna unit, as shown in Figure 3.1. This chapter focuses on what happens to the OFM process when a length of fibre is placed between the headend and the antenna unit - that is when the antenna unit is removed away from the headend as shown in Figure 4.1. The impact of two types of fibre dispersion is considered - namely chromatic, and interposal dispersion.

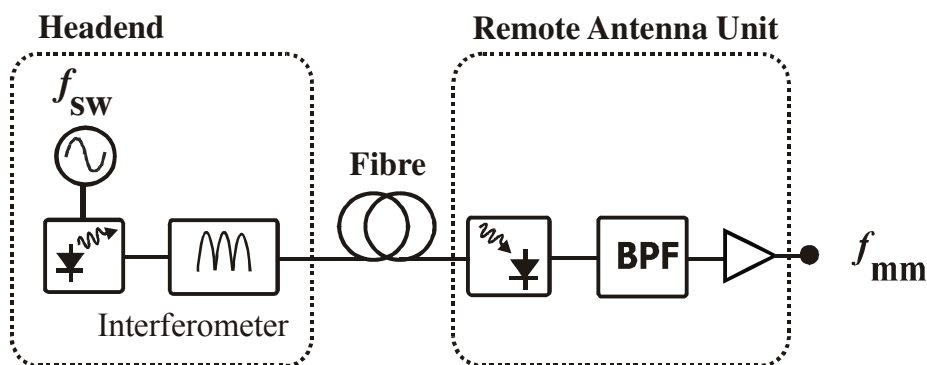


Figure 4.1: OFM system downlink with remotized antenna unit

4.2 Chromatic Dispersion

Chromatic dispersion refers to the wavelength-dependent pulse spreading that occurs as the optical signal propagates along the fibre. There are two contributing factors to chromatic dispersion. The first one is the dependence of the fibre material's refractive index on the wavelength – referred to as material dispersion. The second factor is the waveguide dispersion, which occurs as a result of the dependency of the propagation constant on the wavelength. The end result is that different spectral components arrive at slightly different times, leading to wavelength-dependent pulse spreading, or dispersion.

In many instances, material dispersion is the main contributor to chromatic dispersion. The pulse spreading due to chromatic dispersion is then given by

$$\Delta t_{\text{chrom}} = D(\lambda) \cdot \Delta\lambda \cdot L \quad (4.1)$$

where $D(\lambda)$ is the dispersion parameter (in ps/nm·km), $\Delta\lambda$ is the spectral width of the light source, and L is the length of the fibre. Thus, the broader the spectral width is, the greater the dispersion. For silica fibres, the dispersion parameter, $D(\lambda)$ may be approximated by the Sellmeier [15] equation (4.2) :

$$D(\lambda) = \frac{S_0}{4} \left[\lambda - \frac{\lambda_0^4}{\lambda^3} \right] \quad (4.2)$$

where S_0 is the zero dispersion slope, and λ_0 is the zero-dispersion wavelength, which occurs around 1300 nm. Typical dispersion parameter, $D(\lambda)$ values of silica fibres are -3 ps/nm·km, and -17 ps/nm·km at 1310 nm and 1550 nm respectively [15].

4.3 Impact of Chromatic Dispersion

Chromatic dispersion is caused by the wavelength-dependent propagation times of the different spectral components. In IM-DD systems, the transmission distances of high frequency microwave signals is severely limited by chromatic dispersion, which causes suppression of the transmitted signals at certain lengths. For instance, the transmission distance of a 60 GHz millimetre wave is limited to less than 2 km on standard single mode fibre at 1550 nm, due to chromatic dispersion (see Section 2.2.2, and [27]).

To show the impact of chromatic dispersion on the OFM system, the delivery and generation of the 5th harmonic component (30 GHz) was simulated using the VPI simulation platform. The simulation was carried out at 1550 nm with a dispersion parameter of 16 ps/nm·km, which is equal to that of standard SMF. The fibre length was varied from 0 to 50 km. Figure 4.2 shows the plot of the harmonic strength against the fibre length. The result of the DSB IM-DD system simulation is included for the purpose of comparison.

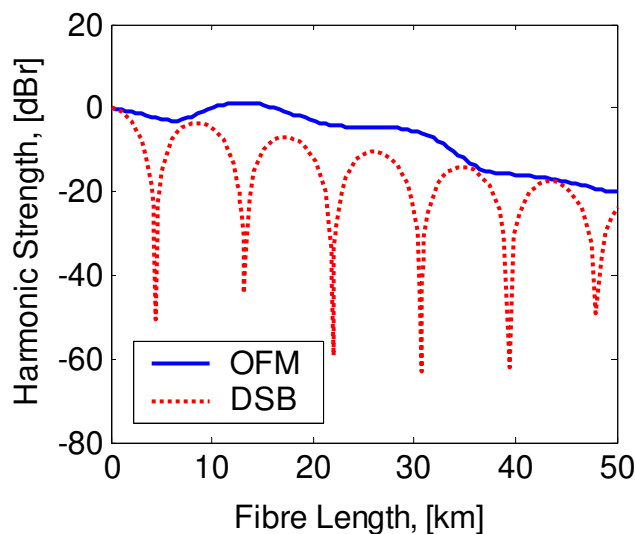


Figure 4.2: Impact of Chromatic Dispersion on the OFM system

The figure shows the amplitude suppression in the DSB IM-DD system caused by chromatic dispersion. Six (6) nulls are encountered in the 50 km fibre length. The first null occurs at just 4.4 km. Other nulls occur around 13 km, 22 km, 30.8 km, 39.2 km, and finally around 48 km. But for the OFM system, no nulls are present throughout the 50 km fibre length. In fact, some gain of about 6 dB occurs between fibre lengths 8 – 35 km. From the foregoing, OFM is clearly chromatic dispersion tolerant. That is, while the span length of the DSB IM-DD RoF system would be limited to less than 4 km, that of the OFM system generating the same 30 GHz microwave signal, but through a 6 GHz sweep signal would extend beyond 50 km.

The monotonically damping amplitude peaks observed for both the DSB and the OFM system are a result of the fibre attenuation, which was 0.2 dB/km, resulting in a total loss of about 20 dB.

The 6 dB gain observed in the OFM system is due to the extra FM-IM conversion taking place in the presence of chromatic dispersion [72]. Figure 4.3 shows what happens to the OFM system when the interferometer is removed. The harmonic strength is strongest between the fibre lengths of 8 – 35 km. This result confirms that the gain observed in Figure 4.2 over these fibre lengths is indeed due to strong FM-IM conversion induced by chromatic dispersion. A similar gain attributed to FM-IM conversion was reported to enhance the modulation efficiency of a directly modulated semiconductor laser for a 7 GHz frequency range [73].

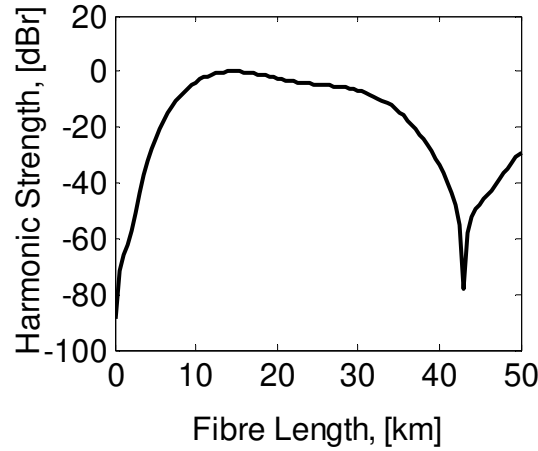


Figure 4.3: Effect of Chromatic Dispersion on the OFM system without an interferometer

4.4 Modal Dispersion

The advantage of multimode fibres (MMFs) over single-mode fibres (SMFs), in general, is their relaxed coupling tolerance, thanks to their larger core diameters, which lead to reduced system-wide installation and maintenance costs. Traditionally, MMFs were made from silica. However, more recently Polymer Optical Fibres (POFs) have also emerged on the scene, promising increased ease of handling and reduced installation costs owing to the more ductile material and larger core size [12], [13], [74]. MMFs allow the propagation of multiple guided modes albeit with different propagation constants. The difference in the mode propagation times leads to intermodal dispersion, which severely limits the fibre bandwidth. As a result of the limited bandwidth, coupled with the associated lower installation and maintenance costs, MMFs have been confined to short link applications such as LANs. In the case of POF, the higher-than-silica attenuation (> 10 dB/km) also inhibits their use in long link applications [13]. Therefore, modal dispersion is the dominant performance limiting factor in MMFs.

For high bandwidth applications, Graded Index (GI) core profiles instead of Step Index (SI) cores, are used to reduce the effects of modal dispersion in MMFs. The objective of the GI profile is to equalise the propagation times of the various propagating modes. The graded refractive index profile can be approximated by the power law equation given by

$$n(r) = \sqrt{n_{cc}^2 \cdot \left[1 - 2\Delta \left(\frac{r}{a} \right)^q \right]}; \quad 0 \leq r \leq a \quad (4.3)$$

$$= n_{cl} \quad ; \quad r > a$$

where q is the index exponent, r corresponds to the cylindrical radial coordinate, n_{cc} and n_{cl} are the refractive indexes of the core centre and cladding respectively, a is the core radius, and Δ is the relative index difference given by

$$\Delta = \frac{n_{cc}^2 - n_{cl}^2}{2n_{cc}^2} \quad (4.4)$$

The refractive index profile is determined by the index exponent, q . If $q = 1$, a linear profile is obtained. If $q = 2$, a parabolic index profile is obtained, and the condition $q = \infty$ corresponds to a step index profile.

4.4.1 Modelling Modal dispersion

Dispersion characteristics of multimode fibres can be studied through either ray optics or modal analysis using Maxwell's wave equations based on the Wentzel-Kramers-Brillouin (WKB) approximation of weakly guided fibres. Both methods are applicable in highly multimode fibres – that is when the normalised frequency (or waveguide parameter) $V \geq 10$, and $V \gg 1$ for the ray optics and the WKB analyses respectively [75].

The total number of guided modes propagating in the multimode fibre is approximated by

$$M = \frac{q}{2(q+2)} \cdot V^2 \quad (4.5)$$

where q is the index exponent, and V is the normalised frequency (or normalised waveguide parameter) given by

$$V = \frac{2\pi a}{\lambda_0} \cdot \sqrt{n_{cc}^2 - n_{cl}^2} \quad (4.6)$$

Therefore, the number of guided modes in GI (with $q = 2$), and SI fibres is approximated by equations (4.7) and (4.8), respectively. From the two equations it is clear that SI fibres support twice as many guided modes as GI fibres of similar physical properties do.

$$M_{GI} \approx \frac{V^2}{4} \quad (4.7)$$

$$M_{SI} \approx \frac{V^2}{2} \quad (4.8)$$

Thus the total number of guided modes depends on the index profile, the core size, the numerical aperture, $NA = \sqrt{n_{cc}^2 - n_{cl}^2}$, and the operating wavelength, λ_0 . For instance a 50 μm core GI-MMF with $NA = 0.2$ will support 342 guided modes at 850 nm and 144 modes at 1310 nm .

For GI fibres it has been shown that the group velocities of the modes are dependent on the mode number, v and that the time, t_v taken by mode v to propagation through distance L of the fibre is given by [75]:

$$t_v = \frac{n_1 L}{c} \left(1 + \frac{q-2}{q+2} \delta + \frac{3q-2}{q+2} \cdot \frac{\delta^2}{2} + \dots \right) \quad (4.9)$$

where δ is known as the profile dispersion and is described by:

$$\delta = \Delta \left(\frac{v}{M} \right)^{\frac{q}{q+2}}; \quad 0 < \delta < \Delta \quad (4.10)$$

Modal dispersion is defined as the propagation time difference between the fastest mode ($\delta = 0$) and the slowest mode ($\delta = \Delta$). Thus for a parabolic index profile with $q = 2$, the pulse spreading, $\Delta\tau$ is

$$\Delta\tau \approx \frac{n_{cc} L}{2c} \Delta^2; \quad q = 2 \quad (4.11)$$

and for the index exponent q not very close to 2, the dispersion is

$$\Delta\tau_{\text{GI}} \approx \frac{n_{cc} L}{c} \cdot \frac{q-2}{q+2} \Delta; \quad q \neq 2 \quad (4.12)$$

For SI fibres, the intermodal dispersion is given by:

$$\Delta\tau_{\text{SI}} \approx \frac{n_{cc} L}{c} \Delta \quad (4.13)$$

The optimum index profile, which produces the minimum intermodal dispersion is determined from the relation $dt_v/d\delta = 0$, leading to the profile dispersion:

$$\delta_0 = \frac{2-q}{3q-2} \quad (4.14)$$

The minimum dispersion occurs when the modes corresponding to $\delta = 0$, and $\delta = \Delta$ take the same amount of time to travel the length of the fibre. The optimum index profile is then found to be [75]:

$$q_0 \approx 2 - 2\Delta \quad (4.15)$$

Now, equation (4.15) suggests that the optimum index is only a function of the fibre's relative index difference, Δ . This is because it was earlier assumed that Δ was not dependent on the wavelength. However, in general Δ is dependent on the wavelength, making the optimum index profile q_0 also a function of the wavelength [75], [76].

4.4.2 MMF Transfer Function

Assuming that each mode i propagates independently with a relative propagation time τ_i , the impulse response of MMF is given by [50], [66]

$$h_{\text{MMF}}(t) = \sum_{i=1}^M c_i \cdot \delta(t - \tau_i) \quad (4.16)$$

where M equals the total number of guided modes, c_i^2 denotes the relative power of mode i . The effects of chromatic dispersion and mode mixing are not taken into account. Using (4.16), the Intensity Modulation Transfer Function (IM-TF) of the MMF may be represented as:

$$|H_{\text{MMF}}(\omega)|^2 = \sum_{i=1}^M \left\{ c_i^4 + 2c_i^2 \cdot \sum_{h=i+1}^M c_h^2 \cdot \cos \omega(\tau_h - \tau_i) \right\} \quad (4.17)$$

Using the above equation, the power transfer functions of 400m, and 2 km of MMF having a core diameter of 50 μm and a NA of 0.2 are plotted in Figure 4.4. The wavelength used is 1310 nm . All the 144 guided modes were included, but to varying degrees of strength. So this is a form of Over-Filled-Launch (OFL) condition. The same launch conditions were used in both cases, that is the same modal power coefficients c_i were used in both plots. Attenuation affects and chromatic dispersion were not taken into account.

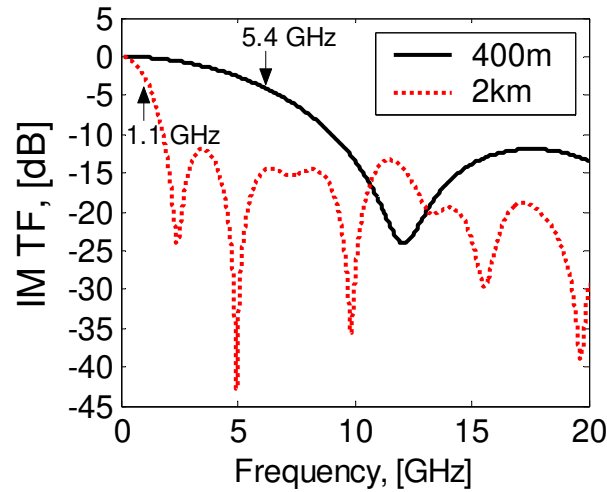


Figure 4.4: Intensity Modulation Transfer Function for 50 μm -core MMF of length (i) 400 m, and (ii) 2 km

It is observed from Figure 4.4 that the -3dB bandwidth of 400m of fibre is about 5.4 GHz. After 2 km the bandwidth drops to 1.1 GHz, i.e. by a factor of 5. This is consistent with the expectation that longer fibre lengths lead to greater modal dispersion as given in equations (4.11) - (4.13).

4.4.3 MMF Bandwidth

From Figure 4.4 the -3dB bandwidths of the two fibre lengths were found to be 5.4 GHz, and 1.1 GHz at 400m and 2 km, respectively. These figures represent a fibre Bandwidth-Length-Product (BLP) of about 2.2 GHz-km under the described launch conditions. State-of-the art MMF have specified bandwidths (measured under OFL conditions) of about 800 MHz-km for silica GI-MMFs and around 500 MHz-km for Perfluorinated (PF) GIPOF [51]. This bandwidth relates to the -3dB (or baseband) bandwidth, and clearly, it is insufficient to meet the increasing demand for high-speed LAN applications, including Gigabit Ethernet for reasonable distances. For this reason, there is a lot of research looking into ways and means of increasing the capacity of MMFs [76] - [81].

As Figure 4.4 shows, the frequency response of MMF does not diminish monotonically to zero after the -3dB bandwidth (the baseband bandwidth), but tends to have repeated passbands beyond that [19]. In recent times, these high order passbands have been used in research to transmit independent streams of data (digital or analogue), in addition to the baseband bandwidth [19], [20], [82], [83]. This is known as Sub-Carrier Multiplexing (SCM). Therefore, in this way, the aggregated transmission capacity of MMF may exceed its baseband bandwidth.

Another way to increase the capacity of MMFs is to use the Under-Filled-Launch (UFL) condition. That is, only some selected modes (or mode groups) are launched in the fibre. Since the propagating modes are fewer under UFL launch conditions, the

difference in propagating times between the fastest and slowest modes is smaller. Thus, inter-modal dispersion is reduced, and the bandwidth increased. The problem with this approach is that the fibre performance may be unstable as it is strongly linked to the actual launch conditions [76]. Fibre performance is also affected by environmental and mechanical factors, and other factors including mode-coupling, modal noise, and Differential Mode Attenuation (DMA), [81], [84] - [87]. However, a stable and reliable performance of a mode-coupling controlled GIPOF fibre link under UFL condition has recently been reported in [78]. In these experiments a high-NA PMMA POF exhibited very low mode-coupling even after 250 m.

It has been stated earlier that intermodal delay determines the fibre bandwidth. This is true in many instances. However, it has also been observed that in general, measured POF bandwidth is not accurately predicted by intermodal delay. A lot of research has been taking place to explain the discrepancy. It has been proposed that in PMMA POF, DMA is responsible for the bandwidth discrepancy, in the absence of mode-coupling, [80]. However, strong presence of mode-coupling has been found to exist in Perfluorinated POF [81]. Both measurements and analyses were based on 100m fibre lengths. As for silica MMFs, it is agreed that they exhibit far less mode coupling compared to POF fibres. This is attributed to the difference in the material properties, [77] - [81].

4.5 Impact of Modal Dispersion on OFM

Neglecting chromatic dispersion, the impulse response of the multimode fibre (MMF) may be represented by equation (4.16), where c_i accounts for the relative strength of mode i . Considering a MZI for the periodic filter, the optical field, $E_{\text{MZI}}(t)$ exiting the MZI is given by equation (A.3). Thus the optical field at the output of the MMF is given by [66]:

$$E_{\text{MMF}}(t) = E_{\text{MZI}}(t) * h_{\text{MMF}}(t) \quad (4.18)$$

$$= \frac{1}{2} E_0 \sum_{i=1}^M c_i \cdot e^{j(\omega_0 t - \omega_0 \tau_i)} \cdot \left\{ e^{j\beta \sin \omega_{\text{sw}}(t - \tau_i)} + e^{j[-\omega_0 \tau + \beta \sin \omega_{\text{sw}}(t - \tau - \tau_i)]} \right\} \quad (4.19)$$

where τ is the path length delay in one arm of the MZI with respect to the other. Taking into account *mode orthogonality* for guided modes, it can be said that each mode propagates along the fibre independently of the others [75]. Therefore, if we ignore *mode coupling* then we can use the optical field associated with each mode given in equation (4.19) to independently compute the detected intensity $I_{\text{MMFi}}(t)$, attributed to each mode at the photodiode as:

$$I_{\text{MMFi}}(t) = \left\langle E_{\text{MMFi}}(t) \cdot E_{\text{MMFi}}^*(t) \right\rangle \quad (4.20)$$

$$= \frac{1}{2} |E_0|^2 c_i^2 \cdot \left[1 + \cos\{\omega_0 \tau + \beta \sin \omega_{\text{sw}}(t - \tau_i) - \beta \sin \omega_{\text{sw}}(t - \tau - \tau_i)\} \right] \quad (4.21)$$

Using the same analysis used in Chapter 3, the total detected intensity is then given by [50]

$$I_{\text{MMF}}(t) = \frac{1}{2} |E_0|^2 \cdot \sum_{i=1}^M c_i^2 \cdot \left[\begin{aligned} & 1 + \cos(\omega_0 \tau) \cdot J_0(z) \\ & + \left\{ 2 \cos(\omega_0 \tau) \cdot \sum_{k=1}^{\infty} \left\{ (-1)^k J_{2k}(z) \cdot \cos \left[2k \cdot \left(\omega_{\text{sw}}(t - \tau_i) - \frac{\omega_m \tau}{2} \right) \right] \right\} \right\} \\ & + \left\{ 2 \sin(\omega_0 \tau) \cdot \sum_{k=1}^{\infty} \left\{ (-1)^k J_{2k-1}(z) \cdot \cos \left[(2k-1) \cdot \left(\omega_{\text{sw}}(t - \tau_i) - \frac{\omega_m \tau}{2} \right) \right] \right\} \right\} \end{aligned} \right] \quad (4.22)$$

where $z = 2\beta \cdot \sin\left(\frac{\omega_{\text{sw}} \tau}{2}\right)$, $\tau = \frac{1}{\text{FSR}}$, and $J_{2k}(\cdot)$ is the Bessel function of the first kind and of the order $2k$. Equation (4.22) shows that the same odd and even harmonic components observed in the OFM system without fibre are generated. However, the generated components are shifted in time. The impact of the FM index and the laser-filter biasing are discussed in Chapter 3.

It can further be shown that even harmonic components are given by

$$I_{2k}(t) = |E_0|^2 (-1)^k \cos(\omega_0 \tau) \cdot J_{2k}(z) \cdot \sqrt{\sum_{i=1}^M \left\{ c_i^4 + 2c_i^2 \sum_{h=1}^M c_h^2 \cos(2k\omega_{\text{sw}}(\tau_i - \tau_h)) \right\}} \cdot \cos \left[2k\omega_{\text{sw}} \left(t - \frac{\tau}{2} \right) - \tan^{-1} \left(\frac{\sum_{i=1}^M c_i^2 \sin(2k\omega_{\text{sw}} \tau_i)}{\sum_{i=1}^M c_i^2 \cos(2k\omega_{\text{sw}} \tau_i)} \right) \right] \quad (4.23)$$

Combining equation (4.23) and equation (4.17) we obtain

$$I_{2k}(t) = |E_0|^2 (-1)^k \cos(\omega_0 \tau) \cdot J_{2k}(z) \cdot |H_{\text{MMF}}(2k \cdot \omega_{\text{sw}})| \cdot \cos \left[2k\omega_{\text{sw}} \left(t - \frac{\tau}{2} \right) - \tan^{-1} \left(\frac{\sum_{i=1}^M c_i^2 \sin(2k\omega_{\text{sw}} \tau_i)}{\sum_{i=1}^M c_i^2 \cos(2k\omega_{\text{sw}} \tau_i)} \right) \right] \quad (4.24)$$

Using a similar approach, we obtain for the odd harmonic components

$$I_{2k-1}(t) = |E_0|^2 (-1)^k \sin(\omega_0 \tau) \cdot J_{2k}(z) \cdot |H_{\text{MMF}}((2k-1) \cdot \omega_{\text{sw}})| \cdot \cos \left[(2k-1) \omega_{\text{sw}} \left(t - \frac{\tau}{2} \right) - \tan^{-1} \left(\frac{\sum_{i=1}^M c_i^2 \sin((2k-1) \omega_{\text{sw}} \tau_i)}{\sum_{i=1}^M c_i^2 \cos((2k-1) \omega_{\text{sw}} \tau_i)} \right) \right] \quad (4.25)$$

Comparing equations (4.24) and (4.25) with equations (3.6) and (3.7) respectively, we conclude that modal dispersion causes the linear scaling in amplitude of the generated harmonic components by the MMF's intensity modulation transfer function, $|H_{\text{MMF}}(\omega)|$ [50], [66]. Figure 4.5 shows what happens when the 400m MMF link whose frequency response is given in Figure 4.4 is used to remotely feed an antenna unit. The strength of generated harmonics is plotted against the FM Index, β . By comparing Figure 4.5 (a) and Figure 3.5, the impact of intermodal dispersion in altering the relative strengths of the generated harmonics is obvious. That is, the 4th harmonic component ($k = 2$) shows a much higher reduction in strength than the 6th component ($k = 3$). This is because the 4th harmonic (12 GHz) is in the vicinity of the dip in the frequency response of Figure 4.4, while the 6th harmonic (18 GHz) coincides with the peak of the first passband beyond the -3dB bandwidth.

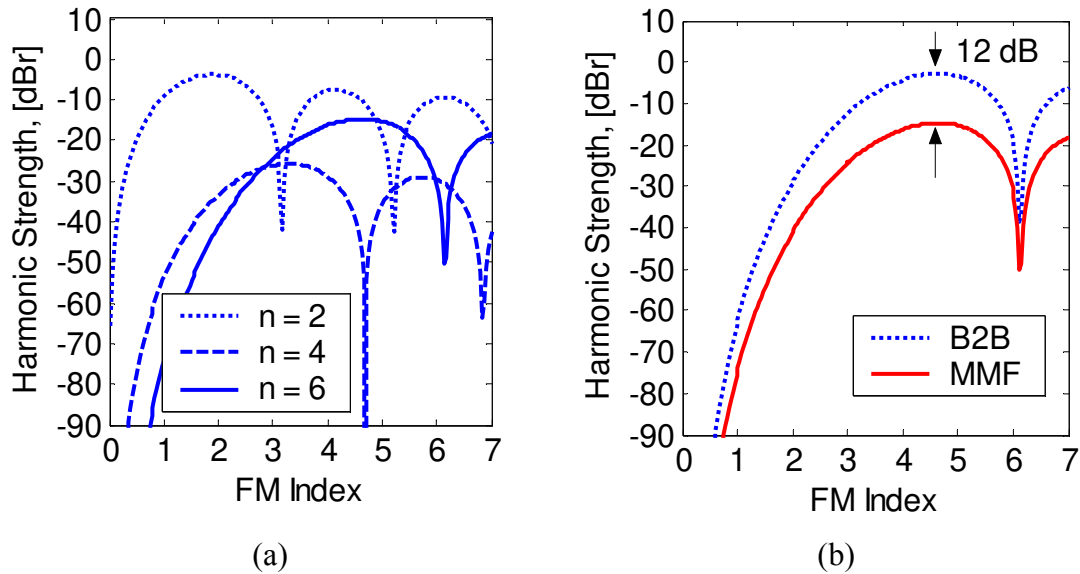


Figure 4.5: Impact of Modal Dispersion on the OFM system (a) even harmonics – $n = 2, 4,$ and 6 (b) 6th harmonic component with and without MMF fibre

Figure 4.5 (b) shows a comparison of the harmonic strengths of the generated 6th harmonic in a system without fibre and one with the 400 m MMF link. A 12 dB attenuation observed is in line with the -12 dB level of the first passband peak in the MMF's transfer function (see Figure 4.4). So, it is clear that OFM can be used to transport microwave signals beyond the -3 dB bandwidth of MMF's by using the high order passbands. This is in a way similar to SCM systems and those RoF systems,

which exploit the high order passbands. However, in the case of OFM, no high-frequency microwave signal sources are required, which is a major operational advantage. The disadvantage of having to transmit through the high order transmission passbands of the fibre is that in applications where the passbands are not stable, adaptive tracking of the position of the passbands may be necessary.

Equations (4.24), and (4.25) also show a new phase term, $\theta_{\Delta\tau}$ which is attributed to modal dispersion. For the odd harmonics, $\theta_{\Delta\tau}$ is given by the expression:

$$\theta_{\Delta\tau} = \tan^{-1} \left(\frac{\sum_{i=1}^M c_i^2 \sin((2k-1)\omega_{sw} \tau_i)}{\sum_{i=1}^M c_i^2 \cos((2k-1)\omega_{sw} \tau_i)} \right) \quad (4.26)$$

In an unstable system, where the propagating modes and the power distribution among them vary significantly over time, they could lead to an increase in phase noise. However, since $\theta_{\Delta\tau}$ depends on the total sum of the modes and their powers, their contribution to phase noise is not expected to be significant.

4.6 Conclusions

OFM does not suffer severe length-dependent signal suppression caused by chromatic dispersion in IM-DD DSB RoF systems. The link length of an IM-DD DSB system delivering a 30 GHz millimetre wave is limited to less than 5 km due to chromatic dispersion. But, using OFM, the link length can be extended beyond 50 km. That is to say OFM is chromatic dispersion tolerant. Therefore, OFM may be used to distribute high-frequency microwave signals over SMF link lengths, which are more than 10 times longer than DSB RoF systems.

In SMF-based systems, attenuation, and phase noise requirements may provide practical limits to link length distances of OFM-based RoF system, and not chromatic dispersion.

It has been shown that OFM can be used to deliver high-frequency microwave signals over multimode fibres. The microwave signals being delivered may exceed the modal bandwidth of the multimode fibre. The amplitudes of the generated harmonics are then scaled by the multimode fibre's intensity modulation transfer function.

CHAPTER

5

Experimental Demonstration of an OFM-based RoF Downlink

5.1 Introduction

Chapters 3 and 4 dealt with theoretical modelling and analysis of the principle of Optical Frequency Multiplication (OFM) for high-frequency carrier generation. This Chapter describes the practical implementation of a RoF downlink employing the principle of OFM. The results of extensive system experiments are used not only to validate the theoretical OFM models, but also to determine the practical challenges that accompany the OFM system approach. Furthermore, the ability of the OFM system to distribute RF signals with different modulation formats via different fibre infrastructure is also experimentally investigated.

The OFM-system comprises a headend, and a Remote Antenna Unit (RAU) as described in Chapter 3. When used as a mere Local Oscillator (LO) generator, no fibre link between the headend and the RAU is needed. However, to deliver RF signals from the headend to a RAU, a fibre link in between is needed. Both SMF and MMF (including Polymer Optical Fibre, POF) links of different lengths were investigated.

The chapter begins by discussing the various electro-optical and opto-electronic components required for the OFM system. The composition of the headend and the simplified RAU are presented. This is followed by system experiments involving the generation of un-modulated LO signals. The quality of the OFM-generated signals, in terms of electrical linewidth and LO phase noise was measured before and after fibre transmission. The measured results were used to validate the OFM models presented in Chapters 3 and 4. Different filter implementations of both the MZI and the FPI

types were explored. These included the fibre-based MZI, the fibre-based FPI, the FBG-based FPI, the semiconductor material-based FPI, and the chip-based MZI. Finally, the up-conversion and remote delivery of modulated RF signals through OFM was demonstrated. Simple Amplitude Shift Keyed (ASK) and complex multilevel modulation formats including xQAM were used. Error Vector Magnitude (EVM) and Bit Error Rate (BER) measurements were performed to determine the performance of the OFM system.

5.2 Optical FM Sources

OFM requires a Frequency Modulated, FM (or Phase Modulated, PM) optical signal. The optical FM/PM source could be a continuously tunable laser source, where a sweep signal, f_{sw} is used to continuously sweep the laser wavelength. However, the tuning speeds of electronically tunable laser sources are still limited to a few hundred MHz at best [88]. That means an OFM system employing a tunable laser as the FM/PM source would not be able to support very high-frequency systems, since very high multiplication factors, and large FM indexes would be required. For instance a tunable laser capable of being driven at 500 MHz, requires an FM index of 54 for optimal 30 GHz operation (60th harmonic) using a filter with the FSR equal to 2.5 GHz. In that case, the phase noise of the generated carrier would be 36 dB higher than that of the sweep signal (see section 3.6.2).

An alternative to the tunable laser FM/PM source is an optical phase modulator. That is, a combination of a CW laser source followed by an optical phase modulator may be used to achieve optical FM [51], [62], [89]. In that case, the applied phase modulation signal must be an integral of the desired frequency modulation signal as described by equation (5.1) [90].

$$m_p(t) = \frac{D_f}{D_p} \int_{-\infty}^t m_f(\sigma) d\sigma \quad (5.1)$$

where D_f is the frequency modulation sensitivity measured in rad/V·s, D_p is the phase modulation sensitivity measured in rad/V, and m_f is the desired FM modulating signal. For a sinusoidal sweep signal, pre-integration of the sweep signal is not required. This makes the sinusoidal swept OFM source simpler as shown in Figure 5.1. In that case, the FM index, β_{FM} is equivalent to the peak phase deviation, $\Delta\theta_{pk}$:

$$\beta_{FM} = \frac{\Delta f_{pk}}{f_{sw}} = \Delta\theta_{pk} = \beta_{PM} \quad (5.2)$$

For non-sinusoidal sweep signals, the need for a high-speed integrator may pose a great challenge, even though non-sinusoidal sweep signals such as the triangular sweep, offer some performance advantages [51].

The PM approach has the advantage that sweep frequencies in the GHz range may be used, because high speed phase modulators are readily available. For this reason the

CW laser-PM combination was used as the FM source in all the reported experiments except for one experiment involving the use of a tunable laser as the FM source.

5.3 FM Index Control

In Chapter 3, the FM index, β_{FM} has been identified as a key parameter in the OFM system. The impact of the FM index on the performance of the OFM system has been explored in Sections 3.2.3, and 3.3.3. It has been established that the relative strength of the generated harmonic components are directly dependent on the FM index. Therefore, control of the FM index is of paramount importance in the OFM system.

On inspection of the harmonic-strength-vs.-FM index plots in Figure 3.5, and Figure 3.12 for both the MZI-, and the FPI-based systems respectively, it is observed that in general higher multiplication factors require larger FM indexes. That means that to practically realise a high-multiplication factor OFM system, the obtainable FM indexes have to be large enough. For instance, an OFM system optimised for a 30 GHz mm-wave delivery using a 6 GHz sweep signal requires an FM index of about 3.4 (5th harmonic) for peak power performance. The theoretically required optimal FM index, increases to 4.7 if the 6th harmonic component is employed in an 18 GHz OFM system, with a sweep signal of 3 GHz.

In order to measure the dynamic response and PM index of an optical phase modulator, it is necessary to transform the phase modulation into intensity modulation. This may be done in many ways. A method, which uses the electro-optically induced birefringence of the modulator and a polarizer to achieve the PM-IM conversion is reported in [91]. Another method, with the ability to measure the optical frequency chirp with a high time resolution is reported in [92]. The latter method was used to measure the actual FM index obtained from the CW laser-phase modulator FM source by first measuring the time-resolved chirp generated by the phase modulator as shown in Figure 5.1. To do this, a tunable Fabry Perot (FP) etalon was used as an optical frequency discriminator to convert the variations in the optical frequency into intensity in real time. The FP had a Free Spectral Range (FSR) equal to 0.5 nm, and was made by *Micron Optics*.

With the FP etalon biased at a linear portion of its transmission curve, the optical signal exiting the etalon was detected and measured by a high-speed sampling scope. By using the *Airy function* given in equation (3.22), which describes the signal transmission through a planar FP etalon, the relationship between the measured voltage (intensity signal) and the corresponding chirp could be established. Assuming that the frequency chirp $\Delta f \ll \text{FSR} / 2\pi$, this relationship is given by equation (5.3) [92]:

$$\frac{V_+(t) - V_-(t)}{V_+(t) + V_-(t)} \approx \Delta f(t) \cdot \frac{2\pi}{\text{FSR}} \sqrt{(1 - T_0) \left[T_0 \frac{(1 + R)^2}{(1 - R)^2} - 1 \right]} \quad (5.3)$$

where Δf represents the signal chirp, V_+ and V_- are the intensity signals measured when the FP etalon is biased at the transmission curve with the positive and negative slopes, respectively.

An example of the time resolved chirp measured for a 2 GHz sweep signal is shown in Figure 5.2. The measurement confirmed the shape of the FM sweep, which was sinusoidal, as shown. From the figure, the peak frequency deviation, Δf_{pk} is about 10 GHz. Thus, by using equation (5.2), the FM index, β_{FM} is determined to be about 5.

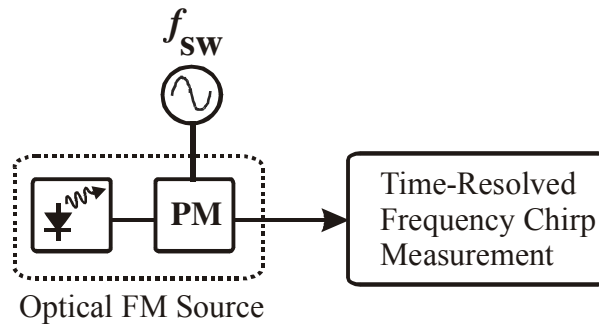


Figure 5.1: Measuring the FM index of the optical phase modulator

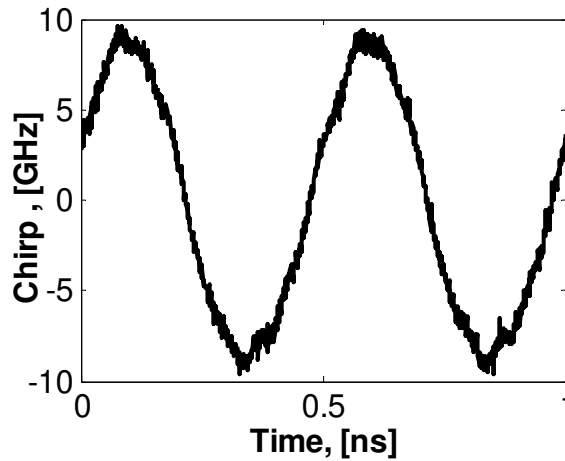


Figure 5.2: Measured time-resolved optical frequency chirp induced by the phase modulator; $f_{sw} = 2$ GHz

From equations (5.1), and (5.2), the FM index, β_{FM} is given by:

$$\beta_{FM} = D_p \cdot V_{pk} \quad (5.4)$$

where V_{pk} is the peak voltage of the phase modulating signal, $m_p(t)$. Therefore, the FM index is directly controlled by controlling the amplitude (i.e. power, P_{sw}) of the

sweep signal, f_{sw} . The sensitivity of phase modulators is normally specified at the half-wave voltage, V_π (i.e. the voltage by which the phase is rotated over π), so that

$$D_p = \frac{\pi}{V_\pi} \quad (5.5)$$

That is, the lower the half-wave voltage, the higher the sensitivity, and the better the OFM up-conversion efficiency.

Using the time resolved chirp measurement method, the phase sensitivity (and half-wave voltage) of a commercially available optical phase modulator (*Sumitomo* TPM1.3-5) was determined for various sweep signal frequencies of interest, i.e. between 1 and 3 GHz. The half-wave voltage was found to vary between 4.0 V, and 4.5 V corresponding to phase sensitivities of 0.785 and 0.70 respectively. These values were within the specified maximum half-wave voltage (< 5 V), but differed from the test value (2.9 V), measured at measured at a lower frequency (100 kHz) and included in the manufacturer's specification sheet of the device.

Equation (5.4) shows that the practical limit to the maximum obtainable FM index from the CW-laser PM source is the maximum power rating of the phase modulator device itself. It was verified that FM index values exceeding 7, could be obtained, without damage to the device.

5.4 Microwave LO Generation with OFM

Because OFM suppresses laser phase noise (see Section 3.5), it is an interesting method for optically generating high-frequency LO microwave, and mm-wave signals. This section describes the experimental realisation of an OFM-based high-frequency LO signal generator.

5.4.1 Experimental Set-up

The basic OFM experimental set-up used for up-conversion, and generation of microwave signals is given in Figure 5.3. A DFB laser emitting in the 1310 nm window was used as the CW laser. The laser was connected to a low-speed (5 GHz) commercially-available phase modulator (*Sumitomo* TPM1.3-5) through an optical isolator to prevent any back reflection into the laser. The phase modulator was driven by a sweep signal, f_{sw} , having a frequency below 3 GHz, and amplified by an electrical high-power driver amplifier (36 dB). The actual sweep signal frequency was dictated by the required microwave frequency, and its harmonic order.

The output of the phase modulator was fed into a custom-made MZI, or other filter. The MZI was made from single mode fibres, and had a path-length delay of about 100 ps, yielding a FSR equal to approximately 10 GHz (see Section 3.2), as shown in Figure 5.4. The transmission characteristics of the MZI were measured by using a tunable laser and a power meter. An isolator was placed between the phase modulator and the interferometer to prevent any light reflections from propagating back into the

phase modulator. Thus, the CW laser, phase modulator, and interferometer made up the OFM system's headend.

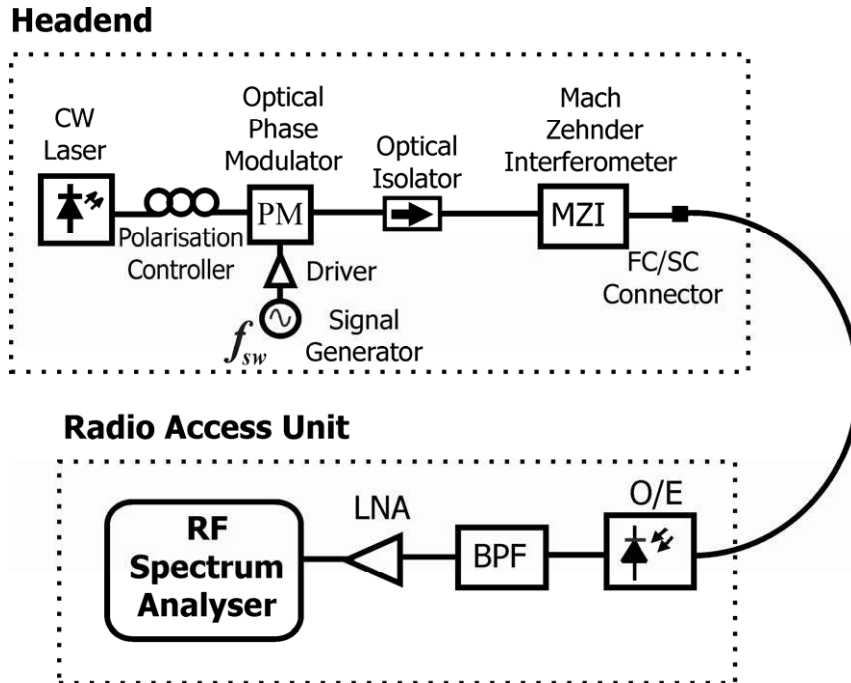


Figure 5.3: OFM Experimental Set-up for Generating Microwave LO Signals

The Radio Access Unit (RAU) comprised a photodetector, a microwave bandpass filter (BPF) to select the required harmonic component and a Low-Noise Amplifier (LNA). A 40 GHz RF spectrum analyser (*Rohde & Schwarz FSQ 40*) was used to analyse the generated microwave signal.

The photodetector was a Schottky type operating at wavelengths 950 nm – 1650 nm. The responsivity, R of the detector was about 0.6 at 1300 nm. The -3 dB bandwidth of the detector was 25 GHz, and it had a 50 μm FC connector for multimode fibre input.

The microwave BPF was a waveguide type fitted with waveguide-to-SMA adapters. The -3 dB bandwidth of the filter was 300 MHz [93]. The filter's centre frequency was adjusted to 17.2 GHz, to coincide with the Dutch license-free RLAN frequency band specified for 17.1 – 17.3 GHz (200 MHz) [93], [94]. The LNA had a gain of 35 dB, a maximum noise figure equal to 7 dB, and an operating bandwidth of 2 to 20 GHz.

In the back-to-back system configuration, the output from the interferometer was connected directly to the photodetector by a short single mode fibre patch cord.

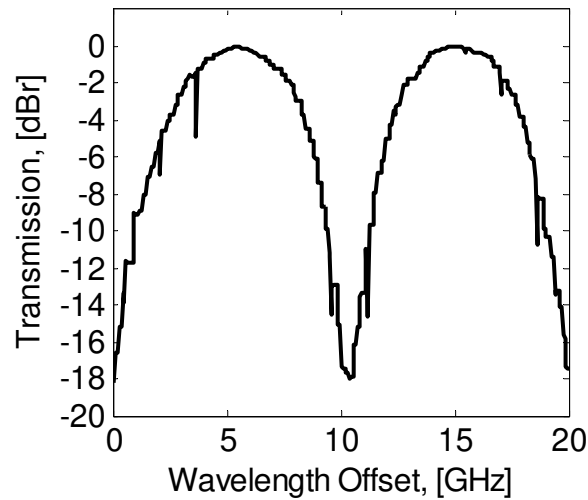


Figure 5.4: Transmission Characteristics of the Fibre-based MZI Filter

5.4.2 Harmonic Component Selection

Figure 5.5 (a) shows the OFM-generated frequency harmonic components before filtering, using the sweep signal, f_{sw} RF power of -8 dBm. The sweep signal frequency, f_{sw} was set to 2.867 GHz in order to generate the target microwave frequency f_{mm} , equal to 17.2 GHz. The target microwave signal was therefore the 6th harmonic component of the sweep signal. The FM index was approximately 4.5. After filtering, all the un-desired harmonics were eliminated as shown in Figure 5.5 (b), leaving only the 17.2 GHz LO.

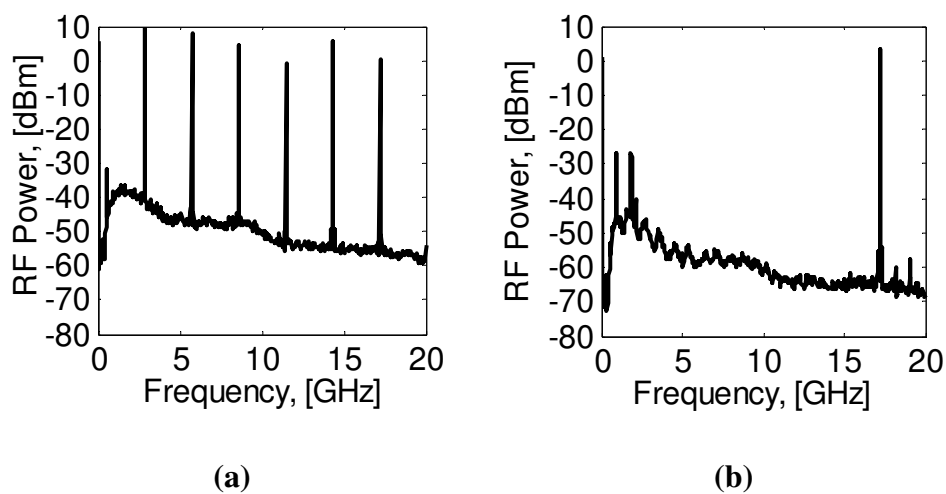


Figure 5.5: OFM Generated Microwave Carriers (a) before filtering, and (b) after filtering

Figure 5.6 shows the time plot of the OFM-generated electrical signal exiting the photodetector, and prior to filtering. The time plot was obtained by replacing the RF Spectrum Analyser with a high-speed sampling scope [95], [96]. In this measurement, the sweep signal frequency was 2 GHz. The figure confirms the illustration of the principle of Optical Frequency Multiplication given in Figure 3.2. That is, a total of 4 transmission peaks of the MZI were traversed in one sweep period. Given that the FSR of the MZI was 10 GHz, it is clear that the peak-to-peak optical frequency deviation, Δf_{pp} , was 20 GHz, in this case.

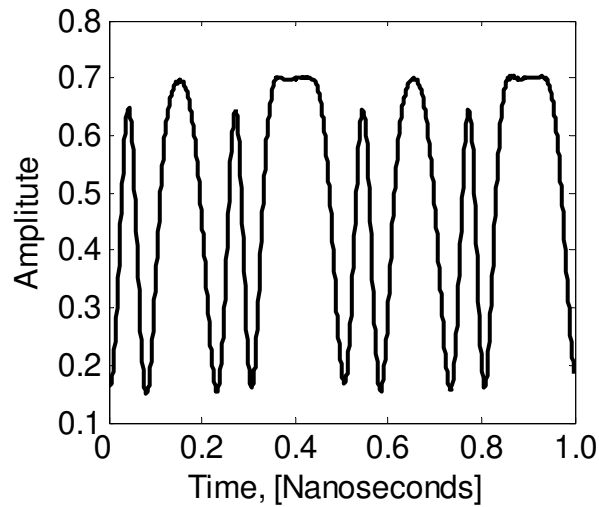


Figure 5.6: Time Plot of the Detected Electrical Signal at the Radio Access Unit of the OFM System Prior to Filtering – $f_{sw} = 2$ GHz.

5.4.3 Impact of FM Index

The impact of varying the FM index, β (i.e. the peak phase deviation, $\Delta\theta$ in this case), was investigated experimentally. The effective RF power, P_{sw} of the sweep signal, f_{sw} applied to the phase modulator was varied from -14 dBm to +30 dBm, and the power of the generated 2nd and 6th harmonic components observed. The result is given in Figure 5.7. It is observed that the amplitude of the various harmonic components varied with the RF power of the sweep signal applied to the phase modulator. The peaks and nulls that are predicted by the OFM model presented in Chapter 3 are also clearly observed.

In order to compare the measured system behaviour with the modelled one (Chapter 3), the measured results were superimposed on the theoretical prediction based on the OFM model of equation (3.5) [97]. The measured results agreed very well with the predicted behaviour as shown in Figure 5.7. It was confirmed that an OFM system using a sweep frequency, f_{sw} of about 3 GHz, and a MZI having a FSR equal to 10 GHz, requires an FM index, β equal to about 5 in order to generate peak power of the

6th harmonic component. Therefore, the prediction of the impact of the FM index based on the OFM model of equation (3.5), and given in Figure 3.5, was verified experimentally.

Furthermore, Figure 5.7 also shows an interesting mapping between the applied RF power of the sweep signal and the effective FM index. If the effective resistance of the phase modulator is known, the effective phase sensitivity, D_p and the half-wave voltage, V_π can quite accurately be determined from Figure 5.7 as well, by using equation (5.4).

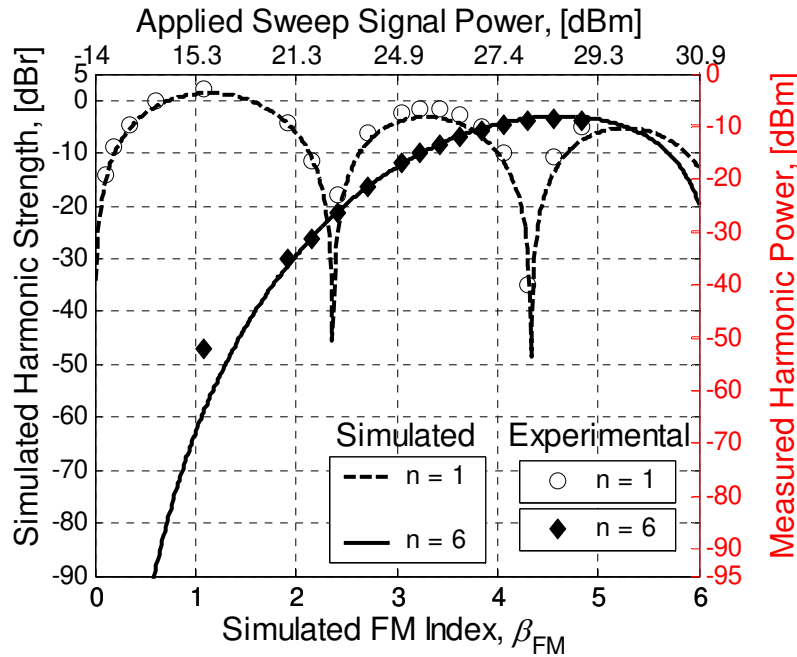


Figure 5.7: Experimental Verification of the Simulated Impact of the FM Index on the Strength of the OFM-Generated Harmonic Components.

5.5 Linewidth and Phase Noise of the OFM Generated Microwave LOs

5.5.1 Impact of Light Source Linewidth

The impact of laser phase noise on the electrical linewidth of the OFM-generated harmonic components has been analysed theoretically in Section 3.5. It has been shown that when operating in the coherent regime (i.e. optical linewidth, $\delta\omega \ll 2\pi \cdot \text{FSR}$), the OFM system eliminates laser phase noise. In order to verify this assertion, the optical linewidth of the laser source was measured and compared with the measured electrical linewidth of the generated LOs.

The optical linewidth of the CW laser was measured by the Delayed Self-Homodyne method [64], [65], [69], [98] - [104]. A 6 km piece of standard single mode fibre was used to de-correlate the two optical signals from the laser. Assuming a group velocity index, v_g of approximately 1.47 for the fibre, the long path delay, τ_p was approximately 30 μs . From equation (5.6) the coherence time, τ_c of a laser with 1 MHz Lorentzian-shaped linewidth is 0.32 μs . Therefore, the incoherent regime condition $\tau_p/\tau_c \geq 1$ was satisfied [69].

$$\tau_c = \frac{1}{\pi\Delta\nu} \quad (5.6)$$

The measured optical linewidth is shown in Figure 5.8a. The measurement confirmed that the linewidth of the DFB laser approximated the Lorentzian shape, as shown by the theoretical curve. The FWHM linewidth of the laser was estimated to be about 0.8 MHz. The FWHM electrical linewidth of the 16 GHz signal (see Figure 5.8b) generated using OFM was found to be less than 20 Hz [95], [96]. This result confirmed the theoretical analysis presented in Section 3.5, which shows that OFM suppresses laser phase noise.

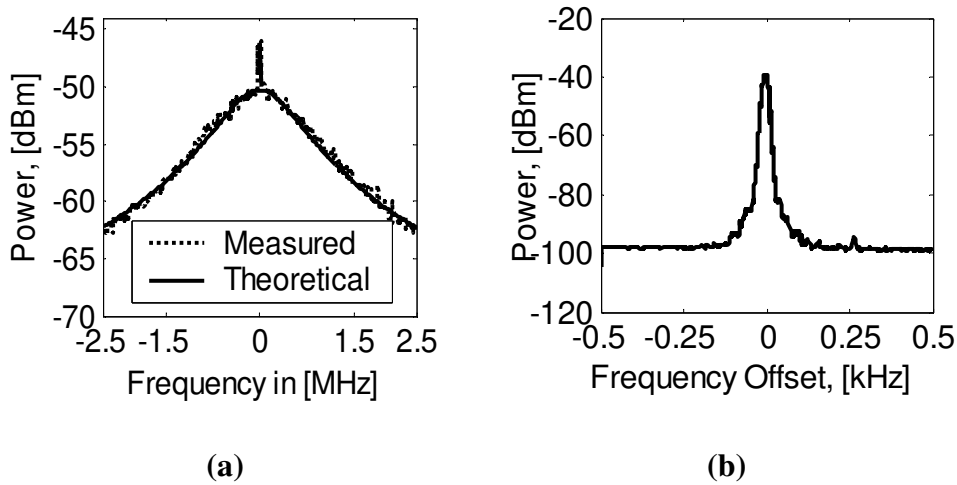


Figure 5.8: Measured Linewidth of (a) the Laser source, (b) an OFM-Generated 16 GHz Microwave Signal

5.5.2 Impact of Sweep Signal Phase Noise

Using an RF spectrum analyser equipped with phase noise measurement capability, the phase noise of the OFM-generated harmonic components was measured [97]. In this measurement, it was imperative to keep the phase noise being measured above that of the measuring equipment itself to avoid characteristic errors. Thus, a signal generator with relatively higher phase noise was used to generate the sweep signal in some of the experiments.

Figure 5.9 shows the measured phase noise of the fundamental and six other harmonic components. Included in Figure 5.9 is the phase noise of the sweep signal itself. At 10 kHz offset the phase noise of the fundamental (3 GHz) was -93 dBc/Hz. The phase noise increased to various levels rising up to -76 dBc / Hz for the 7th harmonic component. The measured increase in phase noise at 10 kHz offset for all the frequency components is given in Table 5.1. The theoretical increase in phase noise due to OFM was estimated using equation (3.43). By comparing the theoretical increase and the measured increase in phase noise, we conclude that the phase noise of the up-converted harmonics varies proportionally to the square of the up-conversion factor, N , with respect to the phase noise of the sweep signal (see section 3.6.2). It is also clear that OFM easily achieves the theoretical performance for both low and high up-conversion factors exceeding 6.

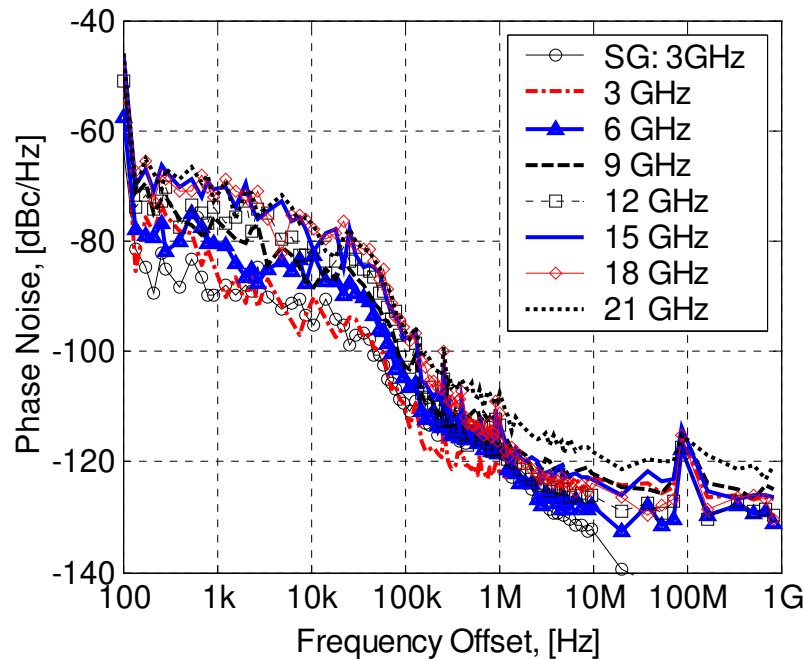


Figure 5.9: Measured Phase Noise of OFM-Generated Microwave LOs (SG = Signal Generator)

Since the phase noise of the OFM generated microwave signals varies proportionally to the square of the multiplication factor relative to the sweep signal phase noise, there are two obvious ways to generate low-phase noise microwave signals – namely, to use a lower multiplication factor (higher sweep signal frequency), or to use a low-phase noise sweep signal. Low frequency electronic LOs with very good phase noise are readily available, making it possible and flexible for the OFM system to meet LO phase noise requirements [89], [97].

Table 5.1 Measured SSB Phase Noise Increase at 10 kHz Offset for OFM Up-Converted Microwave LOs

n	f_{mn} [GHz]	$\Delta L_{\phi}(f_{mn})$ (Measured) [dB]	$\Delta L_{\phi}(f_{mn})$ (Theoretical) [dB]
1	3	0	0
2	6	6	6
3	9	9	9.5
4	12	11	12
5	15	13	14
6	18	15	15.6
7	21	16	16.9

For instance, by using a different sweep signal generator with lower phase noise than the first generator used in the measurements discussed above, the phase noise of an 18 GHz carrier (6th harmonic) was reduced from -80 dBc/Hz to -100 dBc/Hz at offset frequencies between 10 kHz to 100 kHz as shown in Figure 5.10. This represents a 20 dB gain in phase noise reduction. Phase noise is very important because it causes uncertainty during the detection of multi-level modulation formats such as xQAM (used in wireless systems) leading to increased Bit Error Rate (BER). Phase noise also degrades the selectivity of the receiver through reciprocal mixing (see section 3.6.1).

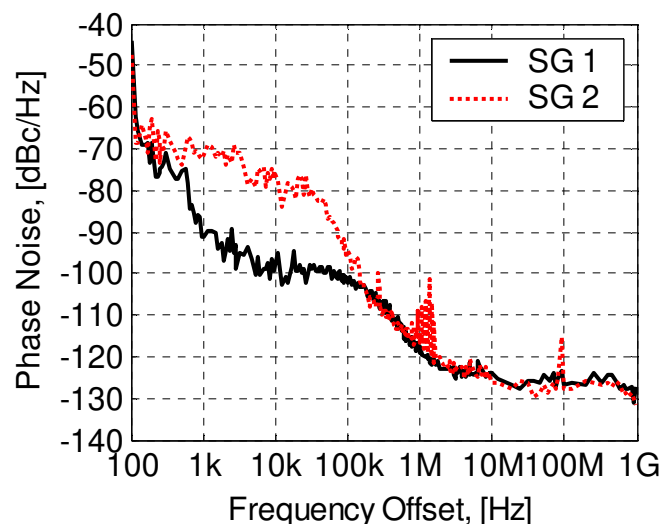


Figure 5.10: Comparison of the SSB Phase Noise of the 18 GHz (6th Harmonic) LO Generated by the OFM System Using 2 Different Sweep Signals

Since the sweep signal generator is stationed at the headend, it can be shared among several radio access units. Thus, the use of a sophisticated sweep signal generator at the headend, if required, would not overly add to the costs pertaining to each RAU.

5.6 Single Mode Fibre-based OFM Downlink

The OFM system was used to up-convert microwave signals delivered to remote RAUs fed by different lengths of single mode fibre [54], [97]. It was observed that apart from the fibre-attenuation-induced loss, there was no other perceivable signal degradation. Figure 5.11 shows a comparison of the phase noise of an 18 GHz signal generated in a back-to-back OFM system with the phase noise of the same mm-wave signal received after 25 km of standard single mode fibre. The phase noise at 10 kHz offset was about -96 dBc / Hz in both cases. No significant change in phase noise was observed.

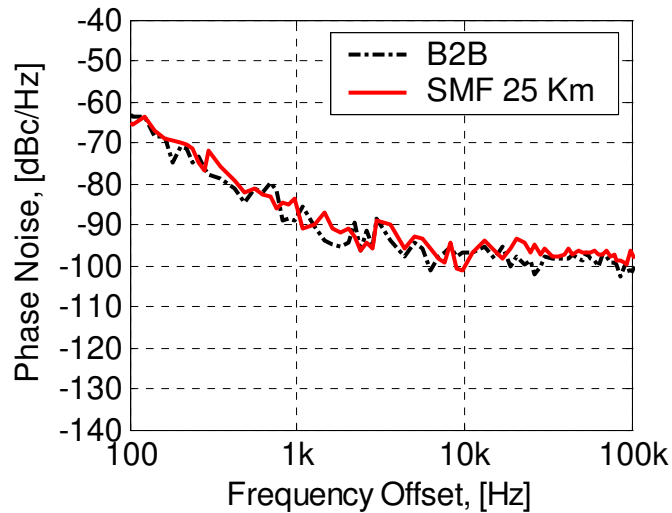


Figure 5.11: Comparison of the SSB Phase Noise of the 18 GHz (6th Harmonic) LO Generated by the OFM System Before and after Transmission over 25 km of Standard SMF.

5.7 Multimode Fibre-based OFM Downlink

To experimentally investigate the capability of the OFM system to perform combined frequency up-conversion and remote delivery of high-frequency microwave carriers over multimode fibre links, the experimental set-up shown in Figure 5.12 was used. Since the headend comprised SMF-pigtailed components, and knowing that the performance of multimode fibres is often strongly linked to the launch conditions as observed in Chapter 4, two methods of coupling to the 50 μm -core diameter MMF link were examined. The first one involved simple SMF-MMF butt-coupling. The second method involved coupling to the MMF through a Mode Scrambler (MS).

5.7.1 Single Mode Fibre Butt-Coupling

Coupling the headend to the fibre was achieved by using simple FC/PC fibre connectors. This is equivalent to central launching. Because the SMF core diameter ($9\ \mu\text{m}$) is much smaller than the MMF core diameter ($50\ \mu\text{m}$), this was also an under-filled launch condition where only the low-order modes were excited. The experiments were repeated numerous times to verify their repeatability.

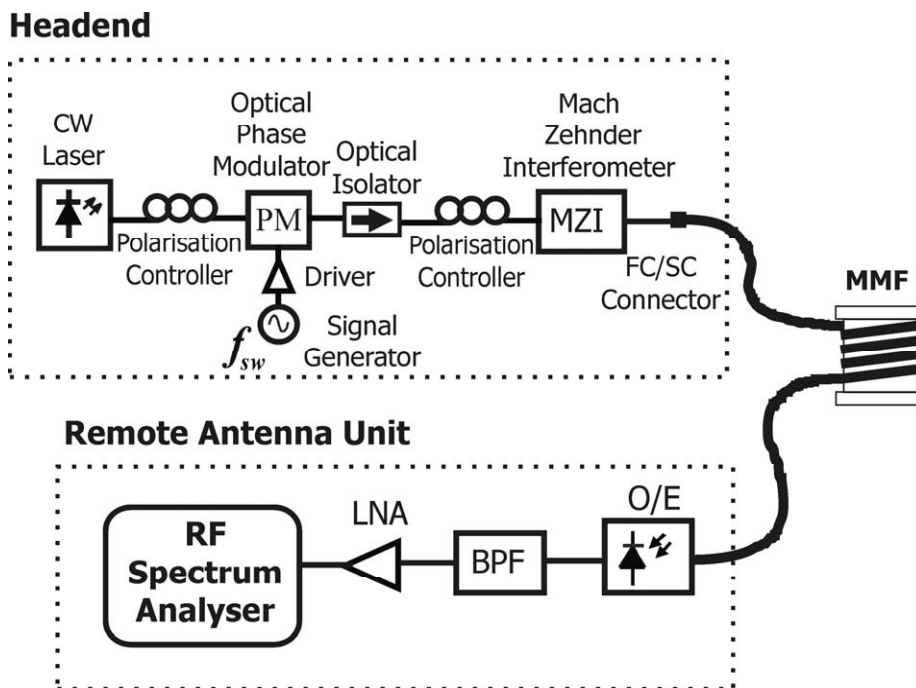


Figure 5.12: OFM System for Frequency Multiplication and Delivery of LOs over 4.4 km MMF

At the RAU, the MMF was coupled to the photodetector, which had a $50\ \mu\text{m}$ -core diameter MMF interface. This ensured that no losses occurred when coupling to the detector, and more importantly eliminated spatial filtering, which causes undesired intensity fluctuations, and modal noise [86], [87].

The frequency response of the MMF under the launch and coupling conditions described above was measured by using an *HP Lightwave Component Analyser* (LCA). In order to make sure that the same optical source used in the OFM system experiments was used in the frequency response measurements, an external Intensity Modulator (IM) was used instead of the LCA's internal modulator and laser (a $1300\ \text{nm}$ Fabry Perot laser). In addition, the effects of all the components were calibrated out, prior to the fibre response measurement. In this way, the measured MMF

response represented the true picture of the MMF link transmission characteristics in the OFM system experiments.

The measured frequency response of the 4.4 km MMF link is given in Figure 5.13. The -3 dB bandwidth was found to be about 950 MHz [54]. Beyond this bandwidth the response was relatively flat with a number of shallow high order passbands clearly visible at frequencies around 3 GHz, 10.2 GHz, 13.1 GHz, and 16.2 GHz. This behaviour is in line with the theory presented in Sections 4.4.2, and 4.4.3. It is clear that under these conditions the fibre may be used for SCM-based systems, and direct RoF transmission, as was reported in [19], [20].

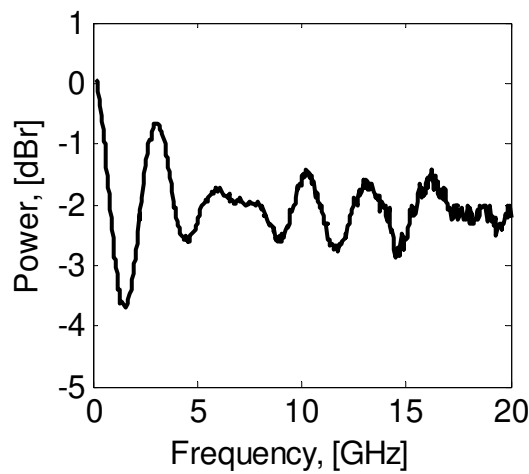


Figure 5.13: Frequency Response of 4.4 km MMF Under SMF Launch

The phase noise of the 17.2 GHz signal generated at the RAU was measured and is given in Figure 5.14. At 10 kHz offset the phase noise was about -92 dBc/Hz. This represents a 5 dB increase over the back-to-back system (see Figure 5.11), which is attributed to the multimode fibre [54]. The cause of this increase may be explained by the new phase term, $\theta_{\Delta\tau}$ (see equation (4.26)) which appears in the MMF-based OFM model developed in Section 4.5. As is stated there, in cases where modal equilibrium is not attained, as it is in this case, this term may fluctuate and contribute to the phase noise of the LO.

Also included in Figure 5.14 is the phase noise of the 17.2 GHz signal generated directly from a high-frequency signal generator (*Rohde & Schwarz SMR 20*). Comparing the SSB phase noise generated by the OFM system and the commercially-available high-frequency electronic signal generator, it is observed that the OFM-based LO generator outperformed the high-frequency electronic signal generator by 10 dB [54].

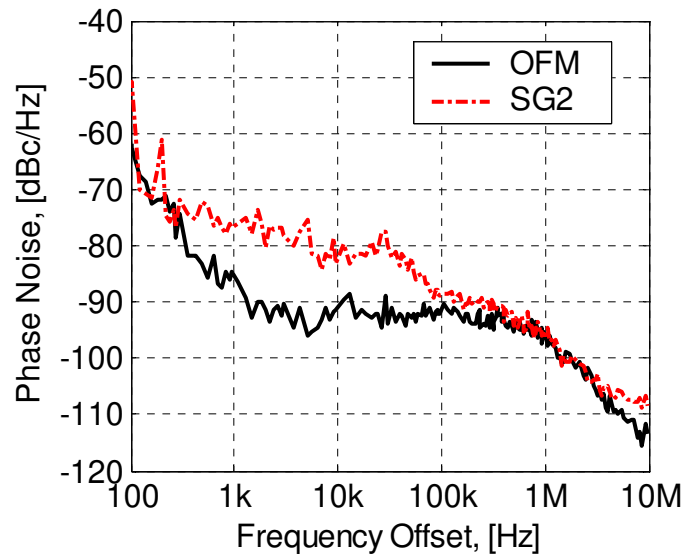


Figure 5.14: Comparison of the SSB Phase Noise of the 17.2 GHz (6th Harmonic) LO Generated after Transmission over 4.4 km MMF and that of the 17.2 GHz LO Generated Directly by a Commercially-Available Electronic Signal Generator

5.7.2 Coupling Through the Mode Scrambler

In order to launch more modes into the multimode fibre, an experimental Mode Scrambler (MS) made by *Draka Fibre*, was placed between the output SMF of the MZI and the MMF link as shown in Figure 5.15. The MS was a Step-Graded-Step index type, with the numerical aperture, N_A equal to 0.3. The core diameter of the MS fibres was 66 μm . Because the core diameter of the MS was larger than that of the MMF, some coupling losses occurred.

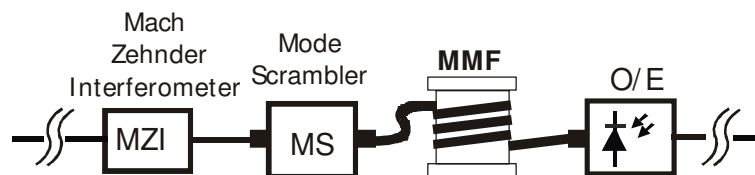


Figure 5.15: Using a Mode Scrambler to Measure the Impact of Modal Dispersion on the OFM System

The impact of using the MS instead of SMF butt-coupling on the frequency response of the MMF was measured, and the result is presented in Figure 5.16. A sharp drop in the -3 dB bandwidth from 950 MHz to about 300 MHz was observed. In addition the high order transmission passbands became narrower, and their peaks more attenuated.

For instance, the peak of a passband at 16.9 GHz is 17 dB below the baseband peak. It was further observed that the measured response was not stable suggesting a non-equilibrium modal distribution situation.

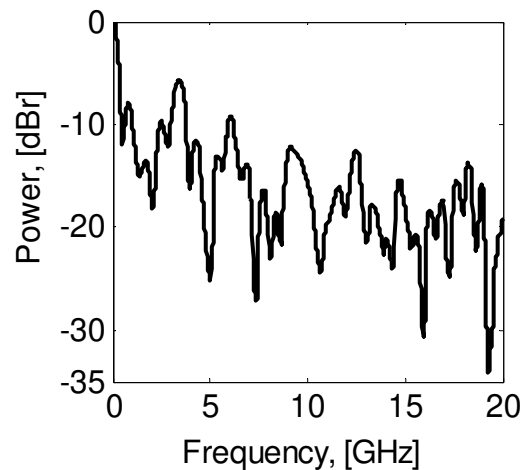


Figure 5.16: Frequency Response of 4.4 km MMF Under Mode Scrambler Launch

In order to determine the effect of the MS on the OFM system, the MS was placed between the MZI in the headend, and the MMF link as shown in Figure 5.15. The power of the generated 17.2 GHz signal measured on the spectrum analyser was -35 dBm. Afterwards, the MS was removed and the photodetector connected directly to the output of the MMF. The measured power of the 17.2 GHz carrier was then -17 dBm, as shown in Table 5.2. The difference in the received optical power was just 1.9 dB, which was due to the MS's coupling losses. The extra 14 dB attenuation experienced by the carrier signal is therefore attributed to the altered MMF frequency response as a result of the MS launch condition.

Table 5.2 Impact of MMF Launch Conditions on the OFM-Generated RF Signals

	MMF Launch Condition		Difference
	SMF-butt	MS	
Received Optical Power	-5.7 dBm	-7.6 dBm	1.9 dB
Generated RF Power	-17 dBm	-35 dBm	18 dB

This result firmly confirms the theoretical model, and analysis presented in Section 4.5, where it was concluded that the OFM-generated harmonics are scaled by the

MMF's intensity modulation transfer function, $|H_{\text{MMF}}(\omega)|$. This means that the level and position of the MMF's passbands are important issues in the MMF-based OFM system, just as they are in SCM-based systems, and others. However, for SMF-based system applications employing the OFM technique, there are no such concerns as OFM is chromatic dispersion tolerant (see Section 4.3).

In order to determine the nature of the actual modes launched into the MMF under the MS-based launch condition, the Far Field Radiation (FFR) patterns of the MS, the SMF, and the MMF were measured. The FOTP-47 Standard was used as a guide [105]. The measurement was performed with the *Goniometric Radiometer*, which is a commercially available Far Field Profiler from *Photon Inc.* This device is capable of performing 3D scans about the optical axis, automatically.

First, the FFR pattern of the SMF pigtail of the DFB laser was measured. Then, the SMF was butt-coupled to one end of the MS and the FFR pattern measured at the other end. Finally, the MS was coupled to the 4.4km MMF link and then the FFR pattern measured at the output of the fibre. The results are presented in Figure 5.17.

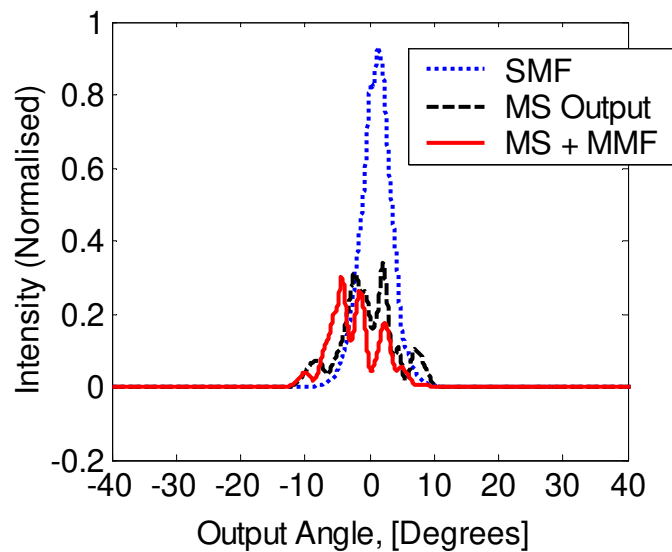


Figure 5.17: Measured Far Field Radiation Patterns from 4.4 km of 50 μm -core MMF Under SMF and Mode Scrambler Launch Conditions

It was observed that the MS distributed the power among several mode groups as opposed to a single mode in the SMF-butt coupling case. Therefore, by using the MS, more modes were launched into the 4.4 km MMF link, resulting in the alteration of the fibre's frequency response given in Figure 5.16. This result is in line with the theoretical fibre modelling discussed in Chapter 4.

It must be mentioned that the non-smooth FFR pattern measured suggests that the MS did not produce a continuous distribution of mode groups [77]. In other words, some mode groups were not excited. This implies that even though more mode groups

appear to have been launched into the MMF link, this was still not an overfilled launch condition (OFL). By comparing the FFR pattern at the input, and the output of the MMF, which is virtually unchanged as shown in Figure 5.17, we can conclude that there was little if any mode coupling in 4.4 km of the silica MMF. This means that even after 4.4 km, modal equilibrium was not attained. This explains why the measured frequency response was not stable [76], [77], [84]. Nevertheless, the MS-based launch condition was sufficiently different from the SMF-butt coupling condition, to enable the demonstration of the impact of modal dispersion on the OFM system.

5.8 Polymer Fibre-based OFM Downlink

Polymer Optical Fibre (POF) offers very attractive features for local networking, because of its easy handling. Due to the ductility of the plastic material, the POF core can be made much larger (120 μm – 1000 μm). The consequent draw back is that the bandwidth is limited by the large number of guided modes, which lead to increased modal dispersion. In addition, POF has a higher attenuation than silica fibres. However, in short-link applications (<500 m) the benefits of easy handling can translate into major system-wide cost savings owing to the reduced installation and maintenance costs [51].

The possibility to use OFM to transport and distribute high-frequency microwave signals over a short (330 m) POF link was explored [96]. The experimental set-up is given in Figure 5.18. The headend was the same as described above, except that in this case, the MZI was placed at the RAU. The same DFB laser emitting in the 1310 nm window was used. A pair of Microscope Objective Lenses (MOL) was used to couple light from the 120 μm -core Graded Index POF (GIPOF) to the Semiconductor Optical Amplifier (SOA)'s SMF pigtail (9 μm mode field diameter). The GIPOF was *Lucina POF* made by *Asahi Glass* from Perfluorinated (PF) polymers, and it had a specified bandwidth-length-product equal to 500 MHz-km, and an attenuation of 25 dB/km. The SOA was used to offset the coupling losses. After the MZI, a Spectrum Analyser and high-speed Sampling Scope, were used to detect the optical signal and to analyse the received electrical signal.

A 16 GHz carrier generated at the GIPOF-fed RAU is given in Figure 5.19. A good CNR was obtained (\approx 50 dB), and there was no degradation of the linewidth of the carrier after transmission on the GIPOF link [96]. Given that the specified bandwidth-length-product of the GIPOF fibre link was 500 MHz-km, all the transported carriers up-to- 20 GHz, were clearly beyond the baseband bandwidth. However, there were a lot of optical losses in this experiment. The total GIPOF fibre loss was about 10 dB, while the coupling loss was more than 15 dB. More importantly, intensity fluctuations of the generated carriers were observed. The intensity fluctuations were caused mainly by modal noise generated during the coupling of the GIPOF fibre to the SMF fibre. Thus, the coupling issue was the main challenge in the realisation of the GIPOF-based OFM system.

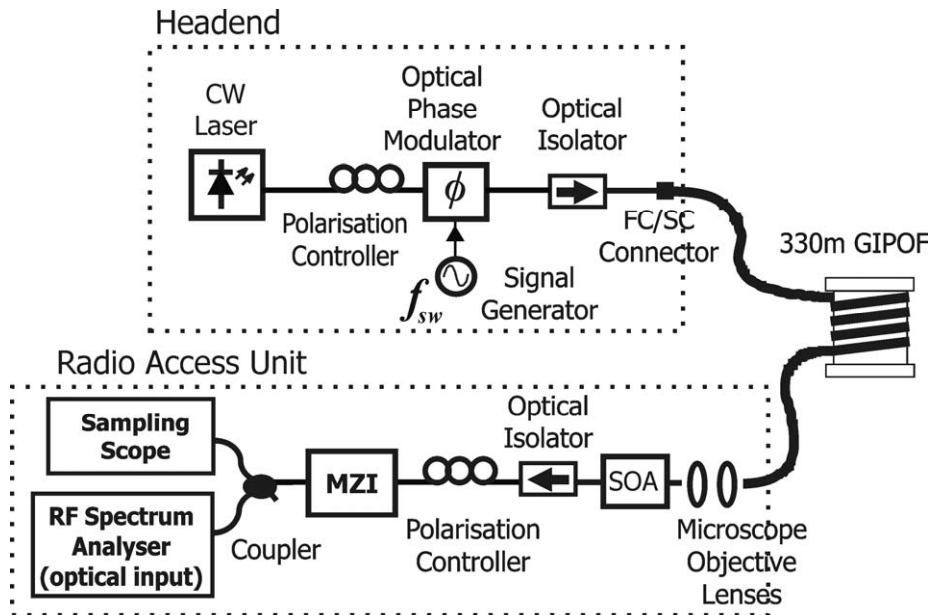


Figure 5.18: OFM Downlink over 330m of Polymer Optical Fibre

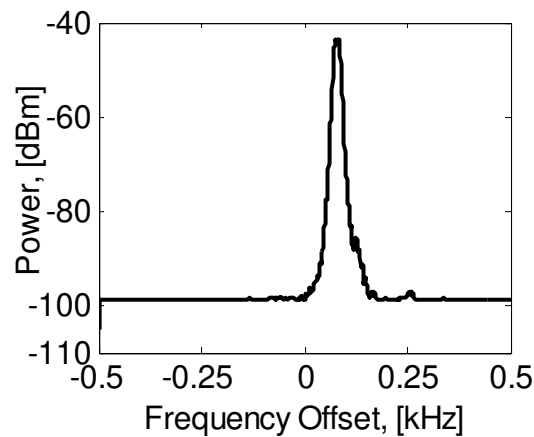


Figure 5.19: A 16 GHz Carrier Generated at a GIPOF Fed Radio Access Unit

In order to investigate the modal noise problem further, the GIPOF's Near Field Pattern (NFP) was examined. The NFP of the GIPOF's end-face was observed on a CCD camera under the SMF-butt coupling launch condition, and using the same 1310 nm DFB laser source, which was used in the OFM experiments. The observed NFP is shown in Figure 5.20.

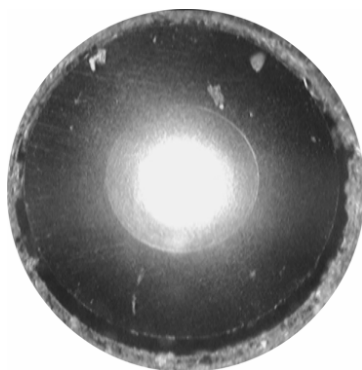


Figure 5.20: Near Field Image of 330 m GIPOF under SMF Butt-Coupling Launch Condition

Figure 5.20 shows that the core of the fibre appears to be fully illuminated. This attests to the perception that strong mode coupling exists in GIPOF [77], [80], especially considering that the fibre length was just 330m. However, variations in the speckle pattern were observed, indicating that modal equilibrium was not attained [86]. Therefore, capturing power from only a section of the GIPOF end-face, also known as *Spatial Filtering*, resulted in the fluctuation of the total received power, or modal noise, which was observed.

When a detector with an active area broad enough to capture all the light from the fibre end-face was used, modal noise seemed to disappear [93]. Thus, several different lens configurations were used to try and reduce the GIPOF-SMF coupling loss, and the modal noise. It was found that high loss and modal noise could not be eliminated from GIPOF-SMF ($120\ \mu\text{m} - 9\ \mu\text{m}$) coupling through lens imaging. However, it was established that appropriate lens imaging could reduce optical intensity fluctuations to very low levels (0.7 dB) if the GIPOF was coupled to a $50\ \mu\text{m}$ MMF instead [93]. These results indicate that POF-detector coupling is an important part of POF-based system, under SMF-butt coupling launch conditions.

5.9 A Tunable Laser-based OFM System

The experiments reported above were all conducted with a CW-laser-Phase-Modulator combination as the FM source. However an electronically Tunable Laser (TL) source may also be used as the FM laser source. In that case, only one device is needed instead of two. The overall OFM headed then becomes simpler and more compact. In addition to that, the use of a TL offers tremendous operational flexibility by making it possible to transparently set the operational wavelength of the system. Thus in a point-to-multipoint OFM system employing WDM, different wavelength resources may be allocated to the RAUs without any hardware modifications to the headend or the RAU of the OFM system [50]. Only the wavelength of the TL is tuned to a different one, leaving the rest of the system unchanged.

In order to experimentally investigate the feasibility of using a TL as the FM source in the OFM system, the CW Laser-Phase Modulator configuration was replaced by a commercially-available (*InTune Technologies*) Grating assisted codirectional Coupler with rear Sampled grating Reflector (GCSR) tunable laser diode, as shown in Figure 5.21 [106]. The GCSR laser provides wide tuning range (>100 nm), high Side Mode Suppression Ratio (SMSR), and has a potential for low-cost fabrication [107], [108]. The device consists of four sections, namely a gain section, a codirectional coupler section, a phase tuning section, and a reflector section as shown in Figure 5.21. By tuning the phase section of the GCSR laser with the sweep signal, a continuous swing in the wavelength was achieved. The GCSR laser was emitting in the 1550 nm window.

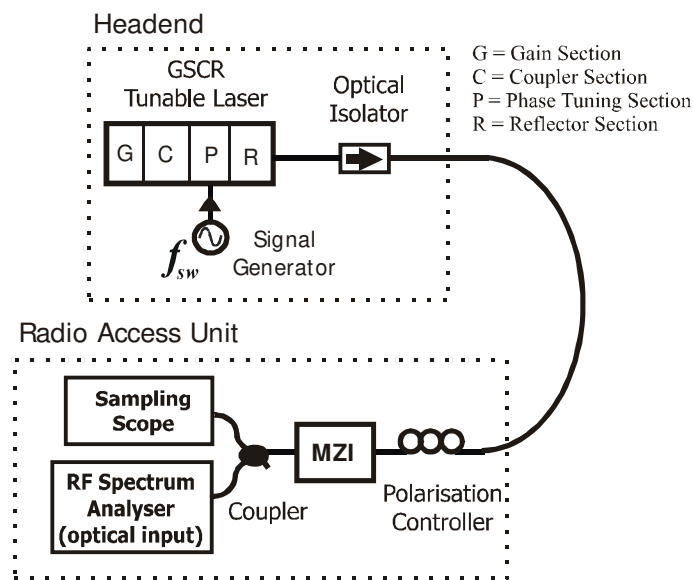


Figure 5.21: Using a Tunable Laser as the FM Optical Source in the OFM System

The power of the sweep signal P_{sw} was equal to 0.0 dBm. After detection of the optical signal received at the RAU, optical frequency multiplication was observed. Figure 5.22 shows the frequency spectrum, and time plot of the electrical signal generated with the 50 MHz sweep frequency. A high frequency up-conversion factor exceeding 10 was observed. From the time plot, the peak optical frequency deviation, Δf could be determined, since the MZI's FSR was known (10 GHz). For instance, the time plot in Figure 5.22 (b) indicates that 3 intensity peaks of the MZI were traversed in one swing period. This means that the peak optical frequency deviation, Δf was equal to 15 GHz, and the FM index, β equal to 300. This is an extremely high FM index. Using equations (5.2), and (5.4), the phase sensitivity, D_p of the GCSR was calculated as 938 rad/V. In contrast, the phase sensitivity of the phase modulator was 1.1 rad/V at 100 kHz, and approximately 0.8 rad/V at 3 GHz. (see Section 5.3). Therefore, the tunable laser offers a phase sensitivity, which is 3 orders of magnitude higher than that of the phase modulator. This means that considering the power of the sweep signal as the input to the OFM system, the GCSR-based system is much more

power efficient than the phase modulator based system. This can translate into major system operational savings. The high efficiency of the GCSR laser is due to the low drive currents required by the laser.

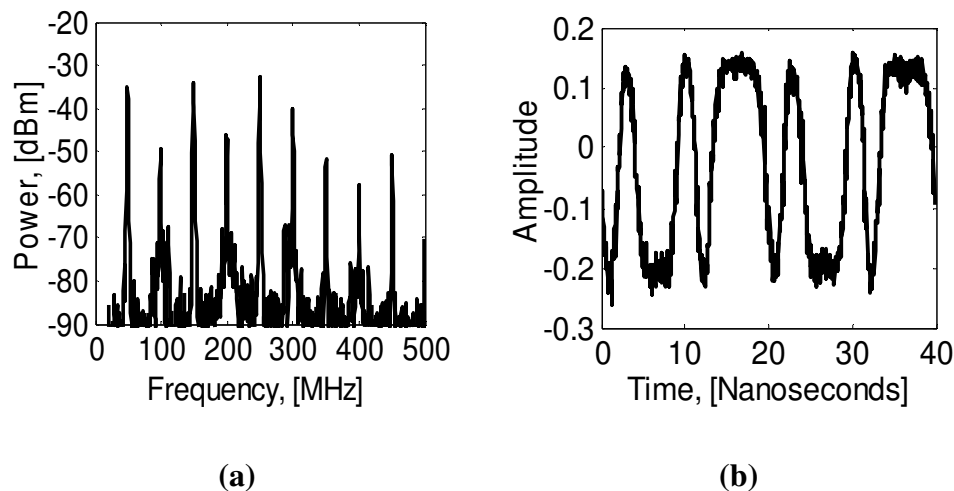


Figure 5.22: Electrical Signal Generated by an OFM System Using a GCSR Tunable Laser as the FM Optical Source (a) Frequency Spectrum, (b) Time Plot

To determine the tuning speed limit of the GCSR, the experiment described above was repeated for different sweep frequencies ranging from 20 MHz to 60 MHz, and the phase sensitivities determined for each sweep frequency. It was observed that the phase sensitivity was higher for the lower frequencies. Furthermore, the phase sensitivity at 60 MHz was 75 % lower than the phase sensitivity obtained with the 20 MHz sweep frequency.

The maximum tuning speed of the laser was less than 100 MHz. Therefore, this particular laser is not useful for a high-frequency OFM system operation. Nevertheless, the obtained experimental results clearly demonstrated the feasibility and potential benefits of using tunable laser sources in WDM-based OFM systems instead of the optical phase modulator.

5.10 Filter Implementations for the OFM System

The OFM experiments discussed above were all carried out with the fibre-based MZI whose transmission characteristics are given in Figure 5.4. However, a number of other interferometric filter implementations were also explored. These include a Fibre-based Fabry Perot Interferometer (FFPI), Fibre Bragg Grating based Fabry Perot Interferometers (FBG-FPI) made in both SMF and MMF, Fabry Perot Interferometer based on Wafer Optical Cavities, and a Chip-based MZI. This section discusses the measured performances of the filters and their pros and cons in terms of practical implementation.

5.10.1 Fibre based Fabry Perot Interferometer

A commercially-available SMF-based Fabry Perot Interferometer with a FSR of 10 GHz was acquired. The FFPI was manufactured by *Micron Optics, Inc* [109]. With no collimating optics, this range of filters are said to be capable of having very high finesse values. In addition, the finesse value of the filter could easily be chosen and specified. The FFPI used in the experiments had a high finesse of 31, and a -3dB bandwidth of 320 MHz. This corresponds to a plate reflectivity, R of 0.9, and a theoretical filter contrast ratio C , of about 26 dB [see equations (3.24) - (3.26)]. The filter was also equipped with a piezoelectric-based tuning mechanism [109].

Using a 1300 nm ASE noise source, the transmission characteristics of the FFPI were measured. The measured FSR of the filter was 10 GHz, as shown in Figure 5.23, in accordance with the specification. Because the resolution and dynamic range of the optical spectrum analyser used for this measurement were limited, a tunable laser and a power meter were used to measure the contrast ratio. The measured contrast ratio was about 25 dB, confirming the specified finesse. Unlike the MZI, the FFPI filter was not sensitive to polarisation changes – a major advantage of using the FFPI instead of the MZI filter.

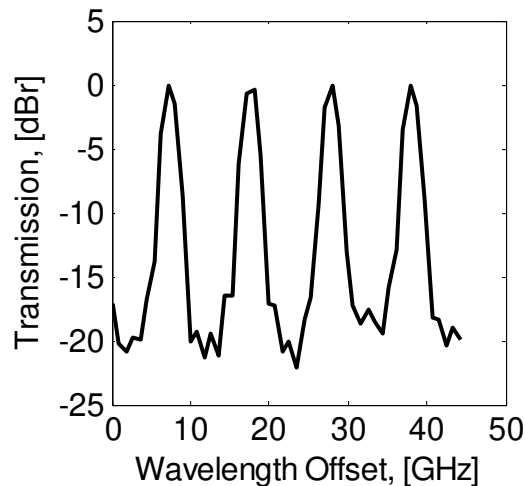


Figure 5.23: Transmission Characteristics of the Fibre-based Fabry Perot Interferometer

Using the FFPI in the OFM system, the received average optical power was 10 dB lower than that of the MZI-based system. This is expected from the different (sharp) response of the FFPI as compared to that of the MZI. With this low optical power the maximum peak power of the generated 17.2 GHz 6th harmonic component was -24 dBm. In contrast, there was sufficient average optical power (≈ 0 dBm) at the output of the MZI-based system to generate RF components of more than 0 dBm. The observed differences in the two systems are in line with the theoretical analysis presented in Chapter 3. That is, a high-finesse FPI-based system is less optical power efficient than a comparable MZI-based system for certain up-conversion factors.

However, the FPI-based system can be made just as efficient as the MZI-based OFM system by using the appropriate finesse, as has been shown in Chapter 3.

In Section 3.3.4 it has been stated that in general, a high finesse value (>10) is not necessary for high harmonic power operation. However, for high up-conversion values and other sweep signal shapes such as the linear sweep, high finesse values may be necessary [51] (see Figure 3.15). Furthermore, since in the OFM system the intensity modulation depth is directly proportional to finesse, a high finesse may be very useful in applications where a high intensity modulation depth is paramount.

5.10.2 Fibre Bragg Grating based Fabry Perot Interferometer

Several samples of Fibre Bragg Grating-based Fabry-Perot Interferometers (FBG-FP) were made by the *Grupo Comunicaciones Opticas* (GCO) of the *Universidad Politecnica de Valencia* (UPV) in Spain for experimentation with the OFM system. The devices were made by writing two FBGs in the fibre, defining an optical cavity in between. The gratings were made in both SMFs and MMFs.

Figure 5.24 shows the transmission characteristics of the MMF-based FBG-FP. The figure shows that interferometric behaviour was achieved. The operating wavelength was around 1318.8 nm . This wavelength is close to the target wavelength of 1310 nm , and it was determined by the Bragg wavelengths of the two gratings.

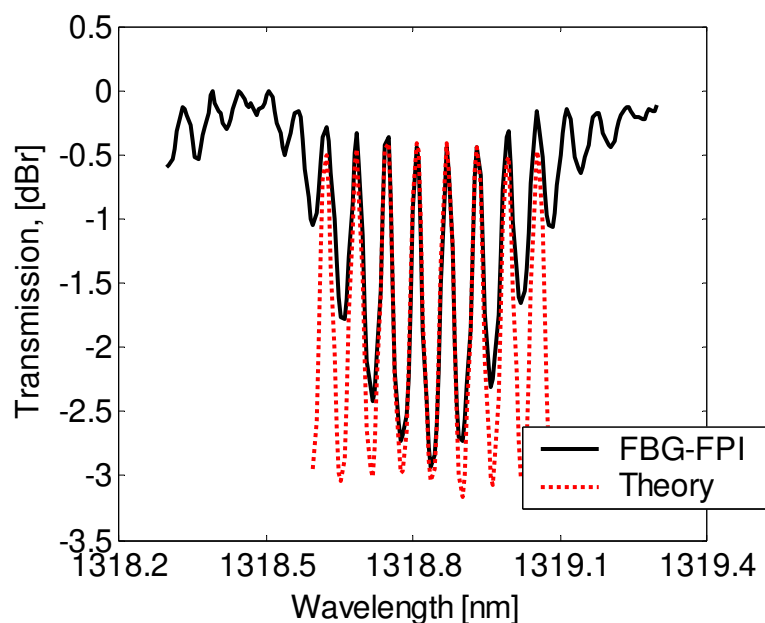


Figure 5.24: Transmission Characteristics of the FBG-based Fabry Perot Interferometer Implemented in a $62.5 \mu\text{m}$ -core MMF.

In order to estimate the FBG-FPI filter parameters, the response of a theoretical FPI computed using the *Airy function* given in equation (3.22) was superimposed on, and

aligned with the measured response, as shown in Figure 5.24. The FSR was then found to be about 10.6 GHz, which was close to the target FSR of 10 GHz. The equivalent reflectivity, R was 0.15, corresponding to a finesse, F_R of just 1.4. This is a low finesse value, which leads to non-optimal harmonic power performance of the OFM system, as indicated in Figure 3.14. The peak loss of the filter was found to be about 4.5 dB.

Using the MMF-based FBG-FPI at the RAU, the strength of the generated 6th harmonic component was -30 dBm, and the CNR > 40 dB [93]. A tunable laser had to be used as the CW laser in these experiments. The CW laser power was 4 dBm. The sweep signal frequency was about 2 GHz. A more detailed description of the experimental results involving the FBG-FPI OFM system has been reported in [93].

The main benefit in using a MMF-based FBG-FPI at the RAU of the OFM system is easy coupling between the filter and the photodetector. But, since the filter may also be placed at the headend as has been shown above, it is better to use a SMF-based FBG-FPI instead, and place it at the headend. SMF-based FBG-FPIs are easier to make and can have better specifications (finesse).

The major draw back in using FBG-FPI filters is that they have interferometric responses for just a small range of wavelengths (see Figure 5.24). That means that accurate positioning of the laser wavelength is required. This can obviously lead to overall OFM system operational challenges relating to laser wavelength alignment.

5.10.3 Wafer-based Fabry Perot Interferometer

Another filter implementation that was experimented with was the use of a piece of semiconductor material as a Fabry-Perot cavity. This approach was inspired by the fact that OFM does not need high-finesse filters (see Chapter 3). Because low-Q filters are easy to make, the OFM system would potentially be of low-cost even if the filter had to be placed at the remote RAU [10], [51], [52], [62], [110].

By carefully cleaving a semiconductor wafer, sufficient reflectivity, R can be achieved at each cleaved facet. The value of the reflectivity obtained can be calculated from the Fresnel equation [15] described as:

$$\rho_p = \frac{-n_2^2 \cos \theta_i + n_1 \sqrt{(n_2^2 - n_1^2 \sin^2 \theta_i)}}{n_2^2 \cos \theta_i + n_1 \sqrt{(n_2^2 - n_1^2 \sin^2 \theta_i)}} \quad (5.7)$$

where ρ_p is the electric field reflection coefficient of the light polarised in the plane of incidence to the facet, n_1 is the refractive index of the medium where light is coming from, n_2 is the refractive index of second medium, which the light enters, and θ_i is the angle of incidence. The intensity reflectance, R_p is calculated from equation (5.8) as:

$$R_p = |\rho_p|^2 \quad (5.8)$$

where ρ_p is the electric field reflection coefficient.

Therefore, cleaved facets of Gallium Arsenide (GaAs), or Indium Phosphide (InP), which have refractive indexes, n equal to 3.4, and 3.37 respectively [111], will exhibit 30 % and 29 % Fresnel reflections, respectively. This reflectivity is enough to form a FPI cavity with a finesse of 2.4 in both cases, which is sufficient to generate (mainly low-order) harmonic components of reasonable strength with the OFM system, (see Section 3.3.4, and [51]).

Two pieces of GaAs, and InP semiconductor materials, were carefully cleaved on both facets, and used in OFM experiments. Both pieces were 400 μm thick. A third piece of InP with a thickness of 3 mm could not be cleaved, and was therefore sawed and then polished. With the target FPI's FSR approximately equal to 10 GHz, the widths of all pieces were about 4.5 mm, calculated from equation (3.21). A special imaging and coupling system was constructed from several translation stages and lenses, giving several degrees of manipulation freedom [51], [93].

Transmission characteristics of all the three wafers were measured. Periodic bandpass responses were measured for cleaved 400 μm thick GaAs, and InP wafers, under SMF launch. Figure 5.25 shows the measured transmission response of the GaAs wafer. The measured FSR was about 9 GHz, which was close to the target. The measured peak loss of the filters was about 6 dB. The measured contrast ratio, C was about 3 dB. This figure was lower than the theoretical contrast ratio of 5 dB, which assumed perfect cleaved facets, and optical beam collimation. The passbands of the FPIs could easily be shifted, say by $\frac{1}{4}$ FSR, by rotating the wafer through 5° using the goniometer on which the wafer was mounted [93].

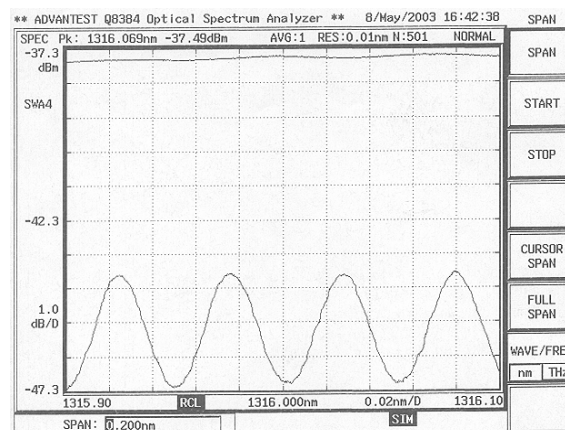


Figure 5.25: Transmission Characteristics of the FPI Made from a Piece of GaAs Semiconductor Material

The 3 mm InP wafer showed no interferometric response. This was attributed to very poor flatness of the facets [93], indicating that the sawing and polishing of the facets

could not achieve sufficient optical flatness required for Fabry-Perot interferometric behaviour [see equations (3.28), and (3.29)].

The 400 μm wafers were successfully used to generate harmonic components in the OFM system, with and without GIPOF fibre. The 6th harmonic component with the power of -45 dBm was generated in the back-to-back system. In the GIPOF-based OFM system, with the FPI placed at the RAU, the power of the 6th harmonic component was about -65 dBm. The low powers were a result of the low intensity modulation depth due to the low contrast ratio and also due to the higher coupling losses.

The advantage of using the wafer-based FPIs was their potential for low cost. However, their performance heavily hinges on good beam collimation, without which their finesse drops sharply due to strong sensitivity to pinhole finesse, F_p [93]. The use of such filters in the OFM system seems feasible, if the filters are placed at the headend rather than at the RAU, where serious coupling issues complicate the system performance.

5.10.4 Chip-Based MZI

A MZI made in a silicon substrate by the *Laboratoire IMEP (Institut de Microélectronique Electromagnétisme et Photonique)* of France [18], [45] was also tested in the OFM system. The filter had a FSR of about 3 GHz and was placed on a peltier element to control the chip's temperature. However, due to high coupling losses (11 dB, optical), the power of the generated 6th harmonic was below -40 dBm, using a sweep signal of 2 GHz. Furthermore, the setting-up of the device was rather complicated and time consuming.

5.11 Stability of OFM-Generated Carriers

In Chapter 3 it is stated that OFM operates in the coherent regime. That means that environmental effects such as temperature are bound to affect the stable performance of the system [69]. The two critical components in the OFM system are the laser source and the interferometer. It has been shown both theoretically and experimentally in the preceding sections of this thesis, that laser phase noise has virtually no impact on the OFM system (see Sections 3.5.2, and 5.5.1). However, the OFM model developed in Chapter 3, and described by equation (3.5) does suggest that the stability of both the laser wavelength and the interferometer are very important aspects of the OFM system. Hence it is desirable to co-locate them at the headend, in order to stabilise them jointly. The potential impact of unstable operation of these two components has been analysed theoretically in Sections 3.2.5 and 3.3.5 for the MZI- and the FPI-based OFM systems respectively. This section investigates the impact of these effects experimentally.

5.11.1 MZI-Based OFM System

The power stability of microwave signals generated through the MZI-based OFM system was measured over time. Figure 5.26 shows the measured stability of the 6th harmonic component (17.2 GHz) for the OFM system employing two different laser sources. The first one was a DFB laser used in most of the experiments described above. The second source was a 1310 nm *HP* tunable laser. It was observed that the intensity of the microwave signal fluctuated by about 10 dB over time in both cases, albeit slowly. However, the nature of the intensity variations was slightly different for each case.

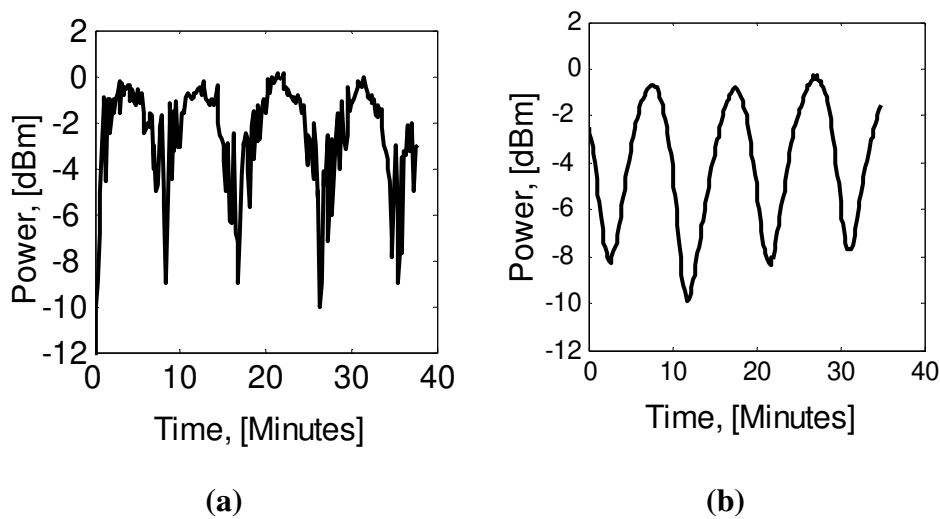


Figure 5.26: Long Term Power Stability of Microwave Carriers Generated by a MZI-based OFM System (a) DFB Laser Source, (b) Tunable Laser Source

By comparing Figure 5.26 (a) and Figure 5.26 (b), it can be said that the DFB laser-based system is affected by two different effects, while the tunable laser source appears to suffer from only one of the two effects. Wavelengths of temperature controlled DFB lasers (as was the case in this case) are known to drift by as much as 0.02 nm (>3 GHz at 1310 nm) or more [56]. On the other hand, the tunable laser used in these experiments had a specified wavelength stability of better than 100 MHz. Therefore, relying on the established fact that laser wavelength drifts cause the intensity of the OFM generated harmonics to fluctuate (see Sections 3.2.5 and 3.3.5), we can conclude that wavelength stability was responsible for the difference in the behaviour of the two systems. That is to say that the faster fluctuations are absent from Figure 5.26 (b) because the tunable laser wavelength was more stable.

The impact of wavelength variations on the OFM system was demonstrated by deliberately tuning the CW laser's wavelength over 0.058 nm (10 GHz), while recording the power of the 5th and the 6th harmonic components. The laser wavelength was varied from 1316.200 nm to 1316.258 nm in steps of 0.001 nm. The results are given in Figure 5.27. The figure shows that the strength of the harmonics

fluctuates as the wavelength varies. For certain wavelengths, the harmonic components are completely eliminated. Furthermore, the peaks of the even harmonic coincide with the minima of the odd harmonic component, and vice versa. This result firmly confirms the theoretical predictions given in Section 3.2.5.

The slower and larger intensity fluctuations observed in Figure 5.26 were investigated further, and found to relate to the stability of the MZI filter. Two of the major factors affecting the stability of the MZI are temperature variations, and the state of polarisation. Temperature variations can cause fluctuations in the lengths of the two interfering arms, leading to fluctuating phase differences. This effect causes the transmission passbands of the MZI to “walk” around [57]. When this happens, the biasing (or wavelength alignment) of the MZI is varied continuously leading to the fluctuation of harmonic intensity.

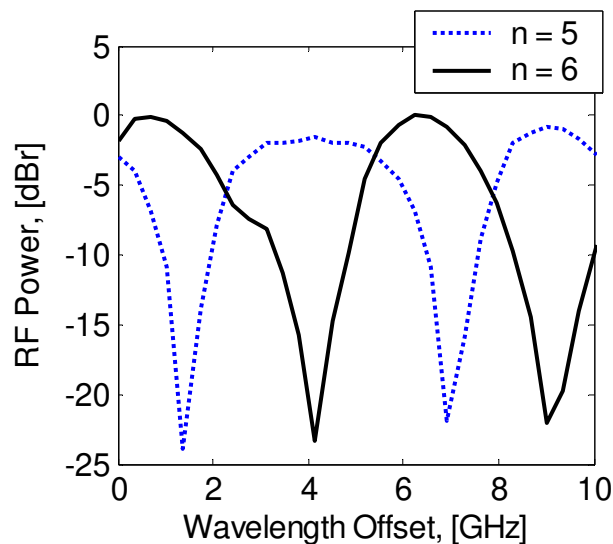


Figure 5.27: Measured Impact of Laser Wavelength Drift on the MZI-Based OFM System

The resulting behaviour is similar to the case when the wavelength is drifting while the filter is stable. This means that the absolute stability of either the laser wavelength or the filter transmission characteristics is not important. What is important is relative stability between the two devices. Therefore, while the DFB laser, and the MZI may be stabilised individually using existing stabilisation techniques and schemes [45], [56], [57], it may be easier and more effective to control the relative stability between the two devices using say, feedback control schemes. This is easier to implement when both devices are co-located in the headend.

Variations in the state of polarisation cause the MZI’s extinction ratio to fluctuate [57]. A reduction in the extinction ratio of the MZI causes a drop in the intensity modulation depth of the OFM system, leading to reduced harmonic strength. Therefore, the MZI-based OFM system requires polarisation stabilisation as well.

This is one of the disadvantages of using the MZI instead of say a FPI, which is not polarisation sensitive (see the following section).

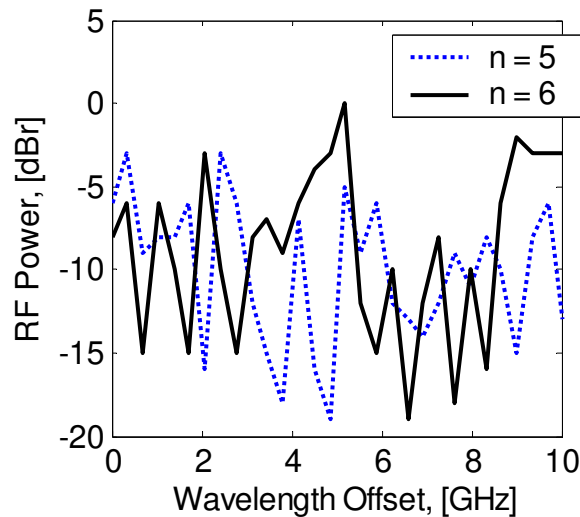


Figure 5.28: Measured Impact of Laser Wavelength Drift on the FPI-based OFM System

5.11.2 FPI-Based System

The measured effect of deliberately introducing laser wavelength perturbations in a FPI-based system is shown in Figure 5.28. The measurement procedure used here was similar to the one used for the MZI-based system whose result is given in Figure 5.27. The FFPI described in Section 5.10.1 was used as the interferometer. It was observed that the intensity fluctuations in the FPI-based system were much sharper than those observed in the MZI-based system. This result confirms the simulated prediction presented in Section 3.3.5. The increased sensitivity to wavelength perturbations observed in the FPI-based OFM system is attributed to the narrower and sharper transmission passbands of the FPI, which had a finesse of 31 and a -3dB bandwidth of just 320 MHz.

Using optical feedback, the relative stability of the FFPI with respect to the laser wavelength was controlled with an external Fibre Fabry Perot Controller (FFP-C). The result is presented in Figure 5.29. It was observed that the wavelength-perturbation-induced harmonic intensity fluctuations were reduced from 10 dB to less than 1 dB. Thus it is concluded that feedback control of the relative laser wavelength-filter characteristics is effective in combating environmentally induced OFM system disturbances. The use of such control circuitry can be made cost effective if the filter is placed at the headend, and shared among several remote RAUs.

The impact of the state of polarisation on the performance FFPI-based OFM system was investigated and found to be virtually negligible (<1 dB). This is because the FPI

is not polarisation sensitive. This is an important advantage of the FPI-based OFM system over the MZI-based system.

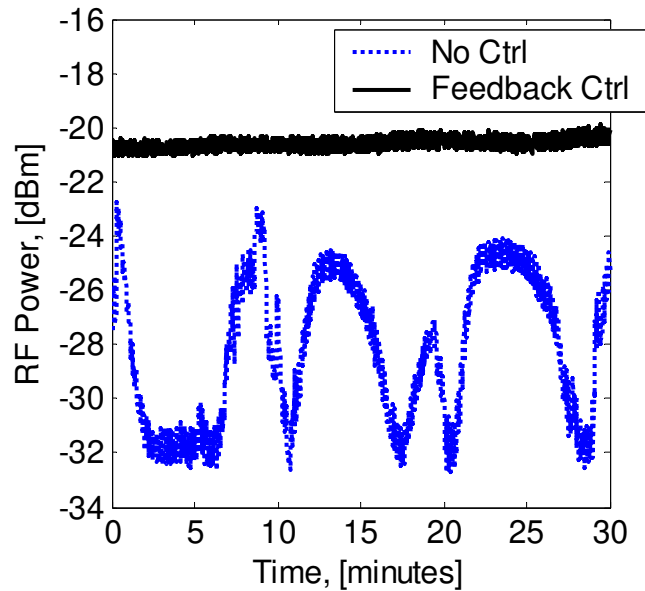


Figure 5.29: Measured Stability of the 6th Harmonic Component Generated with the FPI-Based OFM System Employing a FPI Feedback Loop

5.11.3 Stability of the Chip-based MZI

The stability of a silicon substrate-based MZI was found to be very poor, as shown in Figure 5.30. It was observed that even though the filter was temperature stabilised, it was extremely sensitive to polarisation fluctuations. Furthermore the stabilisation of only the filter cannot produce system stability since laser wavelength fluctuations remain. Given the small FSR (3 GHz) in this case, the system is bound to be even more sensitive to the wavelength fluctuations than the system using the MZI with 10 GHz FSR, as discussed in Section 3.2.5. Therefore the results in Figure 5.30 underscore the importance of stabilising the relative fluctuations between the laser wavelength and the filter, as opposed to the absolute individual stabilisation of the devices, which is more difficult to achieve.

5.12 Transmission and Frequency Up-Conversion of Data Modulated Carriers

The transmission and frequency up-conversion of un-modulated RF signals using OFM have been the focus of the preceding chapters and sections. This section focuses on the modulation of the OFM-generated carriers. In other words, the OFM system is used to perform several functions simultaneously, namely the transportation,

frequency up-conversion, and data modulation of microwave carriers. All processing is carried out with optical signal processing in order to keep the RAU simple.

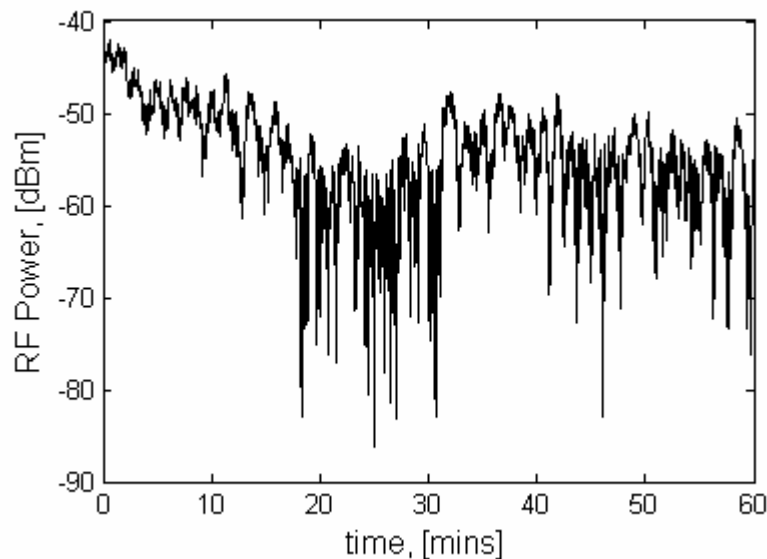


Figure 5.30: Stability of the 6th harmonic Component Generated by the OFM System Using a Chip-Based MZI filter

In order to generate modulated microwave carriers at the RAU, the FM modulated optical signal is also Intensity Modulated (IM) at the headend by the desired baseband data or modulated sub-carrier. Therefore, the optical signal transported over the fibre link is a combined FM and IM signal. The intensity modulation may be performed before or after the frequency modulation. But the maximum modulation bandwidth, or sub-carrier frequency will be limited to less than half of the sweep signal frequency, f_{sw} used [10]. This is because the IM modulation will generate double-sidebands around each of the harmonics generated by the OFM process, which are spaced by the sweep signal frequency.

At the RAU, after photodetection, all the generated harmonic components are intensity modulated with the data applied at the headend. For instance, in the case of a BPSK modulated subcarrier signal of frequency, f_{sc} the generated photocurrent may be represented by equation (5.9) as:

$$I_{\text{PD}}(t) = \frac{1}{2} |E_0|^2 \cdot [m(t) \cos \omega_{\text{sc}} t] \cdot \left\{ \begin{array}{l} 1 + \cos(\omega_0 \tau) \\ \left[J_0(z) + 2 \sum_{k=1}^{\infty} (-1)^k J_{2k}(z) \right] \cdot \cos \left[2k \cdot \left(\omega_{\text{sw}} t - \frac{\omega_{\text{sw}} \tau}{2} \right) \right] \\ + 2 \sin(\omega_0 \tau) \cdot \sum_{k=1}^{\infty} (-1)^k J_{2k-1}(z) \cdot \cos \left[(2k-1) \cdot \left(\omega_{\text{sw}} t - \frac{\omega_{\text{sw}} \tau}{2} \right) \right] \end{array} \right\} \quad (5.9)$$

where $\omega_c = 2\pi f_{\text{sc}}$, and f_{sc} is the subcarrier frequency, and $m(t)$ is the bipolar data signal. The difference between equation (5.9) and equation (3.5) is that in latter case, the amplitude of the electric field is constant while in the former case the amplitude of the field is modulated by the data or subcarrier as shown. The desired frequency harmonic is then filtered and radiated. Therefore, no extra microwave modulation devices, or LOs for frequency up-conversion are required at the RAU. In fact, the RAU is the same, whether it is used to generate modulated carriers or un-modulated carriers. This is the benefit of centralising signal processing functions at the headend in RoF systems. In other words, switching from one standard to another is done simply by changing the signal feed at the headend without the need to up-grade the distribution system and the RAU. In this way, the OFM-based RoF system may support multi-standard operation. Furthermore, OFM does not require high-frequency RF and optical signal processing equipment at the headend because the sub-carrier and the baseband data are both at frequencies much lower than the generated RF signals.

5.12.1 ASK Data Modulation

Figure 5.31 shows the experimental set-up used to generate ASK modulated data. The headend is essentially the same as the one used for LO delivery (e.g. Figure 5.12), except that an external intensity modulator is now placed immediately after the phase modulator. The intensity modulator may also be placed in front of the phase modulator, so that PM and IM are done in reverse order. Direct modulation of the laser could also be used, but the resulting chirp may affect the performance of the system by introducing extra microwave carrier intensity fluctuations due to additional undesired FM-IM conversion in the MZI. A pattern generator was used to generate PRBS data for transmission.

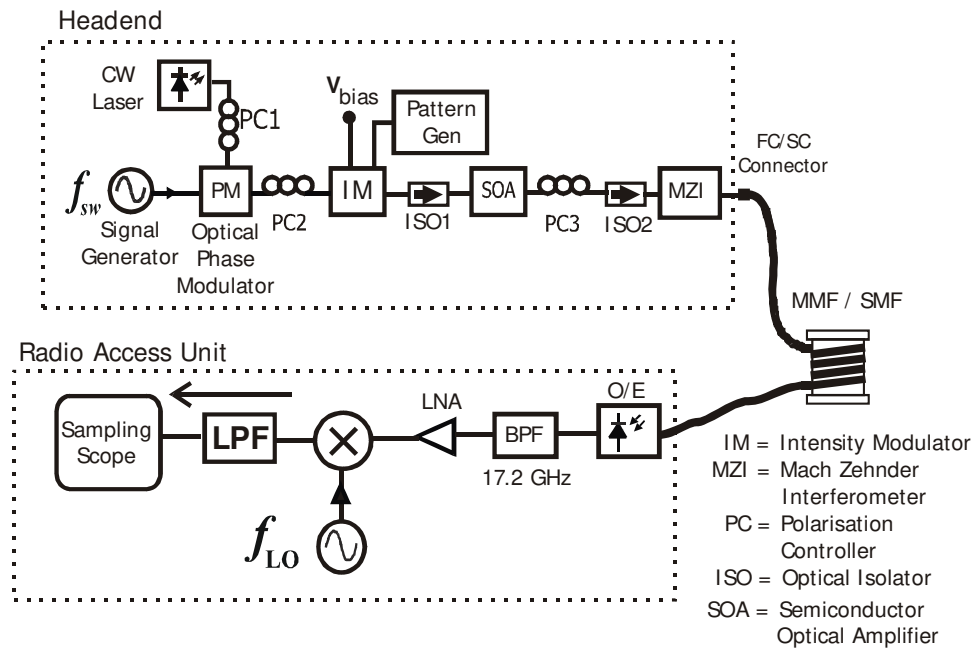


Figure 5.31: Experimental Set-Up for Combined Microwave Carrier Up-Conversion, Transportation, and ASK Data Modulation

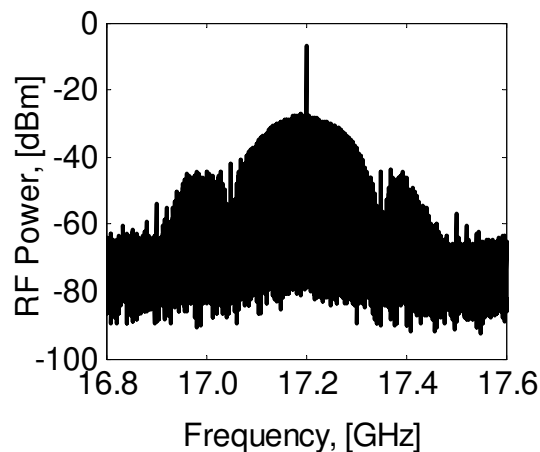


Figure 5.32: Frequency Spectrum of the 150 Mbps ASK Data Modulated 17.2 GHz Carrier Generated by OFM

At the RAU, coherent detection through a double balanced mixer was used to recover the data from the up-converted 17.2 GHz carrier. The mixer had an IF bandwidth of 500 MHz. A 20 GHz signal generator was used to generate the 17.2 GHz LO. The recovered data was analysed on the sampling scope. Figure 5.32 shows the generated 17.2 GHz carrier modulated by ASK data prior to down-conversion. The presence of the PRBS ASK data modulation is clearly visible. Non-coherent detection, such as

envelope detection may also be used. This would avoid the necessity of a phase-locked LO carrier.

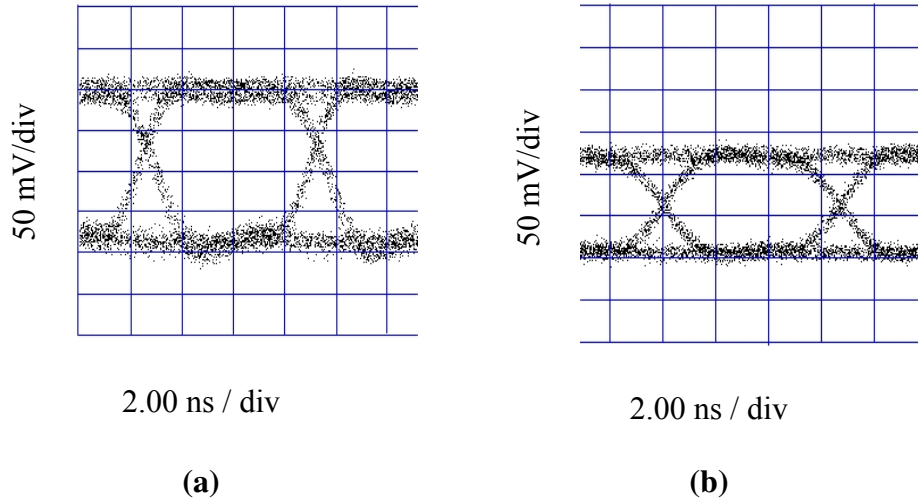


Figure 5.33: Eye Diagrams of Recovered 150 Mbps ASK Data from the OFM-Generated 17.2 GHz (a) Back-to-Back, (b) over 50 km of SMF

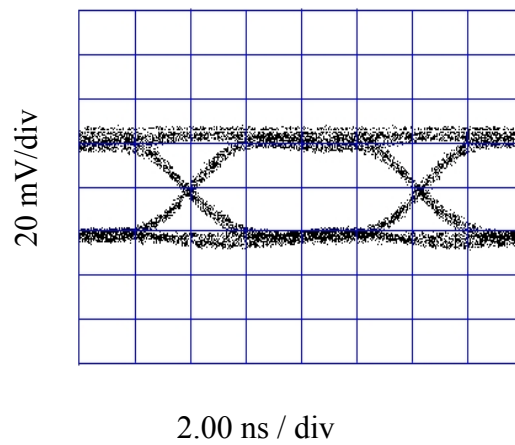


Figure 5.34: Eye Diagram of 120 Mbps ASK Data Recovered from an OFM Generated 17.2 GHz Carrier at a 4.4 km MMF Fed-RAU

Figure 5.33 shows the eye diagrams of the recovered 150 Mbps data before fibre transmission and after transmission over 50 km SMF. Both eye diagrams are clearly open, indicating successful transmission. Similar results, shown in Figure 5.34 were obtained in the 4.4 km MMF-based OFM system, with less than 1 GHz link bandwidth. These results confirm the ability of the OFM system to deliver high-frequency RF signals over both SMF and MMF links (delivered RF signals at frequencies beyond the MMF's modal bandwidth).

The data rate was limited by the filter bandwidth, which was 300 MHz, and also by the IF bandwidth of the mixer, which was 500 MHz. Otherwise, with the sweep signal frequency, f_{sw} equal to 2.87 GHz it should have been possible to transmit data at 1 Gbps or so.

It was observed that the recovered signal was not stable. This was because a standalone signal generator was used to generate the LO signal, such that the phases of the LO and the generated microwave signal were not always synchronised. BER measurements of the ASK modulated data could not therefore be performed since the low bitrate required a relatively long gating time. However, the Q factor of the transmitted signal could be measured during the intervals when the phases were temporarily synchronised. The measured Q-factors were well above 6 indicating the feasibility of obtaining BERs below 10^{-9} [15]. A PLL, locked either on to the 17.2 GHz signal carrier or other transmitted pilot signal for phase reference in the down-conversion circuitry would eliminate such effects by providing a phase-locked LO.

5.12.2 Complex Signal Modulation Formats

Apart from the transmission and generation of simple ASK modulation formats, the capability of OFM to transmit complex modulation formats including BPSK, QPSK, and xQAM was also investigated. Transmission of these multi-level signal formats was achieved by first putting them on a subcarrier, which was then used to intensity modulate the FM optical signal at the headend as shown in Figure 5.35. A *Rohde & Schwarz* Vector Signal Generator (VSG) was used to generate the modulated sub-carriers. Different sub-carrier frequencies were used in the experiments. At the RAU, the 40 GHz (*Rohde & Schwarz FSQ40*) Vector Signal Analyser (VSA) was directly used to analyse the transmitted modulated signal.

An example of the spectrum of the signal recovered after filtering is shown in Figure 5.36. This spectrum was obtained for the case when the sweep signal frequency, f_{sw} was equal to 2.867 GHz, while the subcarrier frequency, f_{sc} was 127 MHz. The FM index, β of the OFM system was optimised for the 6th harmonic as discussed in Section 5.4, and shown in Figure 5.7 ($\beta \approx 4.7$). The 127 MHz subcarrier formed the two sidebands on either side of the 17.2 GHz signal as shown. In Figure 5.36 the subcarrier was modulated with 64QAM data at a symbol rate of 26 MHz, representing a bit rate of 156 Mbps.

The data modulation in the lower side band at 17.093 GHz was examined on the VSA. Clearly open eye diagrams of both the I and the Q components of the recovered 64QAM signal before fibre transmission and after transmission over 4.4 km fibre were obtained as shown in Figure 5.37 [112]. The Error Vector Magnitude (EVM) of the recovered signals was also measured. For the OFM system without fibre transmission, the EVM was 4.2 %. After transmission over 4.4 km of MMF, the EVM increased slightly to 4.7 % indicating a 0.5 % penalty attributed to the fibre link. Other combinations of subcarrier frequencies, modulation formats, and symbol rates were also used [112]. For instance, using the WLAN signal transmission the measured EVM was 4.8 % for the QPSK signal modulation format (18 Mbps) at -3

dBm received optical power. This was well below the 22.39 % maximum EVM specified in the WLAN standard [113].

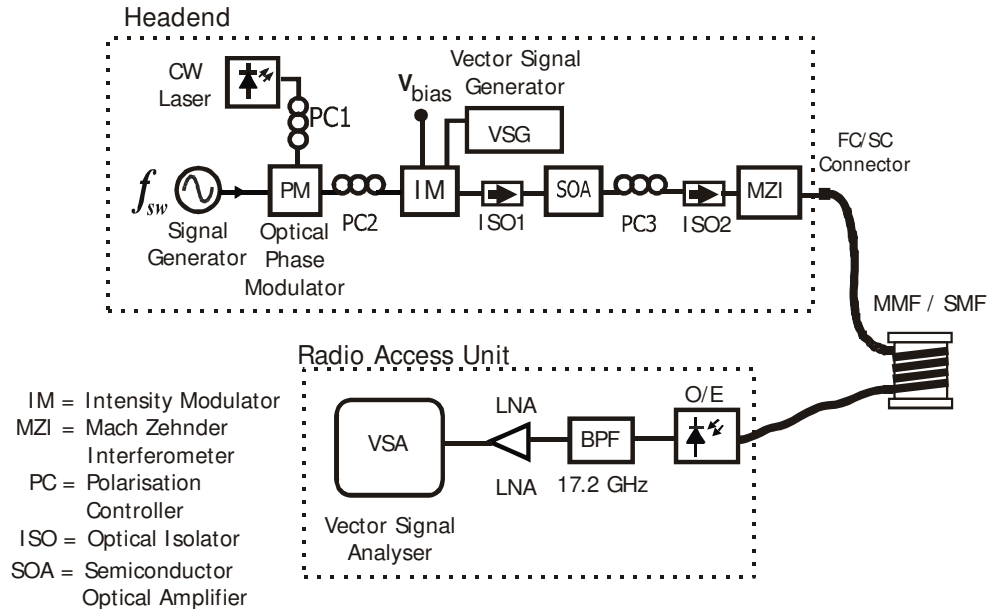


Figure 5.35: Experimental Demonstration of an OFM-Based RoF Downlink for Transportation, Frequency Up-Conversion, and Complex Data Modulation of Microwave Carriers Generated at a Remote Radio Access Unit

The measured EVM values were well within the IEEE 802.11a/g WLAN standard specification for 64 QAM modulation, which is 5.6 % for the data rate of 54Mbps [113]. The successful transmission of other multi-level modulation formats including BPSK, QPSK, and 32 QAM modulation formats was also verified. These results confirmed the capability of OFM to transmit not only simple ASK modulation formats, but complex multi-level modulation formats, including 64QAM, which are commonly used in wireless systems. In these experiments the intensity modulator was used as it was, without any linearization circuitry.

5.12.3 WLAN Signal Up-Conversion and Transmission

The data transmission capabilities of the OFM system were investigated further by using the system to transmit and up-convert IEEE 802.11 a/g WLAN signals. To do this, the VSG was used to generate IEEE 802.11a/g WLAN compliant signals at the subcarrier frequency of 533 MHz. The bit rate of the WLAN signals was 54 Mbps, using OFDM and 64QAM modulation formats. The sweep signal frequency was 3.08 GHz. The FM index of the OFM system was optimised for the 6th harmonic component, being 18.48 GHz, in this case. The spectrum of the unfiltered OFM up-converted signal is shown in Figure 5.38. The two WLAN modulated sidebands are clearly visible. Figure 5.39 shows the OFDM subcarriers present in the Lower Side Band (LSB).

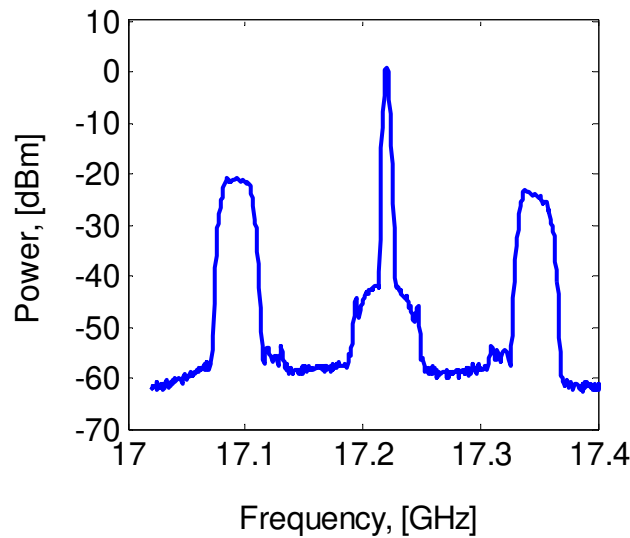


Figure 5.36: Frequency Spectrum of a 64QAM Modulated 17.2 GHz Carrier Generated by the OFM System (Symbol Rate, $R = 26$ MHz).

Using the WLAN digital receiver in the VSA, the WLAN signal in the LSB was recovered and performance measurements carried out. The constellation diagram of the recovered signal, shown in Figure 5.40 confirms the successful frequency up-conversion (from 533 GHz to 18 GHz), and transmission over 4.4 km MMF (<1 GHz -3dB bandwidth) of OFDM WLAN signals.

The optical power impinging on the photodetector was varied and the EVM recorded. The results are summarised in Figure 5.41, where the measured EVM is plotted against the average received optical power. The upper EVM limit defined in the WLAN standard when transmitting 54 Mbps (i.e. 64 QAM), is 5.62 % (-25 dB) [113]. At this value of the EVM, the MMF link shows a total optical power penalty of about 1.7 dB over the whole 4.4 km MMF link. From Figure 5.41, the minimum optical power necessary to obtain an EVM of 5.62 % or less in the 4.4 km MMF-fed OFM system is estimated to be equal to -6.5 dBm. Thus, with say, 0 dBm optical power, MMF link lengths exceeding 10 km should be feasible.

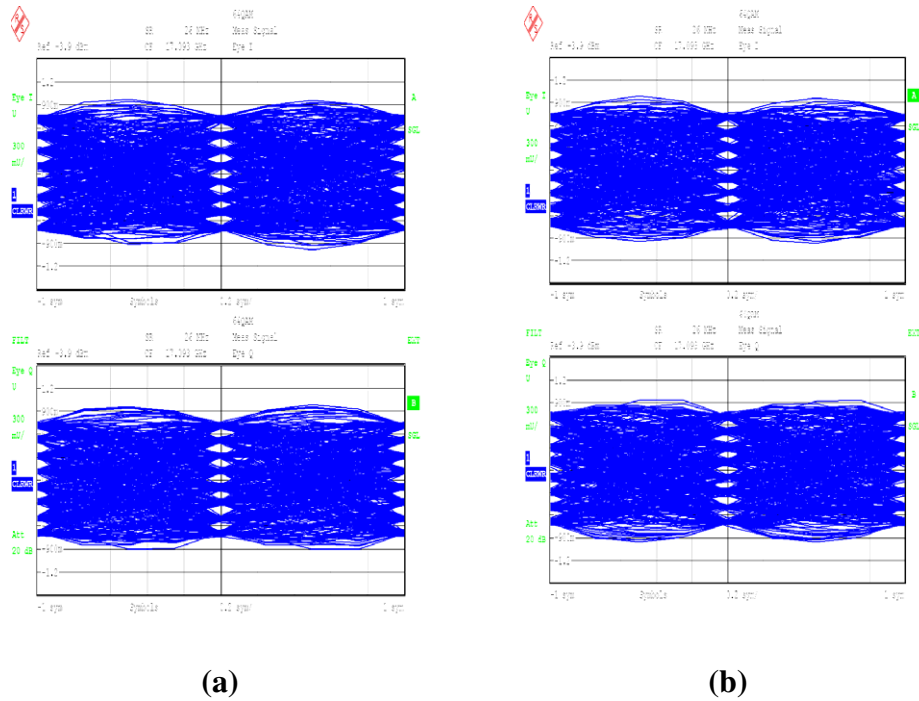


Figure 5.37: Eye Diagrams of 64QAM Data Recovered from a 17.2 GHz Carrier Generated by the OFM System (Symbol Rate, $R = 26$ MHz). (a) Back-to-Back, (b) after 4.4 km MMF

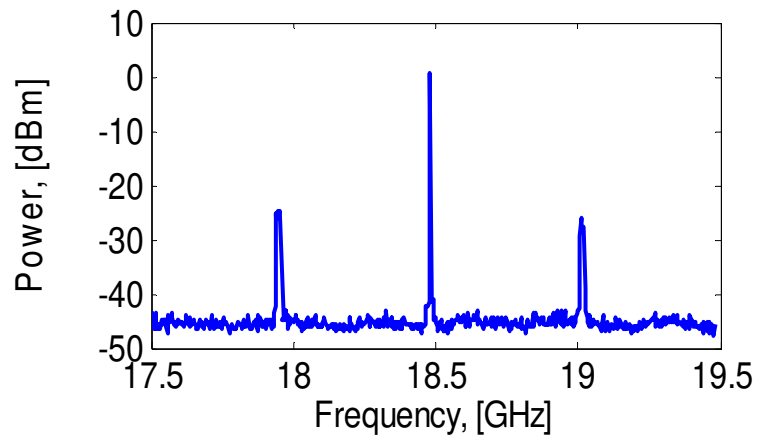


Figure 5.38: Frequency Spectrum of IEEE WLAN 802.11g Signal (54 Mbps) Transported over 4.4km MMF, and Frequency Up-Conversion Using the OFM System

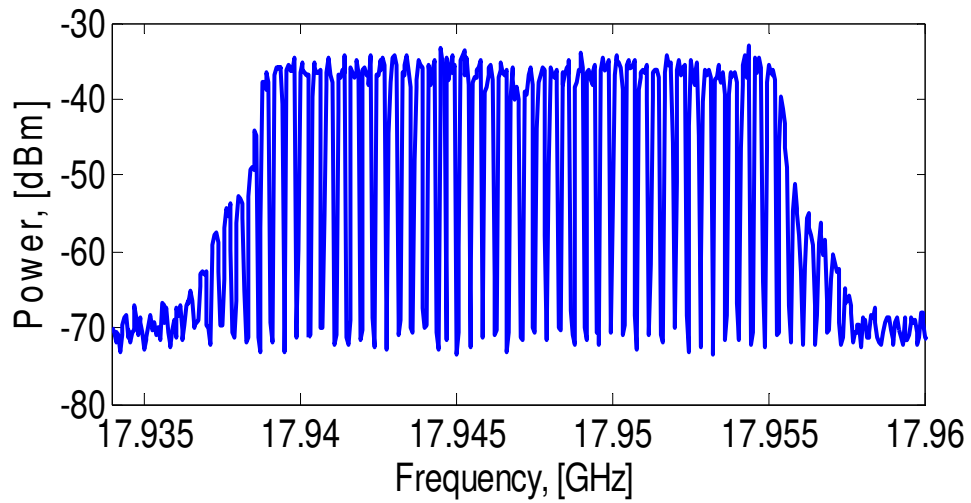


Figure 5.39: Frequency Spectrum of the LSB of the OFM Up-converted WLAN Signal Showing the OFDM Subcarriers

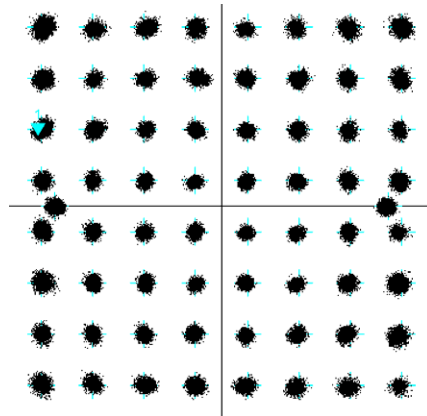


Figure 5.40: Constellation Diagram of the Data Recovered from the OFM Up-converted IEEE WLAN 802.11g Signal (54 Mbps) Transported over 4.4km MMF

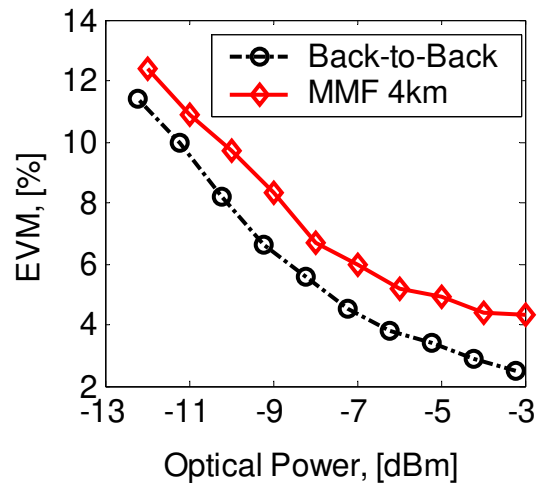


Figure 5.41: Measured EVM against Received Optical Power in an OFM Up-Converted 17.2 GHz 54 Mbps WLAN System

5.12.4 Bit Error Rate Measurements

The BER measurements were done by transmitting the 54 Mbps WLAN signal, and then using the WLAN receiver in the VSA to recover the received data. The measured BER as a function of the received optical power is shown in Figure 5.42. The penalty due to the MMF link at the BER of 10^{-5} is about 1 dB over the 4.4 km MMF link.

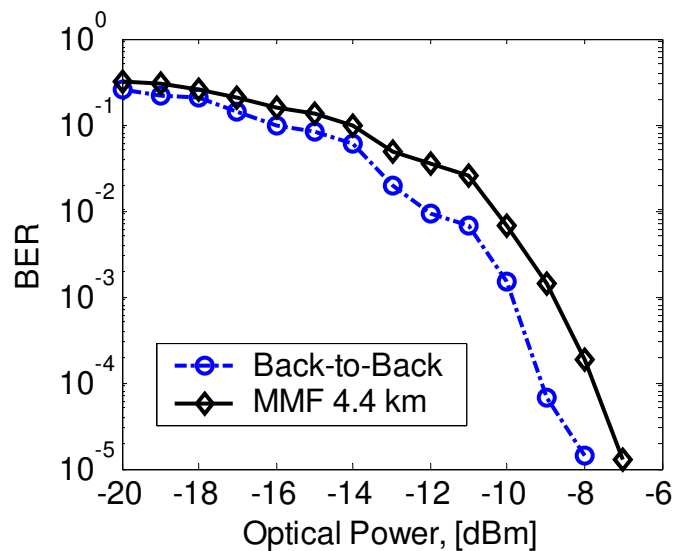


Figure 5.42: BER Measurements on a 54 Mbps WLAN Modulated 18 GHz Signal Generated by OFM and Transmitted over 4.4 km of MMF

5.13 Conclusions

The principle of optical frequency multiplication was demonstrated experimentally. From the extensive experimental investigations, a number of conclusions can be drawn.

The combination of a phase modulator, and a CW laser diode was successfully used as an FM source in the high-frequency-generating OFM system. The use of an electronically tunable laser as the FM source was also demonstrated. The tunable laser option offers a phase sensitivity which is three orders of magnitude higher than that of the phase modulator. However, the tunable laser was limited to tuning speeds below 100 MHz, while the phase modulator could support tuning speeds in excess of 10 GHz or more, if required. The maximum supported data symbol rate (or subcarrier frequency) is limited by this tuning speed.

The impact of the FM index predicted by the OFM system model presented in Chapter 3 was verified. Using a commercially available phase modulator and a tunable laser, sufficient FM indexes for obtaining large multiplication factors exceeding 10 were demonstrated.

The theoretical prediction that OFM suppresses laser phase noise was verified experimentally. Furthermore, it was confirmed that the phase noise of the generated harmonics is determined mainly by the phase noise of the sweep signal and the multiplication factor. Thus, by controlling both, the required phase noise performance can be obtained. OFM was used to transport and generate high-frequency microwave LO signals up-to 21 GHz over SMF and MMF links, with considerably lower phase noise than signals generated directly by a commercially-available electronic signal generator.

Apart from the MZI filter, other filter implementations for use with OFM were investigated. These include the fibre-based Fabry Perot interferometer, the fibre Bragg Grating-based Fabry-Perot, the cleaved semiconductor material optical cavity-based Fabry Perot filter, and the chip-based MZI filter. The MZI filter showed the disadvantage of being polarisation sensitive. The fibre-based Fabry Perot filter had the advantage of easy tunability, and high contrast ratio (finesse). The fibre Bragg Grating-based filter had the disadvantage of a limited operation wavelength range. All OFM systems based on Fabry Perot filters showed negligible sensitivity to polarisation changes.

The amplitude stability of the OFM-generated carriers was found to depend on the relative stability of the laser wavelength and the filter transmission characteristics as predicted by the OFM theoretical model. The intensity fluctuations were successfully eliminated by using feedback control to track the laser wavelength fluctuations in the fibre-based Fabry Perot interferometer.

OFM was successfully used to perform multiple system functions simultaneously – namely signal transport, frequency up-conversion, and carrier modulation with various signal modulation formats. Successful transmission of simple ASK

modulated carriers, and complex multi-level modulation formats including BPSK, QPSK, 32 QAM, and 64 QAM, with low EVMS was demonstrated. OFM downlinks over up-to 50 km SMF and 4.4 km MMF were demonstrated. In addition, the transport, and up-conversion of OFDM signals was demonstrated by using IEEE 802.11 a/g compliant WLAN signals. BER measurements confirmed small penalties due to MMF links. The maximum MMF link length depends on the launching conditions. However, under-filled launch conditions such the SMF-MMF butt coupling method should produce link lengths exceeding 10 km in MMF-fed OFM systems.

CHAPTER

6

Towards a Point-to-Multipoint RoF System Based on OFM

6.1 Introduction

The discussions in the preceding chapters are focussed mainly on the realisation of a RoF downlink by employing the OFM principle. This is because remote delivery of LO signals becomes challenging when high frequencies are involved. For instance, the downlink and uplink transport of wireless signals at frequencies below 6 GHz, can readily be achieved by direct transmission over fibre through the use of intensity modulation of the light from a laser diode and direct detection of that signal by a photodiode (IM-DD, also known as RF over fibre, RFoF). This results in very simple RAUs as no frequency conversion at the RAU is necessary.

At high frequencies, such as mm-waves, the direct transmission of RF signals is more challenging because it requires costly high-frequency electro-optical components, and it is susceptible to dispersion induced amplitude suppression. Therefore, the uplink in mm-wave RoF systems often involve the down-conversion of the upstream signal prior to transmission. That is to say that the RF signal from the mobile unit or wireless terminal unit is first down-converted to an IF and then transmitted over the fibre link (IFoF) through IM-DD. The advantage of transmitting the upstream signal as an IF instead of the RF is that low-cost low-speed electro-optic components may be used at the RAU. However, this approach requires that a high-frequency LO is present at the RAU. This may not be a problem at low-frequencies, where low cost low phase noise MMIC based LO sources are likely to be available [5]. But at mm-waves, it may be more desirable to deliver the LO remotely to the RAU, using whatever RoF techniques that may be appropriate. Therefore, by delivering LO signals from the headend to remote RAUs, the RoF system enables a low-cost uplink solution. This helps to keep the RAU of the high-frequency (mm-wave) wireless system simple, leading to reduced RoF system costs.

This chapter discusses the realisation of a full-duplex RoF system using the OFM RF signal transport principle. Furthermore, the main requirements for, and impediments to the realisation of point-to-multipoint RoF systems based on the OFM principle are also highlighted.

6.2 Full-Duplex RoF System with OFM

The extensive experiments conducted in Chapter 5 confirmed that using OFM, high-frequency mm-wave signals may be transported to remote RAUs fed by either MMF or SMF. The delivered microwave signals exhibit excellent quality, with low phase noise. Therefore, these signals may be used to achieve the uplink in a cost effective manner. This is illustrated in Figure 6.1.

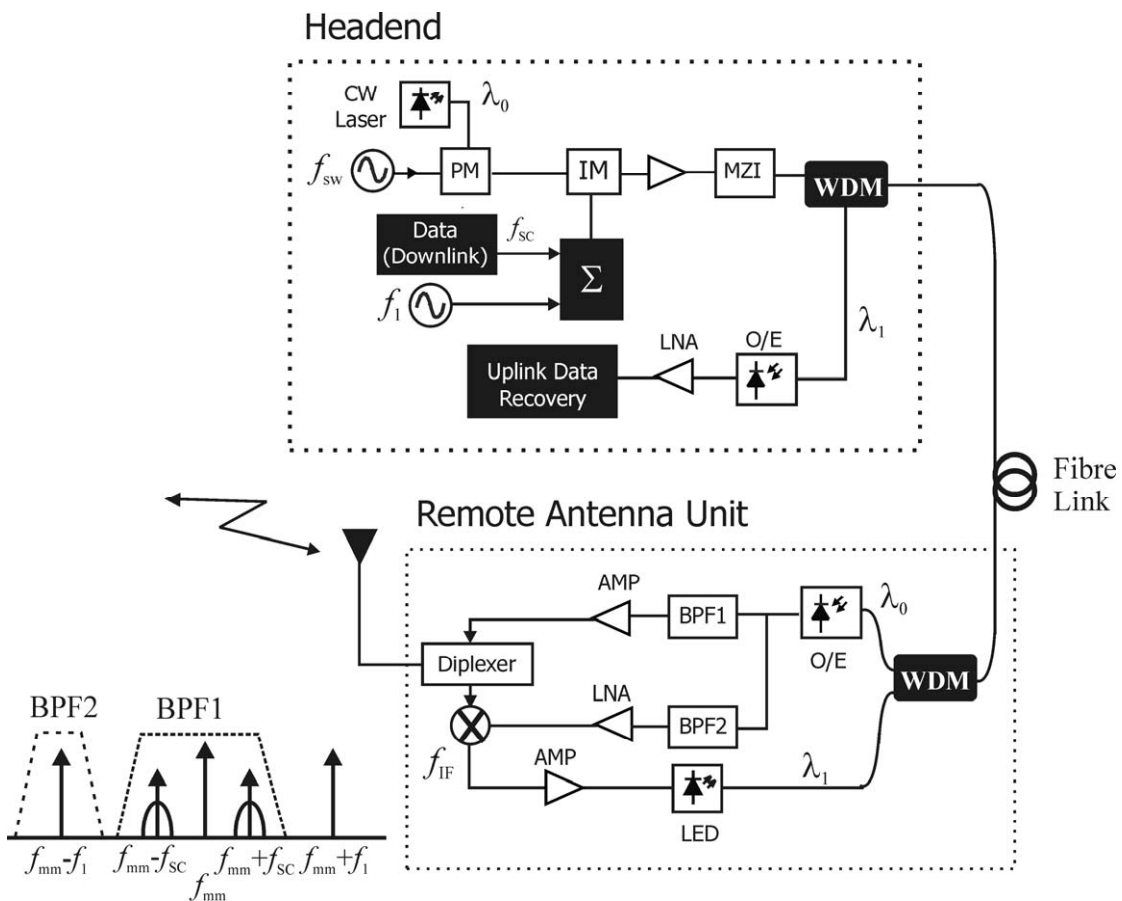


Figure 6.1: Full-Duplex RoF System Employing OFM

The downlink data is transmitted on a subcarrier at the frequency, f_{sc} . The downlink subcarrier together with an appropriately chosen low-frequency signal, f_1 , are added together and used to modulate the intensity modulator. The signal f_1 is not modulated with data. Following optical frequency multiplication at the RAU, the subcarrier

frequencies form sidebands on either side of the multiplied sweep frequency as shown in the figure. The downlink signal is filtered with BPF1 and radiated. One of the two sidebands of the f_1 signal at $f_{LO} = f_{mm} \pm f_1$ may be filtered and used as a LO for the uplink as shown. For instance, if the sweep frequency, f_{sw} equals 3 GHz, and f_1 equals 1.1 GHz, then the frequency of the LO extracted by BPF2 would be 16.9 GHz, assuming an OFM factor of 6. The frequency of the LO may easily be tuned as required, just by adjusting the frequency of f_1 at the headend.

The remotely delivered LO is then used to down-convert the uplink signal coming from the MU/WTU to an IF frequency, f_{IF} . The down-converted signal is transported to the headend via an IM-DD link. Because the IF is at a low frequency, a low cost LED or cheap FP laser diode may be used in the uplink. In this way, the need for a high-frequency LO in the RAU may be eliminated, keeping the RAU simple.

6.3 Point-to-Multipoint OFM System

Figure 6.1 shows a point-to-point bi-directional system with WDM used to multiplex downstream and upstream wavelengths on the same fibre. To achieve a point to multipoint system configuration, WDM may be used, say over a ring network as shown in Figure 6.2 [50]. In this configuration, different wavelengths are used to address different RAUs, which are combined with the Optical Add/Drop Multiplexers, to become Remote Nodes (RNs). The RAU may be configured as illustrated in Figure 6.1, where the remotely delivered LO is used in an IM-DD uplink. The uplink optical source may be delivered remotely, to avoid the necessity of a WDM source at each RN.

An important point to note in Figure 6.2 is that only one interferometer (MZI) is used at the headend. The different wavelengths are swept by separate low-frequency sweep signals, in accordance with the desired mm-wave signals at each RN. Thus, the different nodes may actually operate different wireless standards. The swept optical signals are multiplexed using WDM and then processed simultaneously by the MZI filter, before being fed into the optical ring network. The sharing of the MZI helps to reduce costs, especially if complex filter stabilisation schemes have to be used (see section 5.11).

Because WDM De/Multiplexing devices are more readily available for SMF applications, point-to-multipoint systems based on WDM Multiplexing are more suitable for SMF-fed systems. For MMF-based systems, the star network configuration may be a more suitable option. As for POF-based systems, the star network configuration may be the only option - at least for the moment. In that case, each RAU would be linked by one or two (up-/down-link) separate fibres. This approach may be more suitable for in-building applications, where link lengths are generally short, and where MMFs (including POF) are attractive for their low installation and maintenance costs.

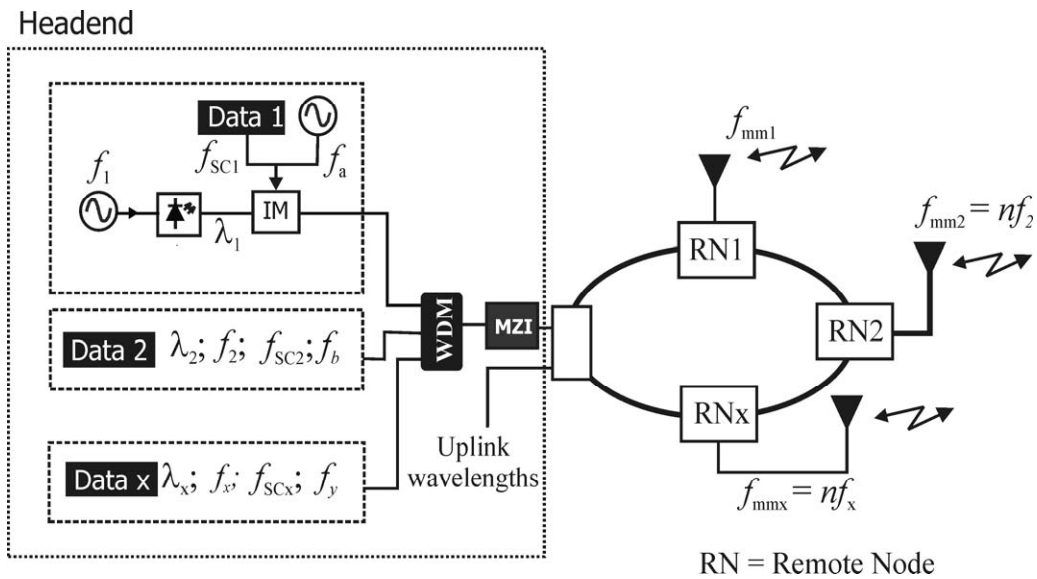


Figure 6.2: Concept of a Point-to-Multipoint RoF Distribution System Using OFM

It must be mentioned that the physical layer performance (link gain, phase noise, dynamic range, complexity, etc.) of RoF systems may not be the only limitation to their application for wireless signal distribution. In the point-to-multipoint system configurations, the nature of the Medium Access Control (MAC) protocol of the wireless system may place limitations on the maximum RoF link distances. This is caused by the fact that by centralising all signal processing functions at the headend, the MUs'/WTUs' access to radio resources at the RAU is also controlled remotely. As a result, the extra signal propagation delay imposed by the RoF link might interfere with the MAC protocol timing boundaries, leading to either poor performance (data throughput) or failure of the MAC protocols themselves.

For instance, the IEEE 802.11 WLAN standard uses Carrier Sense Multiple Access with Collision Avoidance (CSMA/CA) protocol. This is a distributed control mechanism, where each WTU has a fair chance of accessing the medium. If the WTU senses that the medium is busy, or has just successfully transmitted a frame, it executes a *backoff* – waits a random time before attempting to access the medium again [30]. The limits of this wait time, and other time-outs are pre-engineered into the protocol, on the basis of the anticipated maximum cell sizes (air propagation delay). Thus the introduction of extra signal delays owing to the fibre link may cause some of the protocol timing limits to be exceeded, resulting in reduced performance or failure of the protocol altogether. Thus in distributed MAC protocols, only short RoF links may be accommodated. In contrast, centrally controlled MAC protocols such as defined in HyperLAN, and IEEE 802.16 standards, do not suffer such effects. Therefore, centrally controlled MAC protocols are generally perceived to be more suitable for long RoF distribution links [117]. The point to note here is that RoF technology should not be seen as a silver bullet solution for all broadband wireless system signal distribution problems, but rather as a powerful technology with clear

benefits for a wide range of high-capacity systems, especially those requiring a high density of antennas.

It must be mentioned that much research regarding bi-directional and point-to-multipoint RoF systems remains to be done.

CHAPTER

7

Conclusions and Recommendations

7.1 *Conclusions*

This thesis has investigated a concept for up-converting and distributing wireless signals by means of optical fibres. The method referred to as Optical Frequency Multiplication (OFM) involves interferometric filtering of a frequency-swept optical signal in order to generate high-frequency harmonic components of the sweep signal. The behaviour of the OFM system with, and without a fibre link was analysed theoretically and experimentally. Various types of optical fibre have been considered: silica single-mode, silica multimode, and polymer multimode fibres. A mathematical model of the OFM system was developed and used to analyse its behaviour and performance. System simulations with a software tool were also performed. Extensive system experiments were conducted to confirm the predicted behaviour, and performance. The obtained results lead to a number of conclusions.

It has been shown that OFM can be used to realise radio-over-fibre system downlinks between a centralised headend and radio access units. The radio access units may be remoted by both single-mode and multimode fibres. By consolidating the signal processing at the centralised headend, the remote radio access units are significantly simplified. Thus OFM can help reduce system costs in next-generation dense high-frequency broadband wireless systems, where numerous radio access units need to be deployed.

OFM requires a frequency-tunable source to generate a swept optical signal. Such a source could be an electronically tunable laser diode, or a combination of a CW laser and an optical phase modulator. The performance of both options was experimentally investigated. It was found that the tunable laser option has the advantages of low

power operation and a very high phase sensitivity, D_p , which was three orders of magnitude higher than that of the optical phase modulator. However, the operation bandwidth of the tunable laser was limited to less than 100 MHz only, while the optical phase modulator could support multi-GHz operation. For this reason, the combination of the CW laser and the phase modulator was used as the FM source in most of the experiments. With 3 GHz sweep rates, the commercially-available optical phase modulator yielded sufficient FM indexes to achieve frequency multiplication factors exceeding 7.

The impact of laser phase noise on the OFM system was investigated theoretically and experimentally. It was established that OFM suppresses laser phase noise. That means that the phase noise of the OFM-generated carriers is independent of laser phase noise. Therefore, no extra laser phase noise suppression schemes are necessary to generate high purity microwave LOs with OFM. This is an important advantage, which OFM has over other methods such as heterodyning, where PLLs and optical injection locking mechanisms, or dual mode lasers (all of which lead to system complexity) are needed to reduce the effects of laser phase noise.

The phase noise of the OFM-generated harmonic components is dependent on the sweep signal phase noise, and the multiplication factor. It was established that the phase noise of the n^{th} harmonic is proportional to the square of the multiplication factor. Experimental results confirmed the predicted theoretical phase noise performance, which was readily achieved for multiplication factors of up-to 7. Therefore, by using a high-Q sweep signal at the headend, the required LO phase noise performance may be achieved. For instance, a 17.2 GHz LO with SSB phase noise equal to -92 dBc/Hz at 10 kHz frequency offset was generated at a radio access unit remoted by a 4.4 km silica multimode fibre link. This value of phase noise was 10 dB lower than the phase noise of a commercially available high-frequency electronic signal generator. Since the sweep signal frequency is low, and the sweep signal is shared among several remoted radio access units, the impact of the high-Q sweep signal on the cost of the entire point-to-multipoint OFM system should be low.

Since high purity carriers are generated at the remote radio access units, the same carriers may be used to down-convert the uplink data. This eliminates the need for a high-frequency LO in the remote antenna unit, keeping it simple.

Using OFM, large frequency multiplication factors can be obtained. However, since the generation of high order harmonics depends on the FM index, the obtainable multiplication factor is limited by the achievable FM index, β , from the practical point of view. Furthermore, phase noise requirements of the LO to be generated may determine the maximum allowed multiplication factor, due to the increase in phase noise of the up-converted signal.

The intensity of the OFM-generated microwave signals depends on three factors, namely the FM index, β , the interferometers' contrast ratio, and the biasing of the interferometer. In general, higher frequency multiplication factors require larger FM indexes. However, peak harmonic power is obtained only for specific FM indexes. For instance, an OFM system using a sweep signal frequency of 3 GHz, and having an

interferometer (e.g. MZI) with a FSR equal to 10 GHz, requires an FM index equal to 4.7, for optimal generation of the 6th harmonic component. Thus, good control of the FM index is an important part of the OFM system.

The contrast ratio of the interferometer is an important parameter because it determines the effective intensity modulation depth of the OFM system, and thus the conversion efficiency of the system. Different filter implementations of both the MZI and the FPI types were investigated. These include the fibre-based MZI, the fibre-based FPI, the FBG-based FPI, the semiconductor material-based FPI, and the chip-based MZI. The filters had contrast ratios ranging from 3 dB to 25 dB. They were all successfully used in the OFM system. However, because of their varying contrast ratios, the filters produced varying conversion efficiencies. Considering the 17.2 GHz (6th harmonic) carrier, the fibre-based MZI with a measured 20 dB contrast ratio produced carriers of the highest intensity, exceeding 0 dBm. The maximum intensity of the same carrier generated with a fibre-based Fabry Perot interferometer with a 25 dB contrast ratio was -24 dBm. However, it was established that by reducing the contrast ratio (finesse) of the FPI, comparable conversion efficiencies are possible. One of the major differences between the MZI and the FPI filter types is that the contrast ratio of MZI is sensitive to polarisation perturbations, which if not controlled leads to another form of harmonic intensity fluctuations.

The major source of carrier amplitude instability in an OFM system is the biasing of the filter – that is the alignment of the laser's wavelength with the filter's passbands. The alignment of the laser's peak wavelength with the filter's transmission passbands determines the maximum intensity of the generated harmonic components. In general, biasing the filter at the dark spot (i.e. laser wavelength coinciding with the valley of the filter's response), or the bright spot (transmission peak), maximises even harmonic components and minimises the odd harmonic components. The situation is reversed when the filter is biased midway between the valley and the peak (i.e. FSR/4). In that case, it is the odd harmonic components which are maximised, while the even harmonic components are themselves minimised. Fluctuations in the laser's peak wavelength or the filter's response lead to intensity fluctuations of the generated harmonic components. It is therefore important to control the relative stability of the laser wavelength and the filter's response. It was established that rather than stabilise the laser wavelength and the filter separately, it is more effective to control the relative stability, by say feedback control of the filters response to track laser wavelength perturbations. This is easier to achieve if the filter is co-located with the laser at the headend. Using this approach, long-term carrier stability within 1 dB was demonstrated.

OFM can be used to distribute microwave carriers at frequencies well beyond the -3 dB bandwidth of multimode fibres. The amplitude of the generated microwave carriers is scaled by the frequency response of the multimode fibre. From this perspective, an OFM system relies on the same fibre characteristics as an SCM system, which may use higher frequency transmission passbands in multimode fibres. However, the OFM system has several system cost related advantages. For instance, unlike the SCM systems, OFM uses only low-frequency RF processing devices at the headend. The sweep signal has a relatively low frequency, and may be shared among

several radio access units. The modulation devices also operate at relatively low frequencies. Both silica and POF-based MMFs have been investigated. It has been found that Silica glass MMF links of more than 4 km are feasible for mm-wave signal distribution. The maximum link length, which can be bridged with Polymer Optical Fibre (POF) is significantly shorter, owing to its higher attenuation values. Therefore, OFM enables the provision of integrated wired services such as Fast Ethernet, and broadband (e.g. indoor) wireless services on the same in-building (multimode) fibre infrastructure.

OFM can be used to remote radio access units via single-mode fibre links as well. OFM is chromatic dispersion tolerant as it does not suffer from the fibre-length-dependent amplitude suppression, which occurs in IM-DD systems. Therefore, OFM has much longer single-mode fibre length spans than the IM-DD system. It was shown that the single-mode fibre length of a 30 GHz system could be increased from less than 5 km for an IM-DD system, to over 50 km when OFM was used instead of the IM-DD system.

Apart from generating, and transporting un-modulated LOs, OFM can also be used to distribute modulated signals. This is achieved by intensity modulating the FM optical signal with the data or subcarrier to be transmitted, at the headend. The remotely generated up-converted harmonic components are then modulated with the data. No reconfiguration of the remote antenna unit is required. To change from one wireless system standard to another (e.g. WLAN to WiMAX), only the data feed at the headend is altered. The rest of the system remains unchanged (apart from the re-tuning of the BPF at the remote antenna unit, if a completely different transmission frequency is sought). Therefore, OFM has the capability to support multi-standard operation, transparently.

The ability to generate low-phase noise carriers enables OFM to support the distribution of high-quality RF signals modulated with complex multi-level data formats including, BPSK, QPSK, and xQAM besides the simple (ASK) modulation format. For instance, the transmission and generation of a 17.2 GHz signal modulated with 156 Mbps 64 QAM data by a simplified remote antenna unit fed by 4.4 km of MMF was demonstrated. A low EVM of 4.7 % was achieved. Multi-carrier modulation formats such as Subcarrier Multiplexing (SCM), and OFDM, which is used in WLAN standards are also supported. As an example, the up-conversion of IEEE 802.11g WLAN signals from less than 1 GHz to a fully compliant signal at 17.2 GHz was experimentally demonstrated. BER measurements showed a modal dispersion penalty of about 1 dB for a 4.4 km MMF link under restricted launch conditions.

7.2 *Recommendations*

The extensive experimental work covered in this thesis was focussed on the remote delivery of pure high-frequency microwave signals to a significantly simplified Remote Antenna Unit (RAU). However, considering the fact that real-time interactive multimedia services are increasingly becoming an important component of broadband wireless communication services, full-duplex communication is a must for the systems delivering these services. It is therefore imperative to extend the laboratory set-up to implement and demonstrate full-duplex RoF transmission with OFM. One possible way to achieve this, is to use the combination of OFM/IFoF, as described in section 6.2. In addition to realising Full-Duplex Transmission, it is also interesting to investigate methods for achieving simple remote control of some of the RAU functions, when deemed necessary.

Most of the experimental work was conducted at frequencies around 17.2 GHz. This was an interesting frequency to use because of the 200 MHz license-free bandwidth allocated for Radio LANs. In addition, electrical components required for implementing the RAU were easier to acquire. For the purpose of experimentally investigating and validating the performance of the OFM system, this frequency was found to be more than adequate. However, in terms of applicability, it is envisaged that the benefits of the OFM system will be greater at higher operating frequencies such as 60 GHz, due to its ability to offer high multiplication factors, low signal phase noise, and long link lengths, while employing only low frequency electro-optical components at the headend and a simplified RAU. It is therefore, recommended that the OFM laboratory platform be upgraded to cover higher frequencies, including 60 GHz. This will make it possible to explore the use of the OFM system for some of the up-coming high density broadband wireless communication systems. These include the IEEE 802.15 Wireless Personal Area Network (WPAN) standard (57 – 64 GHz), and the IEEE 802.16 Fixed Wireless Access standard (10 – 66 GHz). Clearly, these are application areas, where OFM or other RoF systems promise to be of great benefit.

Appendix

A

Optical Frequency Multiplication based on MZI

A MZI-based OFM system is given in Figure A.1. If the CW wavelength of the tunable laser diode is λ_0 in nm or ω_0 in Hz, and an electronic signal at a frequency, f_{sw} is used to generate the peak optical frequency deviation, Δf_{pk} then the input field to the MZI may be described by [66]:

$$E_{in}(t) = E_0 e^{j[\omega_0 t + \beta \sin(\omega_{sw} t)]} \quad (\text{A.1})$$

where β is the frequency modulation depth of the swept optical signal, defined as the ratio of the peak frequency deviation, Δf_{pk} to the sweep signal frequency, f_{sw} .

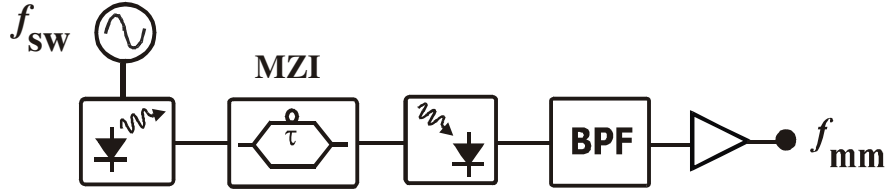


Figure A.1: A MZI-based Optical Frequency Multiplication System

The output from the MZI is then described by

$$E_{MZI}(t) = E_{in}(t) \otimes h_{MZI}(t) \quad (\text{A.2})$$

$$= \frac{1}{2} E_0 \left[e^{j[\omega_0 t + \beta \sin(\omega_{sw} t)]} + e^{j[\omega_0 (t-\tau) + \beta \sin(\omega_{sw} (t-\tau))]} \right] \quad (\text{A.3})$$

where $h_{MZI}(t) = \frac{1}{2} [\delta(t) + \delta(t - \tau)]$ is the impulse response of the MZI filter. The intensity detected by the photodiode is given by

$$I_{PD}(t) = \langle E_{MZI}(t) \cdot E_{MZI}^*(t) \rangle \quad (\text{A.4})$$

$$= \frac{1}{2} |E_0|^2 \cdot \{1 + \cos[\omega_0 \tau + \beta \sin(\omega_{sw} t) - \beta \sin[\omega_{sw}(t - \tau)]]\} \quad (\text{A.5})$$

$$= \frac{1}{2} |E_0|^2 \cdot \left\{ \begin{array}{l} 1 + \cos(\omega_0 \tau) \cdot \cos \left[2\beta \sin\left(\frac{\omega_{sw} \tau}{2}\right) \cdot \cos\left(\omega_{sw} t - \frac{\omega_{sw} \tau}{2}\right) \right] \\ - \sin(\omega_0 \tau) \cdot \sin \left[2\beta \sin\left(\frac{\omega_{sw} \tau}{2}\right) \cdot \cos\left(\omega_{sw} t - \frac{\omega_{sw} \tau}{2}\right) \right] \end{array} \right\} \quad (\text{A.6})$$

By using the Jacobi's identities given in equations (A.7) and (A.8) [115], equation (A.6) can be transformed into equation (A.9), which is a series of Bessel functions.

$$\cos(z \cos \theta) = J_0(z) + 2 \cdot \sum_{k=1}^{\infty} (-1)^k J_{2k}(z) \cdot \cos(2k\theta) \quad (\text{A.7})$$

$$\sin(z \cos \theta) = 2 \cdot \sum_{k=0}^{\infty} (-1)^k J_{2k+1}(z) \cdot \cos[(2k+1)\theta] \quad (\text{A.8})$$

$$I_{PD}(t) = \frac{1}{2} |E_0|^2 \cdot \left\{ \begin{array}{l} 1 + \cos(\omega_0 \tau) \cdot \left\{ J_0(z) + 2 \sum_{k=1}^{\infty} (-1)^k J_{2k}(z) \cdot \cos \left[2k \cdot \left(\omega_{sw} t - \frac{\omega_{sw} \tau}{2} \right) \right] \right\} \\ + 2 \sin(\omega_0 \tau) \cdot \sum_{k=1}^{\infty} (-1)^k J_{2k-1}(z) \cdot \cos \left[(2k-1) \cdot \left(\omega_{sw} t - \frac{\omega_{sw} \tau}{2} \right) \right] \end{array} \right\} \quad (\text{A.9})$$

$$\text{where } z = 2\beta \cdot \sin\left(\frac{\omega_{sw} \tau}{2}\right)$$

References

- [1]. ITU, “World Telecommunication Development Report 2002: Reinventing Telecoms”, March, 2002, available online: <http://www.itu.int/itu-ict/publications/>.
- [2]. Y. Kim, B. J. Jeong, J. Chung, C-S. Hwang, J. S. Ryu, K-H. Kim, and Y. K. Kim, “Beyond 3G: Vision, Requirements, and Enabling Technologies”, IEEE Communications Magazine, 120 – 124, (March 2003).
- [3]. The Industrial Wireless Book, “De-mystifying IEEE 802.11 for Industrial Wireless LANs”, available online at <http://wireless.industrial-networking.com>, May 2005.
- [4]. S. Ohmori, “The Future Generations of Mobile Communications Based on Broadband Access Technologies”, IEEE Communications Magazine, 134 - 142, (December 2000).
- [5]. D. Novak, “Fiber Optics in Wireless Applications”, OFC 2004 Short Course 217, 2004.
- [6]. IEEE 802.16 Working Group on Broadband Wireless Access Standards, “Developing the IEEE 802.16 WirelessMAN® Standard for Wireless Metropolitan Area Networks”, available online at <http://ieee802.org/16/> , May 2005.
- [7]. IEEE 802.15 Working Group for Wireless Personal Area Networks, “IEEE 802.15 WPAN Millimeter Wave Alternative PHY Task Group 3c (TG3c)”, available online at <http://www.ieee802.org/15/pub/TG3c.html>, May 2005.
- [8]. D. Wake, “Radio over Fiber Systems for Mobile Applications” in *Radio over Fiber Technologies for Mobile Communications Networks*, H. Al-Raweshidy, and S. Komaki, ed. (Artech House, Inc, USA, 2002).
- [9]. D. M. Pozar, “*Microwave and RF Design of Wireless Systems*”, (John Wiley & Sons, Inc., 2001).
- [10]. T. Koonen, A. Ng’oma, P. F. M. Smulders, H. P. A. vd. Boom, I. Tafur Monroy, and G. D. Khoe, “In-House networks using Multimode Polymer Optical Fiber for broadband wireless services”, *Photonic Network Communications*, Vol. 5, No. 2, 177-187, (Kluwer, 2003).

-
- [11]. J. J. O'Reilly, P. M. Lane, and M. H. Capstick, "Optical Generation and Delivery of Modulated mm-waves for Mobile Communications", in *Analogue Optical Fibre Communications*, B. Wilson, Z. Ghassemlooy, and I. Darwazeh, ed. (The Institute of Electrical Engineers, London, 1995).
- [12]. Y. Koike, "POF Technology for the 21st Century", in Proceedings of the Plastic Optical Fibres (POF) Conference, 2001, pp 5 - 8.
- [13]. Y. Watanabe, "Current Status of Perfluorinated GI-POF and 2.5 Gbps Data Transmission over it", in Proceedings of OFC '03, USA, 2003, pp. 12 - 13.
- [14]. D. Wake, and K. Beachman, "A Novel Switched Fibre Distributed Antenna System", in Proceedings of European Conference on Optical Communications (ECOC'04), Vol. 5, 2004, pp. 132 - 135.
- [15]. D. K. Mynbaev, L. L. Scheiner, "*Fiber Optic Communications Technology*", (Prentice Hall, New Jersey, 2001).
- [16]. J. Capmany, B. Ortega, D. Pastor, and S. Sales, "Discrete-Time Optical Processing of Microwave Signals", *JLT*, Vol. 23, No. 2, 703 - 723, (2005).
- [17]. B. Carbon, V. Girod, and G. Maury, "Optical Generation of Microwave Functions", in Proceedings of Workshop on Microwave Photonics for Emission and Detection of Broadband Communication Signals, Louvain-la-Nueve, Belgium, 2001.
- [18]. G. Maury, A. Hilt, T. Berceci, B. Cabon, and A. Vilcot, "Microwave Frequency Conversion Methods by Optical Interferometer and Photodiode", *IEEE Trans. On Microwave Theory and Techniques*, Vol. 45, No. 8, 1481 - 1485, (1997).
- [19]. D. Wake, S. Dupont, J-P. Vilcot, and A. J. Seeds, "32-QAM Radio Transmission Over Multimode Fibre Beyond the Fibre Bandwidth", in Proceedings of the IEEE International Topical Meeting on Microwave Photonics (MWP'01), 2001.
- [20]. D. Wake, S. Dupont, C. Lethien, J-P. Vilcot, and D. Decoster, "Radiofrequency Transmission over Multimode Fibre for Distributed Antenna System Applications", *Electronic Letters*, Vol. 37, No. 17, pp 1087 - 1089 (2001).
- [21]. C. Liu, A. Seeds, J. Chadha, P. Stavrinou, G. Parry, M. Whitehead, A. Krysa, and J. Roberts, "Bi-Directional Transmission of Broadband 5.2 GHz Wireless Signals Over Fibre Using a Multiple-Quantum-Well Asymmetric Fabry-Perot Modulator/Photodetector", in Proceedings of the Optical Fiber Communications (OFC) Conference. 2003, Vol. 2, pp. 738 - 740.
- [22]. H. Al-Raweshidy, "Radio over Fibre Technology for the Next Generation" in *Radio over Fiber Technologies for Mobile Communications Networks*, H. Al-Raweshidy, and S. Komaki, ed. (Artech House, Inc, USA, 2002).

-
- [23]. A. Powell, "Radio over Fiber Technology: Current Applications and Future Potential in Mobile Networks – Advantages and Challenges for a Powerful Technology" in *Radio over Fiber Technologies for Mobile Communications Networks*, H. Al-Raweshidy, and S. Komaki, ed. (Artech House, Inc, USA, 2002).
- [24]. Patent No. NL1019047, "Werkwijze en stelsel voor het via een multi-modus optische vezel overdragen van microgolfsignalen", octrooiaanvraag 1019047, indieningsdatum 26 sep. 2001, door A.M.J. Koonen.
- [25]. U. Gliese, T. N. Nielsen, S. Norskov, and K. E. Stubkjaer, "Multifunction Fibre-Optic Microwave Links Based on Remote Heterodyne Detection", *IEEE Trans. On Microwave Theory and Techniques*, Vol. 46, No. 5, 458 - 468, (1998).
- [26]. P. Hartmann, M. Webster, A. Wonfor, J.D. Ingam, R.V. Penty, I.H. White, D. Wake, and A.J. Seeds, "Low-Cost Multimode Fiber-based Wireless LAN Distribution Systems Using Uncooled, Directly Modulated DFB Laser Diodes", in *Proceedings of the ECOC'03*, Vol. 3, 2003, pp. 804 – 805.
- [27]. I. Frigyes, "Basic Microwave Properties of Optical Links: Insertion Loss, Noise Figure, and Modulation Transfer" in *Radio over Fiber Technologies for Mobile Communications Networks*, H. Al-Raweshidy, and S. Komaki, ed. (Artech House, Inc, USA, 2002).
- [28]. J. Capmany, B. Ortega, A. Martinez, D. Pastor, M. Popov, and P. Y. Fongjallaz, "Multiwavelength Single Sideband Modulation for WDM Radio-Over-Fiber Systems Using a Fiber Grating Array Tandem Device", *IEEE Photonics Tech. Letters* Vol. 17, No. 2, 471 - 473, (2005).
- [29]. J. Capmany, D. Pastor, P. Munoz, S. Sales, B. Ortega, and A. Martinez, "WDM-SSB Generation and Dispersion Mitigation in Radio over Fiber Systems with Improved Performance Using an AWG Multiplexer with Flat Top Resonances", in *Proceedings of the International Topical Meeting on Microwave Photonics (MWP 2003)*. 2003, pp. 39 – 42.
- [30]. J. Heiskala, and J. Terry, "*OFDM Wireless LANs: A Theoretical and Practical Guide*", (Sams Publishing, USA, 2002), Chapt. 5.
- [31]. D. Wake, "Optoelectronics for millimetre-wave radio over fibre systems" in *Analogue Optical Fibre Communications*, B. Wilson, Z. Ghassemlooy, and I. Darwazeh, ed. (The Institute of Electrical Engineers, London, 1995).
- [32]. P. Shen, N. J. Gomes, P. A. Davies, W. P. Shillue, P. G. Huggard, and B. N. Ellison, "High-Purity Millimetre-Wave Photonic Local Oscillator Generation and Delivery", in *Proceedings of the International Topical Meeting on Microwave Photonics (MWP 2003)*. 2003, pp. 189 – 192.
- [33]. L. N. Langley, M. D. Elkin, C. Edge, M. J. Wale, X. Gliese, X. Huang, and A. J. Seeds, "Packaged Semiconductor Laser Optical Phase-Locked Loop (OPLL) for Photonic Generation, Processing and Transmission of Microwave Signals", *IEEE Trans. On Microwave Theory and Techniques*, Vol. 47, NO. 7, 1257 - 1264, (1999).

-
- [34]. Y. J. Waen, H. F. Liu, D. Novak, and Y. Ogawa, "Millimeter-Wave Signal Generation from a Monolithic Semiconductor Laser via Subharmonic Optical Injection", *IEEE Photonics Tech. Letters* Vol. 12, NO. 8, 1058 - 1060, (2000).
- [35]. H. Furuta, M. Maeda, T. Nomoto, J. Kobayashi, and S. Kawasaki, "Optical Injection Locking of a 38-GHz-Band InP-Based HEMT Oscillator Using a 1.55- μm DSB-SC Modulated Lightwave", *IEEE Photonics Tech. Letters* Vol. 11, NO. 01, 19 - 21, (2001).
- [36]. C. G. Schaffer, F. H. Lubeck, R. P. Braun, G. Grosskopf, F. Schmidt, and M. Rohde, "Microwave Multichannel System with a Sideband Injection Locking Scheme in the 60 GHz Band", in *Proceedings of the International Topical Meeting on Microwave Photonics (MWP 1998)*. 1998, pp. 67 - 69.
- [37]. S. Fukushima, C. F. C. Silva, Y. Muramoto, and A. J. Seeds, "10 to 110 GHz Tunable Opto-Electronic Frequency Synthesis Using Optical Frequency Comb Generator and Uni-Travelling-Carrier Photodiode", *IEEE Photonics Letters*, Vol. 37, No. 12, 780 - 781, (2001).
- [38]. S. Bennett, B. Cai, E. Burr, O. Gough, and A. J. Seeds, "1.8 THz Bandwidth, Zero-Frequency Error, Tunable Optical Comb Generator for DWDM Applications", *IEEE Photonics Letters*, Vol. 11, No. 5, 551 - 553, (1999).
- [39]. L. A. Johansson, and A. J. Seeds, "Millimeter-Wave Modulated Optical Signal Generation with High Spectral Purity and Wide-Locking Bandwidth Using a Fibre-Integrated Optical Injection Phase-Lock Loop", *IEEE Photonics Tech. Letters* Vol. 12, NO. 6, 690 - 692, (2000).
- [40]. L. A. Johansson, and A. J. Seeds, "36 GHz 140-Mb/s Radio-Over-Fiber Transmission Using an Optical Injection Phase-Lock Loop Source", *IEEE Photonics Tech. Letters* Vol. 13, NO. 8, 893 - 895, (2001).
- [41]. K. E. Razavi, and P. A. Davies, "Semiconductor laser sources for the generation of millimetre-wave signals", *IEE Proc.-Optoelectron.*, Vol. 145, No. 3, 159 - 162, (1998).
- [42]. N. G. Walker, D. Wake and I. C. Smith, "Efficient millimetre-wave signal generation through FM-IM conversion in dispersive optical fibre links", *Electronic Letters*, Vol. 28, No. 21, 2027 - 2028, (1992).
- [43]. J. O'Reilly, and P. Lane, "Remote Delivery of Video Services Using mm-Waves and Optics", *JLT* Vol. 12, NO. 2, 369 - 375, (1994).
- [44]. C. Lim, A. Nirmalathas, D. Novak, and R. Waterhouse, "Millimeter-Wave Broadband Fiber-Wireless System Incorporating Baseband Data Transmission over Fibre and Remote LO Delivery", *JLT*, Vol. 18, No. 10, 1355 - 1363, (2000).
- [45]. G. Maury, B. Cabon, A. Hilt, J-F Le Bigot, "Optical Upconversion of 100 Mb/s BPSK Microwave Subcarrier Signals Using an Unbalanced Mach-Zehnder Interferometer", In *Proceedings of the IEEE International Topical Meeting on Microwave Photonics*, 2000. MWP 2000, pp 179 - 182.

-
- [46]. R. P. Braun, and G. Grosskopf, "Optical Feeding of Base Stations in Millimeter-Wave Mobile Communications", in Proceedings of European Conference on Optical Communications (ECOC'98), 1998.
- [47]. A. Stohr, K. Kitayama, and D. Jager, "Full-Duplex Fiber-Optic RF Subcarrier Transmission Using a Dual-Function Modulator/Photodetector", IEEE Trans. On Microwave Theory and Techniques, Vol. 47, No 7, 1338 - 1341, (1999).
- [48]. R. Heinzlmann, T. Kuri, K. Kitayama, A. Stohr, and D. Jager, "Optical Add-Drop Multiplexing of 60 GHz Millimeter-Wave Signals in a WDM Radio-on-Fibre Ring", in Proceedings of the Optical Fiber Communications (OFC2000) Conference. 2000, pp 137 - 139.
- [49]. T. Ismail, C. Liu, J. E. Mitchel, A. J. Seeds, X. Qian, A. Wonfor, R. V. Penty, and I. H. White, "Full-Duplex Wireless-over-Fibre Transmission Incorporating a CWDM Ring Architecture with Remote Millimeter-Wave LO Delivery Using a Bi-Directional SOA", in Proceedings of the Optical Fiber Communications (OFC) Conference. 2005, paper OThG7.
- [50]. A. M. J. Koonen, A. Ng'oma, M. Garcia Larrode, F. M. Huijskens, I. Tafur-Monroy, and G. D. Khoe, "Novel Cost-Efficient Techniques for Microwave Signal Delivery in Fibre-Wireless Networks", in Proceedings of European Conference on Optical Communications (ECOC'04), Vol. 5, 2004, Stockholm, pp. 120-123.
- [51]. A. Ng'oma, "*Design of a Radio-over-Fiber System for Wireless LANs*", (MTD. Report, Eindhoven University of Technology, Eindhoven, 2002).
- [52]. T. Koonen, A. Ng'oma, H. P. A. vd. Boom, I. Tafur Monroy, P. F. M. Smulders, and G. D. Khoe, "Microwave Signal Transport over Multimode Polymer Optical Fibre Networks for Feeding Wireless LAN Access Points", in Proceedings of the European Conference on Optical Communications (ECOC'02). 2002, Paper 9.2.5.
- [53]. W. M. Hamdy, "*Crosstalk in Direct Detection Optical FDMA Networks*", (Ph.D. Thesis, Massachusetts Institute of Technology, Cambridge, 1991).
- [54]. A. Ng'oma, A. M. J. Koonen, I. Tafur-Monroy, H. P. A. vd. Boom, P. F. M. Smulders, and G. D. Khoe, "Optical Frequency Up-conversion in Multimode and Single-Mode Fibre Radio Systems", in Proceedings of SPIE Vol. 5466, 2004, pp 169 - 177.
- [55]. W. Tomasi, "Electronic communications systems: fundamentals through advanced", (Prentice Hall, New Jersey, 2001).
- [56]. Y. Park, S. K. Lee, and C. J. Chae, "A Novel Wavelength Stabilisation Scheme Using a Fiber Grating for WDM Transmission", IEEE Photonics Tech. Letters Vol. 10, NO. 10, 1446-1448, (1998).
- [57]. L. Ping, L. Deming, H. Dexiu, and S. Junqiang, "Study of Temperature Stability for Fiber-Optic Mach-Zehnder Interferometer Filter", in Proceedings of the 3rd International Conference on Microwave and Millimeter Wave Technology", (IEEE, 2002), pp. 1087 - 1088.

-
- [58]. J. M. Vaughan, "The Fabry Perot Interferometer: History, Theory, and Applications", (Hilger, Bristol, 1989).
- [59]. M. K. Smit, T. Koonen, H. Herrmann, W. Sohler, "Wavelength-selective Devices" in *Fiber Optic Communication Devices*", N. Grote, and H. Venghaus, ed. (Springer, Berlin, 2001).
- [60]. W. S. Gornall, "The World of Fabry-Perots", *Lasers & Applications*, pp 47 – 52 (July, 1983).
- [61]. J. Vobis, D. Derickson, "Optical Spectrum Analysis" in *Fiber Optic Test and Measurement*, D. Derickson, ed. (Prentice Hall Inc., New Jersey, 1998).
- [62]. A. Ng'oma T. Koonen, I. Tafur Monroy, H. P. A. vd. Boom, P. F. M. Smulders, and G. D. Khoe, "Distributing microwave signals via Polymer Optical Fiber (POF) System", in Proceedings of the IEEE/LEOS Benelux Chapter Annual Symposium, 2001, pp 157 - 160.
- [63]. T. Koonen, A. Ng'oma, H. P. A. vd. Boom, I. Tafur Monroy, P. F. M. Smulders, and G. D. Khoe, "Carrying microwave signals in a GIPOF-based wireless LAN", in Proceedings of the Plastic Optical Fibres Conference, 2001, pp 217 - 223.
- [64]. D. M. Baney, W. V. Sorin, "High Resolution Optical Frequency Analysis", in "*Fiber Optic Test and Measurement*", D. Derickson, ed. (Prentice Hall, New Jersey, 1998).
- [65]. M. Nazarathy, W. V. Sorin, D. M. Baney, S. A. Newton, "Spectral Analysis of Optical Mixing Measurements," *JLT* Vol. 7, No., 7, 1083 – 1096, (1989).
- [66]. A. M. J. Koonen, A. Ng'oma, "Integrated Broadband Optical Fiber/Wireless LAN Access Networks", in *Broadband Optical Access Networks and Fiber-to-the-Home*, C. Lin, ed. (John Wiley and Sons, in press).
- [67]. E. Eichen, "Interferometric generation of high-power, microwave frequency, optical harmonics", *Applied Physics Letters*, Vol. 51, 398 – 400 (1987).
- [68]. W. H. Nelson, E. Eichen, and P. Melman, "Interferometric Intensity Noise and Frequency Modulation in single mode semiconductor lasers – Experimental and Theoretical Analysis", in Proceedings of the IOOC – ECOC '85, 1985, pp 729 - 732.
- [69]. B. Moslehi, "Analysis of Optical Phase Noise in Fiber-Optic systems employing a laser source with arbitrary Coherence Time", *JLT*, Vol. LT-4, No. 9, 1334 – 1351, (1986).
- [70]. L. A. Johansson and A. J. Seeds, "Generation and Transmission of Millimeter-Wave Data-Modulated Optical Signals Using an Optical Injection Phase-Lock Loop", *IEEE JLT*, Vol. 21, pp 511 – 520 (2003).
- [71]. A. S. Daryoush, "Phase noise degradation in nonlinear fiber optic links distribution networks for communication Satellites", in "*Microwave Photonics*", A. Vilcot, B. Cabon, and J. Chazelas, ed. (Kluwer Academic Publishers, Netherlands, 2003).

-
- [72]. N. G. Walker, D. Wake, and I. C. Smith, "Efficient Millimetre-wave Signal Generation Through FM-IM Conversion in Dispersive Optical Fibre Links?", *Electronic Letters*, Vol. 28, No. 21, pp 2027 - 2028 (1992).
- [73]. H. L. T. Lee, R. J. Ram, O. Kjebon, and R. Schatz "Enhanced Direct Modulation Efficiency by FM to IM Conversion", in *Proceedings of the IEEE International Topical Meeting on Microwave Photonics (MWP2000)*, 2000, pp 105 - 108.
- [74]. T. Ishigure, A. Horibe, E. Nihei and Y. Koike, "High bandwidth and high numerical aperture graded-index polymer optical fibre," *IEEE Electronic Lett. JLT*, Vol. 30, No. 14, pp 1169 – 1171 (1994).
- [75]. A. Ghatak, K. Thyagarajan, "*Introduction to Fiber Optics*", (Cambridge University Press, 1998).
- [76]. S. E. Golowich, W. A. Reed, A. J. Ritger, "A New Modal Power Distribution Measurement for High-Speed Short-Reach Optical Systems," *JLT.*, Vol. 22, No. 2, pp 457 – 468 (2004).
- [77]. G. Jiang, R. F. Shi, and A. F. Garito, "Mode Coupling and Equilibrium Mode Distribution Conditions in Plastic Optical Fibers," *IEEE Photonics Techn. Lett.*, Vol. 9, No. 8, pp 1128 – 1130 (1997).
- [78]. K. Ohdoko, T. Ishigure, "Propagating Mode Analysis and Design of Waveguide Parameters of GI POF for Very Short-Reach Network Use," *IEEE Photonics Tech. Lett.*, Vol. 17, No. 1, pp 79 – 81 (2005).
- [79]. S. Shaklan, "Measurement of Intermodal Coupling in Weakly guided Multimode Fibre Optics," *Electronic Letters*, Vol. 26, No. 24, pp 2022 – 2024 (1990).
- [80]. T. Ishigure, M. Kano, and Y. Koike, "Which is a More Serious Factor to the Bandwidth of GIPOF: Differential Mode Attenuation or Mode Coupling?" *JLT*, Vol. 18, No. 7, pp 959 - 965 (2000).
- [81]. S. E. Golowich, W. White, W. A. Reed, and E. Knudsen, "Quantitative Estimates of Mode Coupling and Differential Modal Attenuation in Perfluorinated Graded-Index Plastic Optical Fiber," *JLT*, Vol. 21, No. 1, pp 111 - 121 (2003).
- [82]. L. Raddatz, D. Hardacre, I. H. White, R. V. Penty, D. G. Cunningham, M. R. T. Tan, S. -Y. Wang, "High Bandwidth Data Transmission in Multimode Fibre Links Using Subcarrier Multiplexing with VCSELs", *Electronic Letters*, Vol. 34, No. 7, 686 – 688.
- [83]. L. Raddatz, D. Hardacre, I. H. White, R. V. Penty, D. G. Cunningham, M. R. T. Tan, S. -Y. Wang, "High Bandwidth Multimode Fiber Links using Subcarrier Multiplexing in Vertical-Cavity Surface-Emitting Lasers", in *Proceedings of the Optical Fiber Communications (OFC) Conference*. 1998, pp 358 – 359.
- [84]. P. Pepeljugoski, S. E. Golowich, A. J. Ritger, P. Kolesar, and A. Risteski, "Modelling and Simulation of Next-Generation Multimode Fiber Links," *JLT*, Vol. 21, No. 5, pp 1242 – 1255 (2003).

-
- [85]. W. R. White, M. Dueser, W. A. Reed, and T. Onishi, "Intermodal Dispersion and Mode Coupling in Perfluorinated Graded-Index Plastic Optical Fiber," *IEEE Photonics Techn. Lett.*, Vol. 11, No. 8, pp 997 - 999 (1999).
- [86]. R. Dandliker, A. Bertholds, and F. Maystre, "How Modal Noise in Multimode Fibres Depends on Source Spectrum and Fiber Dispersion," *JLT*, Vol. LT-3, No. 1, pp 7 – 12 (1985).
- [87]. A. M. J. Koonen, "Bit-Error-Rate Degradation in a Multimode Fiber Optic Transmission Link Due to Modal Noise," *IEEE JNL on Select. Comms.* Vol. SAC-4, No. 9, (1986).
- [88]. Y. Chien-Huug, L. Chien-Chung, H. Yaw-Wen, and C. Sien, "Fast Wavelength-Tunable Laser Technique Based on a Fabry-Perot Laser Pair With Optical Interinjection", *IEEE Photonics Tech. Lett.*, Vol. 16, No. 3, pp 891 - 893 (2004).
- [89]. A. Ng'oma, A.M.J Koonen, I. Tafur Monroy, H. P. A. vd. Boom, P. F. M. Smulders, F. M. Huijskens, and G. D. Khoe, "Optical Frequency Multiplication for low-phase noise microwave signal generation and delivery", in *Proceedings of the European Conference on Networks & Optical Communications (NOC 2004)*, 2004, pp 237 - 244.
- [90]. L. W. Couch, "*Digital and Analog Communication Systems*", (5th Edition, Prentice Hall, New Jersey, 1997).
- [91]. M. Leversque, M. Tetu, P. Tremblay, and M. Chamberland, "A Novel Technique to Measure the Dynamic Response of an Optical Phase Modulator", *IEEE Trans. On Instrumentation and Measurement*, Vol. 44, No. 5, pp 952 - 957 (1995).
- [92]. S. Tammela, H. Ludvigsen, T. Kajava, and M. Kaivola, "Time-Resolved Frequency Chirp Measurement Using a Silicon-Wafer Etalon", *IEEE Photonics Tech. Lett.*, Vol. 9, No. 4, pp 475 - 477 (1997).
- [93]. A. Giesberts, "*Receiver Design for a Radio over Polymer Optical Fiber System*", (M.Sc. Thesis, Eindhoven University of Technology, Eindhoven, 2003).
- [94]. Dutch National Frequency Register, Internet link: <http://www.at-ez.nl/nfr/>, (14 February 2005).
- [95]. A. Ng'oma, A. M. J. Koonen, I. Tafur-Monroy, H. P. A. vd. Boom, P. F. M. Smulders, and G. D. Khoe, "Low Cost Polymer Optical Fibre based Transmission System for Feeding Integrated Broadband Wireless In-House LANs", in *Proceedings of the IEEE/LEOS Benelux Chapter Annual Symposium*, 2002, pp 214 - 217.
- [96]. A. Ng'oma, I. Tafur-Monroy, A. M. J. Koonen, H. P. A. vd. Boom, P. F. M. Smulders, and G. D. Khoe, "High-Frequency Carrier Delivery to Graded Index Polymer Optical Fibre Fed Next Generation Wireless LAN Radio Access Points", in *Proceedings of European Conference on Optical Communications (ECOC'03)*, Vol. 3, 2003, pp. 508 – 509.

-
- [97]. A. Ng'oma, A. M. J. Koonen, I. Tafur-Monroy, H. P. A. vd. Boom, and G. D. Khoe, "Phase Noise Performance of a Multimode Fibre Based Optical Frequency Multiplication System", in Proceedings of the IEEE/LEOS Benelux Chapter Annual Symposium, 2004, pp 203 - 206.
- [98]. T. Okoshi, K. Kikuchi, and A. Nakayama, "Novel Method for High Resolution Measurement of Laser Output Spectrum", *Electronic Letters*, Vol. 16, No. 16, pp 630 - 631 (1980).
- [99]. H. Tanobe, F. Koyama, and K. Iga, "Spectral Linewidth of AlGaAs/GaAs Surface-Emitting Laser", *Electronic Letters*, Vol. 25, No. 21, pp 1444 - 1445 (1989).
- [100]. K. Iiyama, K. Hayashi, Y. Ida, H. Ikeda, and Y. Sakai, "Reflection-Type Delayed Self-Homodyne/Heterodyne Method for Optical Linewidth Measurements", *JLT*, Vol. 9, No. 5, pp 635 - 640 (1991).
- [101]. M. O. van Deventer, "Comparison of DFB Laser Linewidth Measurement Techniques Results from Cost 215 Round Robin", *Electronic Letters*, Vol. 26, No. 24, pp 2018 - 2020 (1990).
- [102]. R. D. Esman, L. Goldberg, "Simple Measurement of Laser Diode Spectral Linewidth Using Modulation Sidebands", *Electronic Letters*, Vol. 24, No. 22, pp 1393 - 1394 (1988).
- [103]. A. A. Saavedra, R. Passy, J. P. von der Weid, E. Manganote, and A. C. G. Bordeaux, "Measurements of Chirp and Linewidth Enhancement Factor of DFB Semiconductor Lasers Using a Self-Homodyne Interferometric System", in Proceedings of the Microwave and Optoelectronics Conference (IMOC'97), 1997, pp 401 - 405.
- [104]. J. Iannelli, H. Blauvelt, E. Peral, and A. Yariv, "Determination of Dispersion Induced Relative Intensity Noise through Spectral Linewidth Measurements", in the Digest of the LEOS Summer Topical Meetings, 1999, pp 9 - 10.
- [105]. FOTP-47, "*Output Far Field Radiation Pattern Measurement*", Electronic Industries Association (EIA/TIA-455-47B, August 1992).
- [106]. A. Ng'oma, I. Tafur-Monroy, J. J. Vegas Olmos, A. M. J. Koonen, and G. D. Khoe, "Frequency Up-Conversion In Multimode Fiber-Fed Broadband Wireless Networks by Using Agile Tunable Laser Source", *Microwave and Optical Technology Letters*, Vol. 41, No. 1, pp 28 - 30 (2004).
- [107]. P-J Rigole, S. Nilsson, L. Backbom, T. Klinga, J. Wallin, B. Stalnacke, E. Berglind, and B. Stoltz, "114-nm Wavelength Tuning Range of a Vertical Grating Assisted Codirectional Coupler Laser with a Super Structure Grating Distributed Bragg Reflector," *IEEE Photonics Techn. Lett.*, Vol. 7, No. 7, pp 697 - 699 (1995).
- [108]. O. A. Lavrora, D. J. Blumenthal, "Detailed Transfer Matrix Method-Based Dynamic Model for Multisection Widely Tunable GCSR Lasers," *JLT.*, Vol. 18, No. 9, pp 1274 - 1281 (2000).
- [109]. Fibre Fabry-Perot Tunable Filter Datasheet, Micron Optics, Inc. <http://www.micronoptics.com/ffp-tf.htm>

-
- [110]. T. Koonen, A. Ng'oma, H. P. A. vd. Boom, I. Tafur Monroy, P. F. M. Smulders, and G. D. Khoe, "Polymer Optical Fibre Network For Feeding Wireless LAN Antenna Stations", in Proceedings of the XXVIIth URSI GA, 2002, Paper 1833.
- [111]. C. L. Chen, "Elements of Optoelectronics and Fiber Optics", (Irwin, USA, 1996).
- [112]. A. Ng'oma, A. M. J. Koonen, I. Tafur-Monroy, H. P. A. vd. Boom, and G. D. Khoe, "Using Optical Frequency Multiplication to Deliver a 17 GHz 64 QAM Modulated Signal to a Simplified Radio Access Unit Fed by Multimode Fiber", in Proceedings of the Optical Fiber Communications (OFC/NFOEC) Conference. 2005, Paper OWB2.
- [113]. IEEE P802.11a/D7 Standard, LAN/MAN Standard Committee, IEEE Inc., 1999.
- [114]. T. Koonen, Steenbergen, J. Fons, J. Wellen, "Flexible Re-configurable Fiber-Wireless Network Using Wavelength Routing Techniques: the ACTS Project AC349 PRISMA", Photonic Network Communications, Vol. 3, No. 3, 297 - 306, (2001).
- [115]. G. N. Watson, "*A treatise on the theory of Bessel Functions*", (Cambridge University Press, London, 1966).
- [116]. T. Koonen, A. Ng'oma, P. F. M. Smulders, H. P. A. vd. Boom, I. Tafur Monroy, and G. D. Khoe, "In-house networks using Polymer Optical Fibre for broadband wireless applications", in Proceedings of the ISSLS 2002, 2002, pp 285 - 294.
- [117]. M. Garcia Larrode, A. M. J. Koonen, and P. F. M. Smulders, "Impact of Radio-over-Fiber Links on Wireless Access Protocols", in Proceedings of the Nefertiti Workshop on Millimetre Wave Photonic Devices and Technologies for Wireless and Imaging Applications. Jan 2005, CDROM.

List of Publications

- ◆ A. M. J. Koonen, A. Ng'oma, “Integrated Broadband Optical Fiber/Wireless LAN Access Networks”, in *Broadband Optical Access Networks and Fiber-to-the-Home*, C. Lin, ed. (John Wiley and Sons, in press).
- ◆ A. Ng'oma, A. M. J. Koonen, I. Tafur-Monroy, H. P. A. vd. Boom, and G. D. Khoe, “Using Optical Frequency Multiplication to Deliver a 17 GHz 64 QAM Modulated Signal to a Simplified Radio Access Unit Fed by Multimode Fiber”, in Proceedings of the Optical Fiber Communications (OFC/NFOEC) Conference. CA, USA, 2005, Paper OWB2.
- ◆ A. Ng'oma, A. M. J. Koonen, I. Tafur-Monroy, H. P. A. vd. Boom, and G. D. Khoe, “Phase Noise Performance of a Multimode Fibre Based Optical Frequency Multiplication System”, in Proceedings of the IEEE/LEOS Benelux Chapter Annual Symposium, Belgium, 2004, pp 203 - 206.
- ◆ Ton Koonen, Anthony Ng'oma, Maria Garcia Larrode, Frans Huijskens, Idelfonso Tafur Monroy, and Giok-Djan Khoe, “Novel Cost-Efficient Techniques for Microwave Signal Delivery in Fibre-Wireless Networks”, in Proceedings of European Conference on Optical Communications (ECOC'04), Vol. 5, Stockholm, 2004, pp. 120-123 (invited).
- ◆ A. Ng'oma, I. Tafur-Monroy, J. J. Vegas Olmos, A. M. J. Koonen, and G. D. Khoe, “Frequency Up-Conversion In Multimode Fiber-Fed Broadband Wireless Networks by Using Agile Tunable Laser Source”, *Microwave and Optical Technology Letters*, Vol. 41, No. 1, pp 28 - 30 (Wiley, 2004).
- ◆ A. Ng'oma, A. M. J. Koonen, I. Tafur-Monroy, H. P. A. vd. Boom, P. F. M. Smulders, and G. D. Khoe, “Optical Frequency Up-conversion in Multimode and Single-Mode Fibre Radio Systems”, in Proceedings of SPIE Vol. 5466, France, 2004, pp 169 - 177.
- ◆ A. Ng'oma, A.M.J Koonen, I. Tafur Monroy, H. P. A. vd. Boom, P. F. M. Smulders, F. M. Huijskens, and G. D. Khoe, “Optical Frequency Multiplication for low-phase noise microwave signal generation and delivery”, in Proceedings of the European Conference on Networks & Optical Communications (NOC 2004), Netherlands, 2004, pp 237 - 244.

-
- ◆ Ton Koonen, Henrie van den Boom, Anthony Ng'oma, Idelsonso Tafur Monroy, Giok-Djan Khoe, "Novel signal multiplexing methods for integration of services in in-building broadband multimode fibre networks", in Proceedings of the XVth International Symposium on Services and Local access (ISSLS 2004), Edinburgh, 2004.
 - ◆ A.M.J. Koonen, H. P. A. vd. Boom, L. Bakker, J. Zeng, A. Ng'oma, and G. D. Khoe, "Integration of services in short-range multimode Polymer Optical Fibre networks by exploiting the higher-order fibre passbands", in Proceedings of the 13th International Plastic Optical Fibres Conference, Germany, 2004, pp 90 – 97.
 - ◆ A. Ng'oma, A.M.J. Koonen, I. Tafur Monroy, H. P. A. vd. Boom, P. Smulders, and G. D. Khoe, "Towards Multimode-Fibre-Fed Broadband In-door Wireless LANs Operating Above 6 GHz", in Proceedings of the 2nd European Nefertiti Winter School in Microwave Photonics, York, England, 2004.
 - ◆ Ton Koonen, Anthony Ng'oma, Peter Smulders, Henrie van den Boom, Idefonso Tafur Monroy, and Giok-Djan Khoe, "In-House networks using Multimode Polymer Optical Fiber for broadband wireless services", Photonic Network Communications, Vol. 5, No. 2, 177-187, (Kluwer, 2003).
 - ◆ A. Ng'oma, I. Tafur-Monroy, A. M. J. Koonen, H. P. A. vd. Boom, P. F. M. Smulders, and G. D. Khoe, "High-Frequency Carrier Delivery to Graded Index Polymer Optical Fibre Fed Next Generation Wireless LAN Radio Access Points", in Proceedings of European Conference on Optical Communications (ECOC'03), Vol. 3, Italy, 2003, pp. 508 – 509.
 - ◆ A. Ng'oma, A. M. J. Koonen, I. Tafur-Monroy, H. P. A. vd. Boom, P. Smulders, and G. D. Khoe, "Using Multimode Fibres for Broadband In-door Wireless Coverage", in Proceedings of the IEEE/LEOS Benelux Chapter Annual Symposium, Netherlands, 2003, pp 145 - 148.
 - ◆ A. Ng'oma, A.M.J. Koonen, A. Giesberts, I. Tafur Monroy, H.P.A. van den Boom, P.F.M. Smulders and G.D. Khoe, "Feeding broadband wireless services over a multimode polymer optical fibre network", in Proceedings of the IEEE/LEOS Benelux Chapter Workshop on Low-Cost Photonics, June 2003.
 - ◆ A.M.J. Koonen, A. Ng'oma, H.P.A. van den Boom, I. Tafur Monroy, G.D. Khoe, "New techniques for extending the capabilities of multimode fibre networks", in Proceedings of the NOC 2003, 1-3 July 2003, pp. 204-211.
 - ◆ A. M. J. Koonen, H.P.A. van den Boom, A. Ng'oma, I. Tafur Monroy, G.D. Khoe, "Integrated-services in-building POF networks using novel signal multiplexing methods", in Proceedings of the 12th Int. POF conference. 15-17 September 2003; Seattle, Washington, 2003, pp. 44-47.
 - ◆ A. Ng'oma, "Design of a Radio-over-Fibre System for Wireless LANs", (MTD. Report, Eindhoven University of Technology, Eindhoven, 2002).

-
- ◆ Ton Koonen, Anthony Ng'oma, Henrie van den Boom, Idelfonso Tafur Monroy, Peter Smulders, and Giok Djan Khoe, "Microwave Signal Transport over Multimode Polymer Optical Fibre Networks for Feeding Wireless LAN Access Points", in Proceedings of the European Conference on Optical Communications (ECOC'02). Denmark, 2002, Paper 9.2.5.
 - ◆ Ton Koonen, Anthony Ng'oma, Peter Smulders, Henrie van den Boom, Idelfonso Tafur Monroy, and Giok-Djan Khoe, "In-house networks using Polymer Optical Fibre for broadband wireless applications", in Proceedings of the ISSLS 2002, Seoul, 2002, pp 285 - 294.
 - ◆ T. Koonen, A. Ng'oma, H. P. A. vd. Boom, I. Tafur Monroy, P. F. M. Smulders, and G. D. Khoe, "Polymer Optical Fibre Network For Feeding Wireless LAN Antenna Stations", in Proceedings of the XXVIIIth URSI GA, 2002, Paper 1833.
 - ◆ G. D. Khoe, A. M. J. Koonen, P.K.A van Bennekom, H.P.A. van den Boom, A. Ng'oma, T. Monroy, "High capacity polymer optical fibre systems", in Proceedings of the European Conference on Optical Communications (ECOC'02). Denmark, 2002.
 - ◆ A. Ng'oma, A. M. J. Koonen, I. Tafur-Monroy, H. P. A. vd. Boom, P. F. M. Smulders, and G. D. Khoe, "Low Cost Polymer Optical Fibre based Transmission System for Feeding Integrated Broadband Wireless In-House LANs", in Proceedings of the IEEE/LEOS Benelux Chapter Annual Symposium, Netherlands, Netherlands, 2002, pp 214 - 217.
 - ◆ T. Koonen, A. Ng'oma, H. P. A. vd. Boom, I. Tafur Monroy, P. F. M. Smulders, and G. D. Khoe, "Carrying microwave signals in a GIPOF-based wireless LAN", in Proceedings of the Plastic Optical Fibres Conference, Netherlands, 2001, pp 217 - 223.
 - ◆ A. Ng'oma, T. Koonen, I. Tafur Monroy, H. P. A. vd. Boom, P. F. M. Smulders, and G. D. Khoe, "Distributing microwave signals via Polymer Optical Fiber (POF) System", in Proceedings of the IEEE/LEOS Benelux Chapter Annual Symposium, Belgium, 2001, pp 157 - 160.

Samenvatting

Het met draadloze verbindingen afdekken van het domein van de eindgebruiker, buitenshuis zowel als binnenshuis, wordt ontegenzeggelijk een steeds essentiëler deel van breedband communicatie netwerken. Om geïntegreerde breedbandige diensten (welke spraak, data, video, multimedia diensten, en nieuwe diensten met toegevoegde waarde combineren) te kunnen aanbieden, zullen deze systemen hogere overdrachtscapaciteiten moeten leveren die de hedendaagse standaarden van draadloze systemen aanzienlijk te boven gaan. Enkele van deze standaarden zijn de draadloze LAN versies (IEEE802.11a/b/g) welke tot 54 Mbit/s bieden en opereren bij 2.4 GHz en 5 GHz, en de 3G mobiele netwerken (IMT2000/UMTS) die tot 2 Mbit/s bieden en rond 2 GHz opereren. IEEE802.16 of WiMAX is een andere recente standaard die middels vaste draadloze toegang ('fixed wireless access', FWA) de laatste schakel met de eindgebruiker probeert te vormen.

De behoefte aan een hogere capaciteit per oppervlakte-eenheid vergt hogere radio-frekwenties (boven 6 GHz) en kleinere radio-cellen, in het bijzonder in de toepassingen binnenshuis waar deze hoogfrequentie radiogolven enorm hoge verliezen ervaren wanneer zij door muren moeten gaan. Om de kosten van het installeren en het onderhouden van zulke systemen te reduceren is het van wezenlijk belang om de radio-antenne eenheden zo eenvoudig mogelijk te maken. Dit is te bereiken door de signaalbewerkings-functies samen te brengen in een gecentraliseerd hoofdstation, middels radio-over-fiber technologie.

Het onderzoek in dit proefschrift heeft zich geconcentreerd op het gebruik van single-mode zowel als multi-mode fibers om microgolf-signalen te distribueren over op afstand geplaatste vereenvoudigde radio-antenne eenheden. Een alternatieve radio-over-fiber techniek is onderzocht, genaamd optische frequentie-vermenigvuldiging ('Optical Frequency Multiplication', OFM). OFM omvat het periodieke filteren van een in frequentie gezwaaid optisch signaal in het hoofdstation, gevolgd door foto-detektie in de radio-antenne eenheid waaruit de microgolf resulteert. Een betrekkelijk lage zwaai-frekwentie kan gebruikt worden (bv. 3 GHz). Uit de foto-detektie in de radio-antenne eenheid resulteren hoog-frekwente (>21 GHz) harmonischen van de zwaai-frekwentie. De gewenste harmonische wordt geselecteerd middels filtering, versterkt, en uitgestraald door de antenne. Gemoduleerde microgolf draaggolven kunnen gegenereerd worden door het frequentie-gezwaaide optische signaal ook in intensiteit te moduleren.

Middels modelleren, simuleren, en het doen van uitvoerige experimenten is het gedrag en de prestatie van een radio-over-fiber verbinding naar de antenne toe gebaseerd op OFM onderzocht. De resultaten uit de simulaties en de gedetailleerde experimenten hebben aangetoond dat OFM gebruikt kan worden om zeer zuivere hoog-frekvente microgolf signalen te genereren, welke een zeer smal spectrum hebben en een lage enkelzijband fase-ruis. Dit is te danken aan het onderdrukken van de fase-ruis van de laser, wat inherent plaatsvindt in het OFM proces. Deze lage fase-ruis maakt het mogelijk dat met de OFM techniek niet alleen draaggolven gemoduleerd met het simpele ASK data formaat aan de antenne eenheid afgeleverd kunnen worden, maar ook die gemoduleerd zijn met complexe meer-niveau formaten zoals BPSK, QPSK, en x-level QAM. Ook worden signalen ondersteund welke meerdere draaggolven bevatten, zoals signalen met meerdere gemultiplexe hulpdraaggolven, en OFDM signalen zoals gebruikt in draadloze LAN-s. Lage Error Vector Magnitude waarden (minder dan 5%) zijn gemeten voor x-level QAM gemoduleerde signalen, inclusief 64-QAM. Bit-error-rate metingen hebben laten zien dat er circa 1 dB extra zendvermogen nodig is ten gevolge van modale dispersie in een 4.4 km lange multimode fiber verbinding met restrictieve lichtinstraling.

Er is aangetoond dat de OFM techniek tolerant is jegens chromatische dispersie, en dat het single-mode fiber verbindingen kan overbruggen die meer dan tien maal langer zijn (d.w.z. meer dan 50 km) dan systemen welke intensiteitsmodulatie en directe detectie gebruiken; deze laatste hebben te lijden van amplitude-verzwakking ten gevolge van chromatische dispersie. De OFM techniek maakt het ook mogelijk om microgolf signalen af te leveren welke de modale bandbreedte van multimode fibers te boven gaan, door gebruik te maken van de hoger-gelegen doorlaatbanden van de fiber-karakteristieken. Fibers gemaakt van silica glas met lengtes van meer dan 4 km kunnen overbrugd worden. De maximale afstand die met polymeer optische fiber (POF) overbrugd kan worden is aanzienlijk korter, wat te wijten is aan zijn hogere demping per lengte-eenheid. Derhalve kan POF meer aantrekkelijk zijn voor binnenshuis toepassingen waar verbindingen over 500 meter vaak voldoende zijn.

Verschillende implementaties van het Mach Zehnder Interferometer filter, en het Fabry Perot Interferometer filter zijn onderzocht, teneinde hun eenvoud, prestatie, en bruikbaarheid in de omgeving van de eindgebruiker te bepalen. Gevonden is dat de rustgolflengte van de frekwentie-gezwaaide optische bron nauwkeurig afgestemd dient te zijn op de karakteristieken van het periodieke optische filter. Het is daarom te verkiezen om de optische bron en het filter op één plaats te huisvesten. Hiermee is het eenvoudiger om middels elektronische afstemming van het filter (bv. een Fiber Fabry Perot Interferometer) een automatische afstemming op de optische bron te realiseren, wat resulteert in een aanmerkelijke verbetering van de stabiliteit van het OFM systeem.

Het vermogen om hoge frekwentie-vermenigvuldigingsfactoren te realiseren, het goede fase-ruis gedrag, de ondersteuning van alle signaalmodulatie-formaten, en het vermogen om zowel in single-mode als in multi-mode fiber-verbindingen toegepast te kunnen worden, maken de OFM techniek ideaal geschikt voor hoog-frekvente (>5 GHz) breedbandige draadloze communicatie-systemen.

Acknowledgements

Radio-over-Fibre (RoF) technology is a technology that essentially integrates two worlds – the radio world, and the optics world. Therefore, in this integrated world, one has to contend with a double share of problems. Stepping into this field for the first time four years ago, I faced many hurdles and challenges along the way. However, with the help and contributions of many people, we were able to realise a physical working RoF system from a mere idea. To have been part of this transformation has been such an enlightening and satisfying experience. Therefore, it gives me great pleasure to acknowledge and thank the many people who contributed in many various ways to the successful completion of this work.

First and foremost, I wish to thank Prof. Giok-Djan Khoe for giving me the opportunity to work in the Electro-Optical Communications group. Secondly, I am very grateful to my promoter Prof. Ton Koonen for his guidance and all the support, which helped shape the course of this work. Not only did he propose the idea of Optical Frequency Multiplication (OFM), but he also contributed to the theoretical modelling of the system, and to many other aspects of the work. I thank him for the meticulous manner in which he reviewed my thesis, which greatly improved its quality. Thirdly, I thank my direct supervisor, Idelfonso Tafur Monroy, who closely worked with me on this project from its inception to the end. Together, we went through the challenges and difficulties of building a new laboratory platform. I am very grateful for the many discussions we had, especially on the analysis of the theoretical, and experimental results. He also encouraged and supported me with my publications, and reviewed this thesis. Indeed, Idelfonso, without your valuable contribution, this work would not have been accomplished, thank you very much! I would also like to thank Peter Smulders of the ECR group, who provided guidance on the radio aspects of this work. I am also grateful to Bas de Hon, for his useful insights on mode orthogonality, to Prof. Arthur van Roermund for reviewing part of my thesis, and to Gert-Jan Rijckenberg for his thorough review of the thesis.

The building of the laboratory platform presented many challenges. I am grateful to a number of people who helped me with the experimental aspects of the work. I thank Frans Huijskens for constructing the two Mach Zehnder Interferometers, and for his assistance with many practical issues in the lab. I am grateful to Peter van Bennekom for his help with equipment orders and assistance in providing measuring equipment. I thank Henrie van den Boom, and Rene Jonker, who helped me get started with my first experiments, and Huug de Waardt for sharing some of his laboratory equipment. I also thank Fouad Karouta of the OED group who assisted in the preparation of the

wafer-based Fabry Perot cavities, and Piet van Heyningen for allowing me to use his microwave filter. I am grateful to Piet Matthijsse, and Frank Achten of *Draka Fibre* for providing several samples of multimode fibres and an experimental mode scrambler. I also wish to thank Erwin Drenth of *Rohde & Schwarz* for his help in providing the WLAN BER measurement setup, the vector signal generator, and the vector signal analyser. I am grateful to Jan Hendrick den Besten for his assistance in cleaning and setting up the chip-based MZI.

Some of the devices used in the experiments were made by collaborating institutes outside the Netherlands. I am thankful to the group of Prof. Jose Capmany (*Grupo Comunicaciones Opticas*) of the *Universidad Politecnica de Valencia* (UPV) in Spain, for making several samples of the Fibre Bragg Grating-based Fabry Perot Interferometers, which were used in some of the system experiments. Furthermore, I thank Prof. Beatrice Cabon and her group - *Laboratoire IMEP (Institut de Microélectronique Electromagnétisme et Photonique)* of France for allowing us to use their chip-based MZI for system stability measurements. This was done under the auspices of the Nefertiti Network of Excellence (NoE). I also wish to thank Prof. Alwyn Seeds and Dr. John Mitchell, both of *University College London* (UCL) for hosting me during my exchange visit to their RoF laboratories in 2004. That visit was also sponsored by Nefertiti.

Having been part of the ECO group the last few years, I would like to thank all the members of the group for their support in various ways. Two MSc students contributed to this work. Almar Giesberts worked on the development of an OFM-based RoF system receiver, and Almudena Huerta Miranda worked on the simulation of multimode fibre. I thank Susan de Leeuw and Els Gerritsen for their assistance with various administrative matters. I am grateful to Johan van Zantvoort and Jianming Zeng, who worked with me on the Far Field Radiation Pattern measurements, Liu Yong, for the helpful discussions on experimental issues, and J.J. Vegas Olmos, with whom I performed the OFM system experiments using a tunable laser. Over the last few years I had the pleasure of sharing office space with various colleagues. I thank Jacco Kwaaitaal, Eduward Tangdionga, Archi Delphinanto, and Laurens Bakker for the many interesting discussions we had on various issues both technical and non-technical – including social issues.

I am grateful to the Dutch Ministry of Economic Affairs for partly financially supporting this work in the BTS project Broadband Radio@Hand within the BraBantBreedBand (B4) programme. I thank Prof. Erik Fledderus who coordinated the Radio@Hand project for his useful advice and also for accepting to be copromotor of this work. I further thank the Nefertiti FP5 Thematic Network for sponsoring my trips to several interesting workshops on microwave photonics.

I would like to thank a number of people who gave me and my family moral support during the course of this work. I am grateful to Bright Ng'andu, Misheck Mwaba, Paulos Nyirenda, and their families for their support. I also thank Dr. Lemba and Drinah Nyirenda for their support. I further thank our dear friends Tamara, Silvanico, Adora, and Chase who supported us in many ways. I also appreciate the encouragement and support from my family at large. I thank bana kulu, naba shikulu

Chileshe (A.C. Chilambwe), auntie Christine and uncle Golden Ziba, auntie Agnes and uncle Joseph Mutale, and auntie Rose and uncle Evans Mukuka, all of whom have supported me towards this goal.

Finally, I am indebted to my dear wife Ivy, and to our two princesses Chisela and Beene for their love, support, patience, perseverance, and understanding during the many days and nights I had to be away from them. They all truly share in this accomplishment.

Curriculum Vitae

Anthony Ng'oma was born in Kasama (Zambia) in 1969. He completed his secondary school education at Kasama Boys' Secondary School in 1988. In 1989 he entered the University of Zambia (UNZA), where he read for a Bachelor of Engineering degree in Electronic Engineering and Telecommunications. He completed (with Merit) the B.Eng. degree programme in 1994, and soon afterwards joined Computer Technologies Inc. in Lusaka, as a Computer Network Engineer. His duties included computer network design, installation, and maintenance, as well as software development. In August, 1995, he resigned from Computer Technologies Inc. and joined UNZA as a Staff Development Fellow. Soon after, he was offered a scholarship to do a Master of Engineering degree program in Electronic Engineering in collaboration with the University of Twente in Enschede, the Netherlands, under Nuffic's MHO programme. His M.Eng. project work was conducted at the University of Twente between 1995 and 1996 and involved the use of Artificial Intelligence for the control of dynamic non-linear systems.

Following his completion of the M.Eng. degree programme in 1997, he was appointed Lecturer in the Department of Electrical and Electronic Engineering at UNZA. He taught Electronics and Telecommunications courses. In 1999 while at UNZA, he worked for Computer Frontiers Inc. (USA) as a Computer Connectivity Specialist under the US Agency for International Development (USAID) office in Lusaka. He was involved in evaluating and coordinating connectivity projects in Zambia. At the beginning of 2000 he joined the Electro-Optical Communications (ECO) group of the Eindhoven University of Technology to pursue a postgraduate programme of the Stan Ackermans Institute in ICT – the Master of Technological Design (MTD) programme. The title of his MTD thesis was “Design of a Radio-over-Fibre System for Wireless LANs”. Upon completion of the MTD program in 2002, he decided to continue with the PhD research in broadband fibre-wireless systems – the subject of this thesis. This research was executed as part of the Radio@Hand project within the Brabant BreedBand (B4) programme.